Chemical and Redox Non-Innocence in Low-Valent Molybdenum β-Diketonate Complexes: Novel Pathways for CO_2 and CS_2 Activation

Fabio Masero[a], Prof. Dr. Victor Mougel*[a]

[a] Laboratory of Inorganic Chemistry (LAC), Department of Chemistry and Applied Biosciences (D-CHAB), ETH Zurich, Vladimir-Prelog Weg 2, 8093 Zurich, Switzerland. Email: mougel@inorg.chem.ethz.ch

---

Supporting Information

Table of Content:

1. Experimental 6
1.1 General Information 6
2. Synthesis of Isolated Compounds 8
2.1 Homoleptic Mo(III) Complexes 8
2.1.1 Synthesis of [Mo^{III}(^{Me}diket)$_3$] (1) 8
2.1.2 [Mo^{III}(^{tBu}diket)$_3$] (3) 8
2.2 Homoleptic Mo(IV) Complexes 8
2.2.1 [Mo^{IV}(^{Me}diket)$_3$]PF_6 (2) 8
2.2.2 [Mo^{IV}(^{tBu}diket)$_3$]PF_6 (4) 9
2.3 Mo(II) Complexes 9
2.3.1 K[Mo^{II}(^{tBu}diket)$_3$] (5) 9
2.3.2 K(18-crown-6)$_{0.5}$(thf)$_2$[Mo^{II}(^{tBu}diket)$_3$] (5·(18-c-6)$_{1/2}$) 9
2.3.3 K(15-crown-5)[Mo^{II}(^{tBu}diket)$_3$] (5·(15-c-5)) 10
2.3.4 Attempted Preparation of Na[Mo(^{Me}diket)$_3$]by Reduction of [Mo(^{Me}diket)$_3$] with Sodium Naphthalenide 10
2.4 Synthesis of Bis(^{R}diket) Complexes 10
2.4.1 [Mo^{II}(^{tBu}diket)$_2$(py)$_2$] 10
2.4.2 [Mo^{II}(^{tBu}diket)$_2$(PEt_3)$_2$] 10
2.4.3 [Mo^{II}(^{Me}diket)$_2$(py)$_2$] 11
2.4.4 [Mo^{II}(^{Me}diket)$_2$(PEt_3)$_2$] 11
2.5 Synthesis of K[^{tBu}diket] 11
2.5.1 Synthesis of K[^{tBu}diket] 11
2.6 Reaction of K[Mo(^{tBu}diket)$_3$] with CO_2 11
2.6.1 Synthesis of K_2[Mo(^{tBu}diket)$_2$(^{tBu}diket·$^{12}CO_2$)] (6) 11
2.6.2 Synthesis of K_2[Mo(^{tBu}diket)$_2$(^{tBu}diket·$^{13}CO_2$)] (^{13C}6) 12
2.6.3 Synthesis of K_2[Mo(^{tBu}diket)$_2$(^{tBu}diket·CO_2)] using Excess KC_8 12
2.7 Chemical Reduction with CS_2 12
2.7.1 Reduction with 5 12
2.7.2 Reduction with K^0 13

3. Additional Reactivity Studies 14
3.1 Reactivity of Chemically Reduced [Mo(^{Me}diket)$_3$] with CO_2 14
3.2 Reactivity of K[Mo(^{tBu}diket)$_3$] with CS_2 14
3.2.1 In the Absence of 18-Crown-6 14
3.2.2 In the Presence of 18-Crown-6 15
3.3 Deuteration of [Mo(^{Me}diket)$_3$] 17
3.4 Reactivity Studies of 6 18
3.5 Reactivity of K[^{tBu}diket] with CS_2 19
3.5.1 Procedure 19
4. XRD Data 20
4.1 General Procedure 20
4.2 Refinement Details 20
5. NMR Spectroscopy 26
5.1 NMR Spectra of Isolated Metal Complexes 26
5.1.1 Mo(IV) Complexes 26
5.1.2 Mo(III) Complexes 28
5.1.3 Mo(II) Complexes 29
5.2 NMR Spectra of Reaction with CO_2 31
5.3 NMR Spectra of Reaction with CS_2 32
5.4 Reactivity Studies 33
5.4.1 ^{13C}6 + ^{tBu}diketH 33
5.4.2 ^{13C}6 in Methanol-d_4 34
5.4.3 ^{13C}6 in D_2O 35
5.4.4 1 + KC_8 under CO_2 35
5.5 Additional Spectra 36
6. UV-Vis Spectra 37
6.1 ^{Me}diket Supported Complexes 37
6.2 ^{tBu}diket Supported Complexes 37
7. Infrared (IR) Spectroscopy 41
7.1 Reactivity of 5 with $^{12/13}CO_2$ 41
7.1.1 Spectra 41
7.2 Reactivity of 5 with $^{12/13}CS_2$ 42
7.2.1 Procedure 42
7.2.2 Spectra 42
8. EPR Spectroscopy 44
8.1 EPR Spectrum of 6 44
9. Theoretical Calculation of 6 45
9.1 Method 45
9.2 Spin Density Plot 45
9.3 Coordinates of Optimized Geometry 46
10. Electrochemistry 49
10.1 CV Studies 49
10.1.1 CV of 1 49
10.1.2 CV of 2 51
10.1.3 CV of 3 51

10.1.4 CV of 6 53
10.2 Controlled Potential Electrolysis (CPE) under CO_2 53
10.2.1 Attempted Product Identification 54
10.3 Controlled Potential Electrolysis (CPE) in Presence of CS_2 54
10.3.1 Product Analysis 55
11. Proposed Reaction Mechanism 57
12. References 58

Index Supporting Schemes:

Scheme S1: Attempts to isolate and valorize the carboxylated ligand [$^{t\text{Bu}}$diket·CO_2]$^-$ of **6**. 18
Scheme S2: Proposed mechanistic pathways for the formation of **6** *vs.* $K_2[C_2S_4]$. 57

Index Supporting Figures

Figure S1: ^{13}C NMR spectrum in pyridine-d_5 of the crude reaction mixture (pyridine-extraction) after reduction with K^0. 13
Figure S2: UV-Vis spectrum (normalized by concentration [mg·mL^{-1}]) in pyridine of the crude reaction mixture after stoichiometric reduction with K^0 (*solid grey* line). The spectrum of isolated [K(18-crown-6)]$_2$[C_2S_4] is displayed for comparison (*dashed* line). 13
Figure S3: ^{1}H NMR spectrum of the THF-d_8 filtrate. 14
Figure S4: ^{13}C NMR spectrum of the THF-d_8 solid, dissolved in methanol-d_4. 15
Figure S5: ^{1}H NMR spectrum of the THF-d_8 filtrate. 15
Figure S6: ^{13}C NMR spectrum of the THF-d_8 solid, dissolved in methanol-d_4. 16
Figure S7: ^{Me}diket ligand deuteration monitored by ^{1}H NMR spectroscopy: **1** in MeCN-d_3 (*black*, *top*), **1** + [TBA]$_2$[oxalate] in MeCN-d_3 stirred for 24 h (*red*), **1** in methanol-d_4, stirred for 24 h (*orange*) and **1** reduced with KC_8 under CO_2 in MeCN-d_3 (*blue*). 17
Figure S8: ^{13}C NMR spectrum in THF-d_8 of K[$^{t\text{Bu}}$diket] + $^{13}CS_2$ (10 equiv.). 19
Figure S9: ^{13}C NMR spectrum in THF-d_8 of K[$^{t\text{Bu}}$diket] + $^{13}CS_2$ (10 equiv.) after addition of methanol-d_4. 19
Figure S10: ^{1}H NMR spectrum of [Mo(^{Me}diket)$_3$]PF_6 in MeCN-d_3. 26
Figure S11: ^{19}F NMR spectrum of [Mo(^{Me}diket)$_3$]PF_6 in MeCN-d_3. 26
Figure S12: ^{31}P NMR spectrum of [Mo(^{Me}diket)$_3$]PF_6 in MeCN-d_3. 26
Figure S13: ^{1}H NMR spectrum of [Mo($^{t\text{Bu}}$diket)$_3$]PF_6 in MeCN-d_3. 27
Figure S14: ^{19}F NMR spectrum of [Mo($^{t\text{Bu}}$diket)$_3$]PF_6 in MeCN-d_3. 27
Figure S15: ^{31}P NMR spectrum of [Mo($^{t\text{Bu}}$diket)$_3$]PF_6 in MeCN-d_3. 27
Figure S16: ^{1}H NMR spectrum of [Mo(^{Me}diket)$_3$] in MeCN-d_3. 28
Figure S17: ^{1}H NMR spectrum of [Mo($^{t\text{Bu}}$diket)$_3$] in benzene-d_6. 28
Figure S18: ^{1}H NMR spectrum of [Mo($^{t\text{Bu}}$diket)$_3$] in dichloromethane-d_2. 29
Figure S19: ^{1}H NMR spectrum of K(18-crown-6)$_{0.5}$(thf)[Mo($^{t\text{Bu}}$diket)$_3$] in THF-d_8. 29
Figure S20: ^{1}H NMR spectrum of K(15-crown-5)[Mo($^{t\text{Bu}}$diket)$_3$] in benzene-d_6. 30
Figure S21: ^{1}H NMR spectrum of [Mo($^{t\text{Bu}}$diket)$_2$(py)$_2$] in benzene-d_6. 30
Figure S22: ^{1}H NMR spectrum of crude K_2[Mo($^{t\text{Bu}}$diket)$_2$($^{t\text{Bu}}$diket·CO_2)] in THF-d_8. 31
Figure S23: ^{1}H NMR spectrum of recrystallized K_2[Mo($^{t\text{Bu}}$diket)$_2$($^{t\text{Bu}}$diket·CO_2)] in THF-d_8. 31
Figure S24: ^{1}H NMR spectrum of recrystallized [K(18-crown-6)]$_2$[C_2S_4] in Py-d_5. 32
Figure S25: ^{13}C NMR spectrum of recrystallized [K(18-crown-6)]$_2$[C_2S_4] in Py-d_5. 32
Figure S26: ^{13}C NMR spectrum of K[$^{t\text{Bu}}$diket] in THF-d_8. 32
Figure S27: ^{13}C NMR spectrum of **^{13C}6** + $^{t\text{Bu}}$diketH in THF-d_8 after 8 h at ambient temperature. 33
Figure S28: ^{13}C NMR spectrum of K[$^{t\text{Bu}}$diket] in THF-d_8 under $^{13}CO_2$ (1 atm). 33
Figure S29: ^{13}C NMR spectrum of **^{13C}6** in methanol-d_4 after 8 h at ambient temperature. 34
Figure S30: ^{1}H NMR spectrum of **^{13C}6** in methanol-d_4 after 10 min (*maroon*, *top* trace), after 8 h (*dark blue*, *middle* trace) at ambient temperature, and after washing with ^{n}pentane (*light blue*, *bottom* trace). 34
Figure S31: ^{13}C NMR spectrum of **^{13C}6** suspended in D_2O (without filtration). The chemical shift was reference using the residual THF signals. 35

Figure S32: ^{13}C NMR spectra of **1** + KC_8 (1 equiv.) in methanol-d_4 under $^{12}CO_2$ (1 atm, *light blue*, *top* trace) and $^{13}CO_2$ (1 atm, *dark blue*, *bottom* trace). 35
Figure S33: ^1H NMR spectrum of K[Mo($^{t\text{Bu}}$diket)$_3$] (crude) in benzene-d_6. Small amounts of **3** (indicated within the spectrum) could be removed by treatment with crown ether (18-crown-6 or 15-crown-5) which allowed for purification by recrystallization (see Figure S19 and Figure S20). 36
Figure S34: UV-Vis spectrum of [Mo($^{\text{Me}}$diket)$_3$]PF_6 in MeCN (d = 2 mm). 37
Figure S35: UV-Vis spectrum of [Mo($^{t\text{Bu}}$diket)$_3$]PF_6 in THF (d = 2 mm). 37
Figure S36: UV-Vis spectrum of [Mo($^{t\text{Bu}}$diket)$_3$] in THF (d = 2 mm). 37
Figure S37: UV-Vis spectrum of K[Mo($^{t\text{Bu}}$diket)$_3$] in THF (d = 2 mm). 38
Figure S38: UV-Vis spectrum of K(15-crown-5)[Mo($^{t\text{Bu}}$diket)$_3$] in THF (d = 2 mm). 38
Figure S39: UV-Vis spectrum of K(18-crown-6)[Mo($^{t\text{Bu}}$diket)$_3$] in THF (d = 2 mm). 38
Figure S40: UV-Vis spectrum of K_2[Mo($^{t\text{Bu}}$diket)$_2$($^{t\text{Bu}}$diket·CO_2)] in THF (d = 2 mm). 39
Figure S41: Overlayed UV-Vis spectra of [Mo($^{t\text{Bu}}$diket)$_3$], K[Mo($^{t\text{Bu}}$diket)$_3$] and K_2[Mo($^{t\text{Bu}}$diket)$_2$($^{t\text{Bu}}$diket·CO_2)], respectively, in THF (d = 2 mm). 39
Figure S42: UV-Vis spectrum of [Mo($^{t\text{Bu}}$diket)$_2$(py)$_2$] in THF (d = 2 mm). 39
Figure S43: UV-Vis spectrum of [Mo($^{t\text{Bu}}$diket)$_2$(PEt_3)$_2$] in THF (d = 2 mm). 40
Figure S44: UV-Vis spectrum of [K(18-crown-6)$_2$] in MeCN (*left*) and pyridine (*right*) (d = 2 mm). .40
Figure S45: IR spectra of [Mo($^{t\text{Bu}}$diket)$_3$] (*top*, *red*), K[Mo($^{t\text{Bu}}$diket)$_3$] (*middle*, *light turquoise*), and K_2[Mo($^{t\text{Bu}}$diket)$_2$($^{t\text{Bu}}$diket·$^{12}CO_2$)] (*bottom*, *green*). 41
Figure S46: IR spectra of K_2[Mo($^{t\text{Bu}}$diket)$_2$($^{t\text{Bu}}$diket·$^{12}CO_2$)] (*top*, *green*), and K_2[Mo($^{t\text{Bu}}$diket)$_2$($^{t\text{Bu}}$diket·$^{13}CO_2$)] (*middle*, *turquoise*). The subtraction of the two spectra is displayed below (*light blue*). 41
Figure S47: IR spectra of chemically reduced **1** exposed to $^{12}CO_2$ (*top*, *green*), and $^{13}CO_2$ (*middle*, *turquoise*). The subtraction of the two spectra is displayed below (*light blue*). 42
Figure S48: FT-IR spectra of reactivity studies with $^{12/13}CS_2$ (KBr pellet). The spectrum in *light blue* corresponds to the subtraction of the spectra obtained from K[Mo($^{t\text{Bu}}$diket)$_3$] + $^{12}CS_2$ (*yellow*) and K[Mo($^{t\text{Bu}}$diket)$_3$] + $^{13}CS_2$ (*orange*). The spectra of K[Mo($^{t\text{Bu}}$diket)$_3$] (*turquoise*), [Mo($^{t\text{Bu}}$diket)$_3$] (*red*) and [K(18-crown-6)]$_2$[C_2S_4] were obtained from independently isolated compounds. More details are given in the text above. 43
Figure S49: X-Band EPR spectrum of K_2[Mo($^{t\text{Bu}}$diket)$_2$($^{t\text{Bu}}$diket·CO_2)] (*black*) and its simulated spectrum (*blue*). Collection parameters: c = 2 mM (in 2-MeTHF), T = 20 K, microwave frequency 9.5 GHz. Simulation parameters: S = 1/2, g = (1.994, 1.979, 1.932), A($^{95/97}$Mo)=(63.6, 48.8, 73.3) with g-strains of (0.026, 0.023, 0.035) and A-strains of (37.4, 59.4, 94.9). 44
Figure S50: Qualitative molecular orbital diagram of [Mo($^{t\text{Bu}}$diket)$_2$($^{t\text{Bu}}$diket·CO_2)]$^{2-}$ with the most relevant molybdenum-based molecular orbitals (*black* boxes) and the spin density (*orange* box). 45
Figure S51: CV (scan rate ν = 100 mV·s^{-1}, 2nd scan) of [Mo($^{\text{Me}}$diket)$_3$] (1 mM) in $TBAPF_6$/MeCN (0.1 M). A $TBAPF_6$/MeCN (0.1 M) background measurement is displayed as a grey dotted line, formal Mo oxidation states are indicated in black. 49
Figure S52: CV of [Mo($^{\text{Me}}$diket)$_3$] (1 mM) in $TBAPF_6$/MeCN (0.1 M) with varying scan rate ν (see Figure legend) of the Mo(III)/Mo(II) (*left*) and of the Mo(III)/Mo(IV) redox couple (*right*). 49
Figure S53: Randles-Ševčík plot of [Mo($^{\text{Me}}$diket)$_3$] (1 mM) in $TBAPF_6$/MeCN (0.1 M) of the Mo(III)/Mo(II) (*left*) and of the Mo(III)/Mo(IV) redox couple (*right*). 50
Figure S54: CV (2nd scan) of [Mo($^{\text{Me}}$diket)$_3$] (1 mM) in $TBAPF_6$/MeCN (0.1 M) under argon (*black* trace) and under CO_2 (*light blue* trace) at ν = 20 mV·s^{-1} (*left*) and ν = 100 mV·s^{-1} (*right*). 50
Figure S55: CV (2nd scan) of [Mo($^{\text{Me}}$diket)$_3$] (1 mM) in $TBAPF_6$/MeCN (0.1 M) under argon (*black* trace) and in presence of 1 equiv. of CS_2 (*yellow* trace) at ν = 20 mV·s^{-1} (*left*) and ν = 100 mV·s^{-1} (*right*). 51
Figure S56: CV of [Mo^{III}($^{\text{Me}}$diket)$_3$] (*black* trace) and [Mo^{VI}($^{\text{Me}}$diket)$_3$]PF_6 (*orange* trace) at a scan rate ν = 100 mV·s^{-1} in $TBAPF_6$/MeCN (0.1 M). 51
Figure S57: CV (scan rate ν = 100 mV·s^{-1}, 2nd scan) of [Mo($^{t\text{Bu}}$diket)$_3$] in $TBAPF_6$/MeCN (0.1 M) (*left*) $TBAPF_6$/THF (0.1 M) (*right*). A $TBAPF_6$/MeCN (0.1 M) and $TBAPF_6$/THF (0.1 M) background measurement is displayed as a grey dotted line, formal Mo oxidation states are indicated in black. Note that the solubility of [Mo($^{t\text{Bu}}$diket)$_3$] in $TBAPF_6$/MeCN (0.1 M) is < 1 mM. 51
Figure S58: CV of [Mo($^{t\text{Bu}}$diket)$_3$] (1 mM) in $TBAPF_6$/THF (0.1 M) with varying scan rate ν (see Figure legend) of the Mo(III)/Mo(II) (*left*) and of the Mo(III)/Mo(IV) redox couple (*right*). 52
Figure S59: Randles-Ševčík plot of [Mo($^{t\text{Bu}}$diket)$_3$] (1 mM) in $TBAPF_6$/THF (0.1 M) of the Mo(III)/Mo(II) (*left*) and of the Mo(III)/Mo(IV) redox couple (*right*). 52

Figure S60: CV (2nd scan) of [Mo($^{t\text{Bu}}$diket)$_3$] (1 mM) in TBAPF$_6$/THF (0.1 M) under argon (*black* trace) and under CO_2 (*light blue* trace) at ν = 20 mV·s^{-1} (*left*) and ν = 100 mV·s^{-1} (*right*).....52
Figure S61: *left:* CV of K_2[Mo($^{t\text{Bu}}$diket)$_2$($^{t\text{Bu}}$diket·CO_2)] (1 mM) in TBAPF$_6$/THF (0.1 M) at a scan rate of ν = 100 mV·s^{-1} in anodic (*top*) and cathodic (*bottom*) scan direction. *right:* Comparison of CV of [Mo($^{t\text{Bu}}$diket)$_3$] (1 mM) and K_2[Mo($^{t\text{Bu}}$diket)$_2$($^{t\text{Bu}}$diket·CO_2)] (1 mM) in TBAPF$_6$/THF (0.1 M) at a scan rate of ν = 100 mV·s^{-1}. 53
Figure S62: Analysis after CPE (under Ar (*black*), under CO_2 (*light blue*) and under $^{13}CO_2$ (*dark blue*) by ^{13}C NMR spectroscopy, after extraction with D_2O. On the left, a zoom on 210 ppm < δ < 150 ppm is displayed. 54
Figure S63: ^{13}C NMR spectrum after electrolysis in TBAPF$_6$/MeCN (in MeCN-d_3).....55
Figure S64: ^{13}C NMR spectrum of yellow precipitate formed after electrolysis in TEABF$_4$/MeCN (in methanol-d_4). 55
Figure S65: ^{13}C NMR spectrum of the working compartment solution after electrolysis in TEABF$_4$/MeCN (taken to dryness, in methanol-d_4). 56
Figure S66: Product analysis after CPE (with TEABF$_4$ as supporting electrolyte) by UV-Vis spectroscopy in methanol. 56

1. Experimental

1.1 General Information

If not stated otherwise, all manipulations were conducted under air- and water free conditions under argon, either using standard glovebox (Vigor) or Schlenk-line techniques. All glassware was stored overnight at 120 °C and cooled under dynamic vacuum. Caps, valves, syringes *etc.* containing plastic and/or Teflon were dried overnight in a vacuum oven (T = 60 °C, p = 10^{-3} mbar) prior to use. Dry solvents were obtained from a solvent purification system (Vigor), degassed by three consecutive freeze pump thaw cycles, and stored in a glove box, in J. Young-valve equipped flasks over activated molecular sieves (for additional purification details, see Table S1). Deuterated solvents were degassed by three consecutive freeze pump thaw cycles and purified according to Table S2. Commercially available chemicals were used as received or purified according to Table S3. ***NMR*** spectra were obtained on a 300 MHz Bruker Avance III, Bruker AVANCE DRX 500 MHz NMR, or Cryo-Probe Bruker Avance III 500 MHz spectrometer. ^{1}H and ^{13}C NMR spectra were referenced to residual protonated solvent signals. ***Solution Magnetic Susceptibility*** measurements were performed via ^{1}H NMR spectroscopy using Evans' method with diamagnetic corrections.[1, 2] A capillary containing the same deuterated solvent was placed in the NMR tube prior to the measurement. The results were recorded in triplicate and the mean value is given with the corresponding standard deviation. ***UV-Vis*** spectra were collected inside an argon filled glove box with an Agilent Cary 60 instrument, which was connected by an optical fiber to a dip probe (path length d = 2 mm). ***FT-IR*** spectra were recorded on a Nicolet iS5 spectrometer (Thermo Scientific), located inside an Ar-filled glove box. Minimal amounts of sample were mixed with KBr and pressed into a pellet. ***X-Band EPR*** spectrum was recorded on a Elexsys E500 EPR spectrometer (Bruker Biospin, Rheinstetten, Germany) equipped with an ESR-900 helium flow cryostat (Oxford Instruments, Oxfordshire, UK) and a Super-High-Q resonator (Bruker) at 9.5 GHz. The spectrum was processed and simulated using Matlab (The Mathworks, Natick, MA, USA) and EasySpin.[3] ***Elemental analyses*** were performed by the Mikrolabor ETH Zurich on a LECO TruSpec Micro spectrometer. Details on ***electrochemistry*** can be found in Section S8.

Table S1: List of used solvents, supplier and purification.

Solvent	Supplier	Purification
Acetonitrile (MeCN)	Sigma-Aldrich	From SPS, stored over 3 Å MS.
Benzene	Sigma-Aldrich	Distilled from K/benzophenone, stored over 4 Å MS.
Diethyl ether (Et_2O)	Sigma-Aldrich	From SPS, distilled from K/benzophenone, stored over 4 Å MS.
Dimethoxyethane (DME)	Sigma-Aldrich	Distilled from K/benzophenone, stored over 4 Å MS.
Hexamethyldisiloxane (HMDSO)	Sigma-Aldrich	Distilled from Na/benzophenone, stored over 4 Å MS.
Methanol (MeOH)	Acros	Stored over 3 Å MS.
Ethanol (EtOH)	Sigma-Aldrich	From SPS, stored over 3 Å MS
^{n}Pentane	Sigma-Aldrich	From SPS, stored over 4 Å MS.
Pyridine (Py)	Sigma-Aldrich	Distilled from K/benzophenone, stored over 4 Å MS.
Tetrahydrofuran (THF)	Sigma-Aldrich	From SPS, distilled from K/benzophenone, stored over 4 Å MS.
Toluene (PhMe)	Chemie Brunschwig	From SPS, stored over 4 Å MS.

Table S2: List of used deuterated solvents, supplier and purification.

Solvent	Supplier	Purification
MeCN-d_3	Sigma-Aldrich	Stored over 3 Å MS (2 x 48 h)
Benzene-d_6	Sigma-Aldrich	Distilled from K/benzophenone, stored over 4 Å MS.
Dichloromethane-d_2	Chemie Brunschwig	Distilled from CaH_2, stored over 4 Å MS.
Chloroform-d	Sigma-Aldrich	Distilled from CaH_2, stored over 4 Å MS.

Methanol-d_4	Sigma-Aldrich	Stored over 3 Å MS.
Pyridine-d_5	Acros	Distilled from K/benzophenone, stored over 4 Å MS.
THF-d_8	Sigma-Aldrich	Distilled from K/benzophenone, stored over 4 Å MS.

Table S3: List of commercially available compounds.

Reagent	**Supplier**	**Purification**
Acetylacetone (^{Me}diketH)	Sigma-Aldrich	
Ammonium chloride (NH_4Cl)	VWR	
Ammonium molybdate ($(NH_4)_6Mo_7O_{24}\cdot 4H_2O$)	Acros	
Carbon disulfide ($^{12}CS_2$)	Acros	Degassed by freeze pump thaw (3x) and stored over 4 Å MS.
^{13}Carbon disulfide ($^{13}CS_2$)	Sigma-Aldrich	
15-crown-5	Appollo Scientific Ltd.	Degassed and stored over molecular sieves (4 Å).
18-crown-6	Appollo Scientific Ltd.	Sublimed under vacuum (10^{-3} mbar).
Dipivaloylmethane ($^{t\text{Bu}}$diketH)	Fluorochem	Degassed by freeze pump thaw (3x).
Ferrocenium hexafluorophosphate ($FcPF_6$)	Sigma Aldrich	
Graphite	Acros	
Hydrochloric acid (HCl, 37 wt%)	Sigma-Alrdich	
$Mo(CO)_6$	Sigma Aldrich	Sublimed under vacuum (10^{-3} mbar) at ambient temperature.
Naphthalene	Sigma-Aldrich	Sublimed under vacuum (10^{-3} mbar).
Potassium (K^0)	Acros	Washed with ^{n}pentane (2x) and dried under vacuum (10^{-3} mbar).
Potassium bromide (KBr)	Sigma-Aldrich	Dried under high vacuum (10^{-6} mbar) at 290 °C.
Potassium hydride (KH)	Sigma Aldrich	Washed with ^{n}pentane (2x) and dried under vacuum (10^{-3} mbar).
Silver hexafluorophosphate ($AgPF_6$)	Sigma Aldrich	
Sodium Ingot 99.95%	Sigma Aldrich	
Sodium chloride (NaCl)	VWR	
Sulfuric acid (H_2SO_4)	VWR	
Tetrabutyl ammonium hexafluorophosphate ($TBAPF_6$)	Fluorochem	Recrystallized from hot ethanol (2x) and dried at 80 °C for 48 h und high vacuum (p = 5 μbar).
Tin shots (Sn)	Sigma Aldrich	

Table S4: List of previously reported compounds prepared by synthesis.

Compound	Purification	Reference
Potassium graphite (KC_8)		Kaner *et al.*[4]

2. Synthesis of Isolated Compounds

2.1 Homoleptic Mo(III) Complexes

2.1.1 Synthesis of [Mo^{III}(^{Me}diket)$_3$] (1)

Combined and modified procedures from Shibahara *et al.*[5] and Larson *et al.*[6]
In a 500 mL Erlenmeyer flask, $(NH_4)_6Mo_7O_{24}\cdot 4H_2O$ (5.0 g, 30.1 mmol, 1.0 equiv.) was dissolved in concentrated HCl (100 mL). Tin metal shots (20 g, 168.5 mmol, 5.6 equiv.) were added and the solution was stirred at 100 °C in a boiling water bath. The solution turned from yellow green, to dark green and to a final color of red brown within 11 min. NH_4Cl (5 g, 73.5 mmol, 3.1 equiv.) was added and the solution was heated for further 2 min. before cooling it in an ice bath for 1 min. The solution was filtered through a glass sintered frit and saturated with gaseous HCl (generated by dropwise addition of concentrated H_2SO_4 to solid NaCl in a separate Schlenk flask) by bubbling for 1 h. The red solution was stored at 4 °C for two days. After filtration, washing with cold methanol and drying *in vacuo*, $(NH_4)_3[MoCl_6]$ was obtained as a salmon-orange colored crystalline solid in quantitative yields (10.9 g, 30.0 mmol).
^{Me}diketH (32 mL, 312 mmol, 10.4 equiv.) was dissolved in degassed, deionized water (250 mL) at 50 °C. $(NH_4)_3[MoCl_6]$ (10.9 g, 30.0 mmol, 1.0 equiv.) was added as a solid and the reaction mixture was stirred for 1 h and 30 min at 50 °C. The obtained mixture was stored 4 °C overnight affording the precipitation of brown/dark purple crystals. The solvent was removed by filtration and the remaining solid was dried *in vacuo*, affording [Mo(acac)$_3$] (3.25 g, 8.26 mmol, 27.4% based on $(NH_4)_6[Mo_7O_{24}\cdot 4H_2O]$) as a dark purple crystalline solid. All spectroscopic data is in agreement with previous reports.[6] We have redetermined the magnetic susceptibility and also report here the ^{1}H NMR spectrum in benzene-d_6 and MeCN-d_3:
μ_{eff} = 3.5(3) μ_B (Evans-method). ^{1}H NMR (benzene-d_6, 300 MHz) δ[ppm] = 129.54 (s, 18H, CH_3) , 41.73 (s, 3H, C*H*). ^{1}H NMR (MeCN-d_3, 300 MHz) δ[ppm] = 126.60 (s, 18H, CH_3), 41.33 (s, 3H, C*H*).). This data is in accord with previous literature reports.[7]

2.1.2 [Mo^{III}($^{t\text{Bu}}$diket)$_3$] (3)

In a 500 mL Schlenk flask, [Mo(CO)$_6$] (11.41 g, 43.22 mmol, 1.0 equiv.) and $^{t\text{Bu}}$diketH (54.1 mL, 259.3 mmol, 6.0 equiv.) were combined and suspended in Toluene (*ca.* 200 mL). The flask was connected to a reflux condenser and the reaction mixture was refluxed for 24 h. After cooling down to ambient temperature, the mixture was degassed by one freeze-pump-thaw cycle. Then, the reaction was again refluxed for 24 h. The last two steps were repeated three times. After cooling down to ambient temperature, all volatiles were removed under reduced pressure. Excess [Mo(CO)$_6$] and $^{t\text{Bu}}$diketH were distilled off under reduced pressure (T = 80 °C, p = 0.005 mbar). The remaining red solid material was recrystallized twice from hot acetonitrile (-35 °C). Filtration followed by drying *in vacuo* afforded the title compound as a dark red/brown, crystalline solid. Yield (1st crop): 16.44 g (25.46 mmol, 58.6%). Anal. Calcd for $C_{33}H_{57}MoO_6$, C, 61.38; H, 8.90. Found: C, 61.37; H, 8.77. μ_{eff} = 3.62(9) B.M. (Evans-method). ^{1}H NMR (CD_2Cl_2, 500 MHz) δ[ppm] = 44.19 (3H (C*H*), br), 6.78 (54H (CH_3), br). ^{1}H NMR (C_6D_6, 500 MHz) δ[ppm] = 46.11 (3H (C*H*), br), 7.03 (54H (CH_3), br). UV-Vis (0.21 mM in THF): λ_{max} [nm] ([$10^3 \cdot M^{-1} \cdot cm^{-1}$]) = 283 (31.2), 393 (7.3), 452 (4.5). Single crystals suitable for XRD analysis were grown by slowly cooling a saturated acetonitrile solution to -35 °C.

2.2 Homoleptic Mo(IV) Complexes

2.2.1 [Mo^{IV}(^{Me}diket)$_3$]PF$_6$ (2)

$AgPF_6$ (140 mg, 0.55 mmol, 1.1 equiv.) was added to a stirred solution of [Mo(^{Me}diket)$_3$] (197 mg, 0.50 mmol, 1.0 equiv.) in DME (*ca.* 5 mL). The reaction mixture was stirred at ambient temperature for one hour and then filtered by centrifugation. The obtained solid was extracted with acetonitrile and the resulting bright orange/red solution was concentrated to 2 mL. Slow diffusion of diethyl ether

into the concentrated acetonitrile solution afforded dark red crystals. The crystalline solid was filtered off and dried *in vacuo*. Yield (1st crop): 170 mg (0.32 mmol, 64%). Anal. Calcd for $C_{15}H_{21}F_6MoO_6P$, C, 33.47; H, 3.93. Found: C, 33.21; H, 3.76. μ_{eff} = 2.68 B.M. (Evans-method). ^{1}H NMR (MeCN-d_3, 300 MHz) δ[ppm] = 106.36 (s, 3H ($^{diket}CH$)), 85.56 (s, 18H (CH_3)). ^{19}F NMR (MeCN-d_3, 282 MHz) δ[ppm] = -72.85 (d, J = 706.4 Hz, (PF_6)). ^{31}P NMR (MeCN-d_3, 121 MHz) δ[ppm] = -144.59 (hept, J = 702.9 Hz, PF_6^-). UV-Vis (0.5 mM in MeCN): λ_{max} [nm] ([$10^3 \cdot M^{-1} \cdot cm^{-1}$]) = 283 (8.6), 333 (5.8), 365 (5.6), 441 (3.0, sh). Single crystals suitable for XRD analysis were grown in the same way as described above for isolation.

2.2.2 [Mo^{IV}(^{tBu}diket)$_3$]PF$_6$ (4)

$AgPF_6$ (56 mg, 0.22 mmol, 1.1 equiv.) was added to a stirred solution of [Mo(^{tBu}diket)$_3$] (130 mg, 0.20 mmol, 1.0 equiv.) in DME (*ca.* 8 mL). The reaction mixture was stirred at ambient temperature for one hour and then filtered by centrifugation. The filtrate was taken to dryness and the obtained red residue was washed with ^{n}pentane (2 x 3 mL) followed by Et_2O (2 x 3 mL). Drying *in vacuo* afforded the title compound as a bright orange/red solid Yield: 129 mg (0.16 mmol, 82%). Anal. Calcd for $C_{33}H_{57}F_6MoO_6P$, C, 50.13; H, 7.27. Found: C, 50.11; H, 7.02. μ_{eff} = 2.66(15) B.M. (Evans-method, MeCN-d_3). ^{1}H NMR (MeCN-d_3, 500 MHz) δ[ppm] = 113.99 (s, 3H ($^{diket}CH$)), 1.25 (s, 54H (CH_3)). ^{19}F NMR (MeCN-d_3, 471 MHz) δ[ppm] = -72.94 (d, J = 706.6 Hz, (PF_6)). ^{31}P NMR (MeCN-d_3, 202 MHz) δ[ppm] = -144.63 (hept, J = 706.5 Hz, PF_6^-). UV-Vis (0.25 mM in THF): λ_{max} [nm] ([$10^3 \cdot M^{-1} \cdot cm^{-1}$]) = 257 (16.0), 322 (7.8), 373 (7.6), 442 (4.9, sh). Single crystals suitable for XRD analysis were grown by slow diffusion of ^{n}pentane into a saturated THF-solution at ambient temperature.

2.3 Mo(II) Complexes

2.3.1 K[Mo^{II}(^{tBu}diket)$_3$] (5)

In a 50 mL Schlenk flask, [Mo(^{tBu}diket)$_3$] (1.29 g, 2.0 mmol, 1.0 equiv.) was dissolved in Et_2O and cooled to -35 °C. In 5 mL vial, KC_8 (296 mg, 2.2 mmol, 1.1 equiv.) was suspended in Et_2O and cooled to -35 °C. The KC_8 suspension was added dropwise to the [Mo(^{tBu}diket)$_3$] solution. The resulting mixture was stirred for 30 min. while slowly warming to ambient temperature. After filtration through a short pad of celite, all volatiles were removed under reduced pressure affording the title compound as a dark green crystalline solid (1.23 g, 90%). *Note:* The here described procedure afforded the title compound in sufficient purity for further reactions. However, its very high solubility in both polar (*e.g.* acetonitrile) as well as apolar (*e.g.* ^{n}pentane) solvents prohibited the preparative purification by recrystallization, and hence these samples were always contaminated by small amounts of [Mo(^{tBu}diket)$_3$] starting material (visible by ^{1}H NMR). Nevertheless, we were able to grow single crystals amenable for XRD studies, either from acetonitrile or ^{n}pentane (both at -35 °C). Details on the corresponding solid-state structures can be found in Section S4. In order to obtain analytically pure material, we have found that treatment with crown ether (*e.g.* 18-crown-6) afforded the corresponding Mo(II) complex with more advantageous solubility properties (*vide infra*).

2.3.2 K(18-crown-6)$_{0.5}$(thf)$_2$[Mo^{II}(^{tBu}diket)$_3$] (5·(18-c-6)$_{1/2}$)

In a 20 mL scintillation vial, [Mo^{III}(^{tBu}diket)$_3$] (200 mg, 0.31 mmol, 1.0 equiv.) was dissolved in THF (*ca.* 10 mL) and cooled to -35 °C. In a separate vial, KC_8 (50 mg, 0.36 mmol, 1.2 equiv.) was suspended in THF and cooled to -35 °C. The KC_8 suspension was added dropwise to the [Mo(^{tBu}diket)$_3$] solution. The resulting mixture was stirred for 30 minutes while slowly warming to ambient temperature. After removal of graphite by centrifugation, a solution of 18-crown-6 (50 mg, 0.19 mmol, 0.6 equiv.) in THF (*ca.* 2 mL) was added to the dark green filtrate and stirred at ambient temperature for 4 h. All volatiles were removed under reduced pressure and the obtained solid was washed with benzene (2 x 6 mL) followed by ^{n}pentane (3 x 6 mL). The remaining solid was dried *in vacuo*, affording the title compound as a dark black crystalline solid (180 mg, 0.19 mmol, 60%). Anal. Calcd for $C_{47}H_{85}KMoO_{11}$, C, 58.73; H, 8.91. Found: C, 58.74; H, 8.92. μ_{eff} = 2.6(2) μ_B (Evans-method). ^{1}H NMR (THF-d_8, 300 MHz) δ[ppm] = 8.36 (s, br), 5.42 (s, br), 4.13 (s, br), 3.66 (s, CH_2, 18-crown-6) 3.62 (m, CH_2, K(thf)), 1.77 (m, CH_2, K(thf)). UV-Vis (0.23 mM in THF): λ_{max} [nm] ([$10^3 \cdot M^{-1} \cdot cm^{-1}$]) = 283 (20.7), 380 (3.7), 431 (1.9, sh), 657 (2.6). Single crystals suitable

for XRD analysis were grown by slow diffusion of ^{n}pentane into a saturated solution of THF at ambient temperature.

2.3.3 K(15-crown-5)[Mo^{II}(^{tBu}diket)$_3$] (5·(15-c-5))

In a 20 mL scintillation vial, [Mo^{III}(^{tBu}diket)$_3$] (323 mg, 0.50 mmol, 1.00 equiv.) was dissolved in THF (*ca.* 8 mL) and cooled to -35 °C. In a separate vial, KC_8 (74 mg, 0.55 mmol, 1.1 equiv.) was suspended in THF (*ca.* 2 mL) and cooled to -35 °C. The KC_8 suspension was added dropwise to the [Mo(^{tBu}diket)$_3$] solution. The resulting mixture was stirred for 30 minutes while slowly warming to ambient temperature. After removal of graphite by centrifugation, a solution of 15-crown-5 (109 μL, 0.55 mmol, 1.1 equiv.) in THF (*ca.* 2 mL) was added to the dark green filtrate and stirred at ambient temperature for 4 h. All volatiles were removed under reduced pressure. The obtained solid was washed with ^{n}pentane (2 x 5 mL) and extracted with benzene (10 mL). Slow diffusion of ^{n}pentane (20 mL) resulted in the precipitation of dark black crystals. After filtration, the remaining solid was dried *in vacuo*, affording the title compound as a dark black crystalline solid (220 mg, 0.24 mmol, 48%, only the first crop was collected). Anal. Calcd for $C_{89}H_{157}K_2Mo_2O_{22}$, C, 57.80; H, 8.56. Found: C, 57.97; H, 8.51. μ_{eff} = 2.6(3) μ_B (Evans-method). ^{1}H NMR (benzene-d_6, 500 MHz) δ[ppm] = 9.13 (s, br), 5.91 (s, br), 5.48 (s, br), 4.33 (s, br), 3.26 (s, CH_2, 15-crown-5), 2.52 (s, br). UV-Vis (0.26 mM in THF): λ_{max} [nm] ([$10^3 \cdot M^{-1} \cdot cm^{-1}$]) = 284 (17.8), 380 (3.0), 431 (1.6, sh), 644 (2.3). Single crystals suitable for XRD analysis were grown by slow diffusion of ^{n}pentane into a saturated solution of benzene at ambient temperature.

2.3.4 Attempted Preparation of Na[Mo(^{Me}diket)$_3$]by Reduction of [Mo(^{Me}diket)$_3$] with Sodium Naphthalenide

This compound was only isolated as blue powder by precipitation. Due to inherently low solubility in most common organic solvents, no meaningful analytical data could be obtained. Despite multiple attempts, we also did not succeed in crystallizing this compound for structural characterization by single crystal XRD.

In a 5 mL scintillation vial, a solution of naphthalene (164 mg, 1.27 mmol, 1.0 equiv.) in THF (4 mL) was added to elementary sodium (41 mg, 1.79 mmol, 1.4 equiv.) and stirred at ambient temperature for 1 h, forming a dark green solution of sodium naphthalenide. In a 20 mL Schlenk flask, [Mo(^{Me}diket)$_3$] (501 mg, 1.27 mmol, 1.0 equiv.) was dissolved in Et_2O (6 mL). The freshly prepared sodium naphthalenide solution was added dropwise and the resulting mixture was stirred for 25 min. at ambient temperature. A dark blue solid precipitated, which was separated by filtration and washed with Toluene (3 x 5 mL) and Et_2O (2 x 5 mL). After drying *in vacuo*, **^{Me}Mo(II)** was obtained as a dark blue powder (234 mg). Anal. Calcd for $C_{15}H_{21}MoNaO_6$, C, 43.28; H, 5.08. Found: C, 43.87; H, 5.00.

2.4 Synthesis of Bis(^{R}diket) Complexes

2.4.1 [Mo^{II}(^{tBu}diket)$_2$(py)$_2$]

In a 25 mL scintillation vial, cold pyridine (3 mL, -35 °C) was added dropwise to solid K[Mo(^{tBu}diket)$_3$] (137 mg, 0.20 mmol, 1.0 equiv.). The resulting deep purple solution was stirred for one hour at ambient temperature. All volatiles were removed under reduced pressure and the obtained residue was extracted with ^{n}pentane. Removal of the solvent *in vacuo* afforded the desired product as a dark purple solid. Yield: 130 mg (0.20 mmol, 100%). Anal. Calcd for $C_{32}H_{48}MoN_2O_4$, C, 61.92; H, 7.80; N, 4.51. Found: C, 61.87; H, 8.12; N, 4.48. μ_{eff} = 2.77(9) μ_B (Evans-method, benzene-d_6). ^{1}H NMR (benzene-d_6, 500 MHz) δ[ppm] = 28.88 (br, Py, *arom.* C*H*), 18.47 (br, 2H (^{diket}C*H*)), 10.89 (br, Py, *arom.* C*H*), 0.88 (s, 36H (^{diket}CH_3)), --4.58 (br, Py, *arom.* C*H*). UV-Vis (0.25 mM in THF): λ_{max} [nm] ([$10^3 \cdot M^{-1} \cdot cm^{-1}$]) = 228 (7.6), 254 (12.3), 327 (2.4), 385 (1.1), 541 (9.5), 580 (9.9), 907 (10.3 (br)).

Single crystals suitable for XRD analysis were grown by cooling a saturated solution in Et_2O to -35 °C.

2.4.2 [Mo^{II}(^{tBu}diket)$_2$(PEt$_3$)$_2$]

In a 20 mL scintillation vial, cold (-35 °C) PEt_3 (*ca.* 1 mL) was added dropwise to K[Mo($^{t\text{Bu}}$diket)$_3$] (132 mg, 0.19 mmol, 1.0 equiv.). The resulting dark purple solution was stirred for three hours while warming to ambient temperature. All volatiles were removed under reduced pressure. The resulting dark purple residue was triturated with Et_2O (2 x 2 mL) and extracted with ^{n}pentane (*ca.* 5 mL). All volatiles were removed under reduced pressure. The obtained crude was recrystallized from ^{n}pentane at -35 °C. Anal. Calcd for $C_{34}H_{68}MoO_4P_2$, C, 58.44; H, 9.81. Found: C, 58.30; H, 9.88. μ_{eff} = 2.83(11) μ_B (Evans-method, benzene-d_6). ^{1}H NMR (benzene-d_6, 500 MHz) δ[ppm] = 20.65 (br, 2H ($^{\text{diket}}$C*H*)), 6.48 (br, 18H (PEt_3, C*H*$_3$)), 0.57 (s, 36H ($^{\text{diket}}$C*H*$_3$)), -15.96 (br, 12H (PEt_3, C*H*$_2$)). UV-Vis (0.25 mM in THF): λ_{max} [nm] ([$10^3 \cdot M^{-1} \cdot cm^{-1}$]) = 225 (10.3), 270 (15.5), 353 (8.4), 513 (5.7), 541 (9.5), 547 (8.8), 820 (12.5 (br)).

Single crystals suitable for XRD analysis were grown by cooling a saturated solution in Et_2O to -35 °C.

The following two compounds were not isolated, but only identified by single crystal XRD:

2.4.3 [Mo^{II}(^{Me}diket)$_2$(py)$_2$]

In a 25 mL scintillation vial, cold pyridine (3 mL, -35 °C) was added dropwise to solid **^{Me}Mo(II)** (20 mg). The resulting deep purple solution was stirred for one hour at ambient temperature. After filtration, slow diffusion of Et_2O at ambient temperature led to the precipitation of dark purple crystals, which were analyzed by single crystal XRD.

2.4.4 [Mo^{II}(^{Me}diket)$_2$(PEt_3)$_2$]

In a 20 mL scintillation vial, cold (-35 °C) PEt_3 (*ca.* 1 mL) was added dropwise to solid **^{Me}Mo(II)** (19 mg). The resulting deep purple solution was stirred for one hour at ambient temperature. All volatiles were removed by filtration and the obtained residue was extracted with ^{n}pentane. Recrystallization from ^{n}pentane at -35 °C led to the precipitation of deep purple crystals, which were analyzed by single crystal XRD.

2.5 Synthesis of K[$^{t\text{Bu}}$diket]

2.5.1 Synthesis of K[$^{t\text{Bu}}$diket]

In a 20 mL scintillation vial, potassium hydride (180 mg, 4.5 mmol, 0.9 equiv.) was added portion wise to a stirred solution of $^{t\text{Bu}}$diketH (920 mg, 5.0 mmol, 1.0 equiv.) in Et_2O/THF (1:1, *ca.* 20 mL) at -35 °C. The reaction mixture was stirred at for 30 minutes while slowly warming to ambient temperature. After filtration, all volatiles were removed under reduced pressure and the obtained residue was washed with ^{n}pentane (2 x 5 mL). The final solid was dried *in vacuo* affording the title compound as a colorless powder. ^{1}H NMR (THF-d_8, 500 MHz) δ[ppm] = 5.35 (s, 1H ($^{\text{diket}}$C*H*)), 1.06 (s, 18H (C*H*$_3$)). ^{13}C NMR (THF-d_8, 126 MHz) δ[ppm] = 197.8 (s, *C*=O), 86.4 (s, *C*H), 41.9 (s, C_q), 29.7 (s, *C*H$_3$).

Single crystals suitable for XRD analysis were grown by cooling a saturated solution in a mixture of THF/^{n}pentane to -35 °C.

2.6 Reaction of K[Mo($^{t\text{Bu}}$diket)$_3$] with CO_2

2.6.1 Synthesis of K$_2$[Mo($^{t\text{Bu}}$diket)$_2$($^{t\text{Bu}}$diket·$^{12}CO_2$)] (6)

In a 100 mL, J-Young valve equipped round bottom flask, Et_2O (*ca.* 20 mL) was saturated with CO_2. A solution of K[Mo($^{t\text{Bu}}$diket)$_3$] (342 mg, 0.5 mmol) in Et_2O (*ca.* 5 mL) was added by syringe and the solution was stirred at ambient temperature for 30 min. An abrupt color change from dark green to dark red/brown was observed. All volatiles were removed under reduced pressure. The obtained solid was washed with ^{n}pentane (3 x 10 mL). The ^{n}pentane washings were taken to dryness, affording a dark red/brown solid, which was identified as [Mo($^{t\text{Bu}}$diket)$_3$] (*m* = 238 mg, 0.37 mmol). The remaining solid was extracted with THF, resulting in a green solution. The THF extracts were taken to dryness (m_{crude} = 119 mg) and recrystallized by slow evaporation of THF into HMDSO.

Filtration followed by drying *in vacuo* afforded the title compound as a green powder. Yield: 80.3 mg (0.11 mmol, 22%). Anal. Calcd for $C_{34}H_{57}K_2MoO_8 \cdot (HMDSO)_{1/2}$, C, 52.33; H, 7.83. Found: C, 52.63; H, 7.51. μ_{eff} = 1.7(2) μ_B (Evans-method). ^{1}H NMR (THF-d_8, 500 MHz) δ[ppm] = 2.38 (br), 1.20 (br). UV-Vis (0.29 mM in THF, d = 2 mm): λ_{max} [nm] ([$10^3 \cdot M^{-1} \cdot cm^{-1}$]) = 233 (12.5), 284 (19.0), 372 (4.0), 682 (1.4, br).

Single crystals suitable for XRD analysis were grown by slow evaporation of a saturated solution (DME or THF) into HMDSO at ambient temperature.

2.6.2 Synthesis of K_2[Mo($^{t\text{Bu}}$diket)$_2$($^{t\text{Bu}}$diket·$^{13}CO_2$)] (^{13C}6)

The ^{13}C-labelled complex was prepared with a slightly modified procedure:

In a 100 mL, J-Young valve equipped Schlenk flask, K[Mo($^{t\text{Bu}}$diket)$_3$] (342 mg, 0.5 mmol) was dissolved in THF and degassed by three consecutive freeze-pump-thaw cycles. $^{13}CO_2$ (1 atm, 2.7 mmol, 5.4 equiv.) was condensed into the frozen reaction mixture. The reaction mixture was slowly warmed to ambient temperature and stirred for 30 min. An instant color change from dark green to brown was observed. All volatiles were removed under reduced pressure. The obtained residue was washed with ^{n}pentane (5 x 4 mL) and then extracted with THF. The green extraction solution was taken to dryness affording the title compound as a dark green solid (46 mg, 0.060 mmol, 12%).

The compound was used for reactivity studies and spectroscopic analyses without further purification.

2.6.3 Synthesis of K_2[Mo($^{t\text{Bu}}$diket)$_2$($^{t\text{Bu}}$diket·CO_2)] using Excess KC_8

To support the proposed mechanistic pathway, and to prepare the title complex with improved yields, we have evaluated the reaction of K[Mo($^{t\text{Bu}}$diket)$_3$] with CO_2 in the presence of excess reducing agent (KC_8). Here, K[Mo($^{t\text{Bu}}$diket)$_3$] was generated *in-situ* by treatment of [Mo($^{t\text{Bu}}$diket)$_3$] with KC_8 (1.1 equiv.). An additional equivalent of KC_8 was added in two steps, resulting in a significantly higher yield as compared to the original procedure with only 1 equivalent of reducing agent (Section 2.6.1).

Procedure: In a 100 mL, J-Young valve equipped round bottom flask, [Mo($^{t\text{Bu}}$diket)$_3$] (323 mg, 0.5 mmol, 1.0 equiv.) was dissolved in Et_2O (*ca.* 10 mL) and saturated with CO_2. A suspension of KC_8 (74 mg, 0.55 mmol, 1.1 equiv.) in Et_2O (*ca.* 3 mL) was added by syringe and the solution was stirred at ambient temperature for 10 min. Additional suspensions of KC_8 (41 mg, 0.3 mmol, 0.6 equiv.) in Et_2O (*ca.* 3 mL), followed by KC_8 (20 mg, 0.15 mmol, 0.3 equiv.) in Et_2O (*ca.* 3 mL), were added by syringe and the solution was stirred at ambient temperature for further 10 min. All volatiles were removed under reduced pressure. The obtained residue was washed with ^{n}pentane (3 x 10 mL). The ^{n}pentane washings were taken to dryness, affording a dark red/brown solid, which was identified as [Mo($^{t\text{Bu}}$diket)$_3$] (*m* = 162 mg, 0.25 mmo) (^{1}H NMR and UV-Vis spectroscopy). The remaining solid was extracted with THF, resulting in a green solution. The green extraction solution was taken to dryness affording the title compound as a dark green solid (184 mg, 0.24 mmol, 48%) (^{1}H NMR and UV-Vis spectroscopy).

2.7 Chemical Reduction with CS_2

2.7.1 Reduction with 5

In a 25 mL scintillation vial, CS_2 (237 μL, 4 mmol, 20 equiv.) was dissolved in THF (7 mL). A solution of K[Mo($^{t\text{Bu}}$diket)$_3$] (137 mg, 0.20 mmol, 1.0 equiv.) and 18-crown-6 (58 mg, 0.22 mmol, 1.1 equiv.), dissolved in THF (3 mL), was added and the reaction mixture was stirred at ambient temperature for one hour. An instant color change from dark green to brown/red occurred and a dark solid precipitated. All volatiles were removed under reduced pressure and the obtained dark residue was extracted with ^{n}pentane. The removal of the solvent *in vacuo* afforded [Mo($^{t\text{Bu}}$diket)$_3$] in quantitative yields (129 mg, 0.2 mmol). The remaining solid was recrystallized by slow diffusion of ^{n}pentane into a saturated solution of the crude in pyridine, affording [K(18-crown-6)]$_2$[C_2S_4] as a dark green crystalline solid (70 mg, 0.092 mmol, 92%). ^{1}H NMR (Py-d_5, 500 MHz) δ[ppm] = 3.60 (CH_2). ^{13}C NMR

(Py-d_5, 125 MHz) δ[ppm] = 269.7 (CS_2), 71.1 (CH_2). UV-Vis (0.24 mM in Py, d = 2 mm): λ_{max} [nm] ([$10^3 \cdot M^{-1} \cdot cm^{-1}$]) = 302 (10.7), 391 (19.5) 391 (7.0, sh). UV-Vis (0.15 mM in MeCN, d = 2 mm): λ_{max} [nm] ([$10^3 \cdot M^{-1} \cdot cm^{-1}$]) = 294 (11.9), 352 (17.0), 392 (5.5, sh).

2.7.2 Reduction with K^0

Potassium metal (19.5 mg, 0.5 mmol, 1.0 equiv.) and THF (5 mL) were placed into a 25 mL scintillation vial. A solution of 18-crown-6 (132 mg, 0.5 mmol, 1.0 equiv.) and CS_2 (600 μL, 10 mmol, 20.0 equiv.) in THF (5 mL) was added and the reaction was stirred at ambient temperature for 48 h. The reaction mixture was filtered by centrifugation and the remaining solid was extracted with pyridine. The crude product was obtained after removal of all volatiles under reduced pressure as a dark green solid (158 mg). Analysis by ^{13}C NMR and UV-Vis spectroscopy was used to identify and quantify the crude product. ^{13}C NMR (Py-d_5, 125 MHz) δ[ppm] = 271.7 (CS_3, CS_3^{2-}), 269.7 (CS_2, $C_2S_4^{2-}$), 70.8 (CH_2, 18-crown-6)) (Figure S1). UV-Vis (0.32 mM in Py, d = 2 mm): normalized absorption at λ = 353 nm [$mg^{-1} \cdot mL$] = 3.80 (Figure S2). Final calculated yield of $[K(18\text{-crown-6})]_2[C_2S_4]$: 0.15 mmol, 60%.

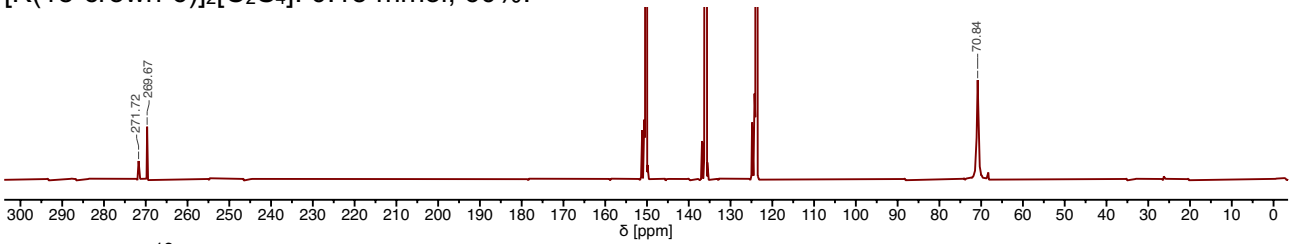

Figure S1: ^{13}C NMR spectrum in pyridine-d_5 of the crude reaction mixture (pyridine-extraction) after reduction with K^0.

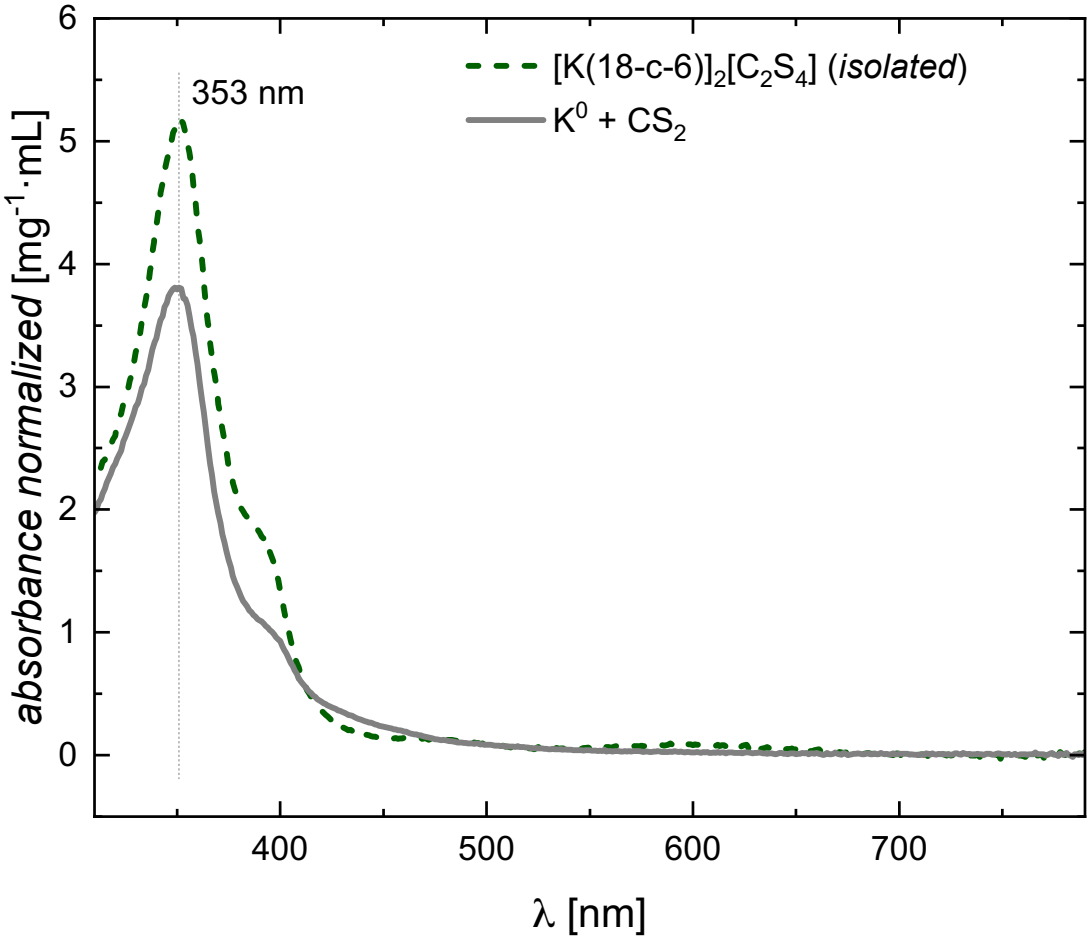

Figure S2: UV-Vis spectrum (normalized by concentration [$mg \cdot mL^{-1}$]) in pyridine of the crude reaction mixture after stoichiometric reduction with K^0 (*solid grey* line). The spectrum of isolated $[K(18\text{-crown-6})]_2[C_2S_4]$ is displayed for comparison (*dashed* line).

3. Additional Reactivity Studies

3.1 Reactivity of Chemically Reduced [Mo(^{Me}diket)$_3$] with CO_2

The dark green solid, obtained by reduction of **^{Me}Mo(III)** with KC_8 displayed limited solubility in polar solvents such as THF. Exposure of such THF solutions to excess CO_2 led to an abrupt color change from deep green to brown red, accompanied by the precipitation of a grey/green solid. The filtrate was identified by ^{1}H NMR to be **^{Me}Mo(III)**, whose formation was already indicated by the CV measurement under CO_2. However, the ^{1}H NMR spectrum (in MeCN-d_3) of the precipitated solid displayed a substantial change: while the peak of the central methine proton (C*H*) remained unchanged (δ = 41.3 ppm), the signal assigned to the six protons of the methyl groups (2x CH_3) of the ^{Me}diket ligand at δ = 126.6 ppm split into three distinct features, located at a slightly higher chemical shift (δ = 131.3, 129.7 & 127.9 ppm, see Section S3.3, Figure S7, *blue* trace). We thus suggest that the methyl groups are the reactive site of the reduced metal complex with CO_2. However, the same ^{1}H NMR pattern evolved, when **^{Me}Mo(III)** was stirred in MeOH-d_4 for 24 h (see Section S3.3, Figure S7, *orange* trace). Hence, we concluded that the characteristic signals at $\delta(^1H)$ > 125 ppm are not related to any reactivity with CO_2, but originate from deuteration of the ligand. Very likely, KC_8 acts as a base and promotes deuteration of the terminal methyl groups. Nevertheless, these experiments showed, that CO_2 reacts with the reduced (Mo(II)) species and promotes its reoxidation to Mo(III). To elucidate the CO_2-based product of this redox reaction, we further focused on ^{13}C NMR spectroscopy. Unfortunately, all THF-d_8 solutions containing paramagnetic Mo species are ^{13}C NMR silent. However, extraction of the conceivably carboxylated mixture with methanol-d_4 allowed for ^{13}C NMR analysis: two signals at $\delta(^{13}C)$ = 176.0 & 161.4 ppm appeared, both of which remarkably increased in intensity when same experiments were conducted with ^{13}C labelled $^{13}CO_2$ (see Figure S32). Combined with investigations performed on **^{tBu}Mo(II)** + CO_2, we tentatively assign these two major signals to the carboxylated ligand (K[^{Me}diket·$^{13}CO_2$]) and potassium methyl carbonate (K[$O_2{}^{13}COCD_3$]), respectively (see Section S3.3 for details).

3.2 Reactivity of K[Mo(^{tBu}diket)$_3$] with CS_2

3.2.1 In the Absence of 18-Crown-6

In a 5 mL scintillation vial, 0.2 M stock solution $^{13}CS_2$ (110 μL, 0.022 mmol, 1.1 equiv.) in THF-d_8 was diluted with THF-d_8 (0.4 mL). A solution of K[Mo(^{tBu}diket)$_3$] (13.7 mg, 0.020 mmol, 1.0 equiv.) in THF-d_8 (0.4 mL) was added dropwise and the reaction was stirred for 20 min at ambient temperature. The color changed instantly from dark green to brown/red and a solid precipitated. The reaction mixture was filtered by centrifugation. The filtrate was directly analyzed by ^{1}H NMR spectroscopy, revealing the clean formation of [Mo(^{tBu}diket)$_3$] (δ_H = 47.42 ppm (C*H*), 7.02 ppm (CH_3)) (Figure S3). The solid was dissolved in methanol-d_4 and analyzed by ^{13}C NMR spectroscopy. Potassium tetrathiooxalate ($K_2[^{13}C_2S_4]$, δ_C = 269.2 ppm)[8], potassium methyl xanthate-d_3 (K[$^{13}CS_2OCD_3$], δ_C = 234.4 ppm)[9] and potassium 2-thioxo-1,3-dithiol-4,5-dithiolate ($K_2[^{13}C_3S_5]$, δ_C = 210.5 ppm (*C*=S), 142.5 ppm (*C*S_2))[10] were identified as the main $^{13}CS_2$-derived products (Figure S4). Note that the methyl carbon of potassium methyl xanthate-d_3 is not visible in the ^{13}C NMR spectrum because it is a non-labelled carbon and fully deuterated at the same time.

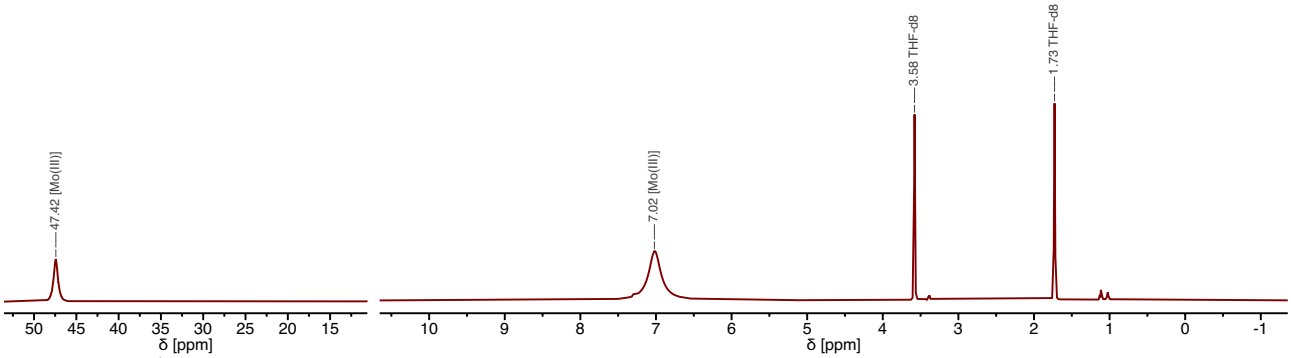

Figure S3: ^{1}H NMR spectrum of the THF-d_8 filtrate.

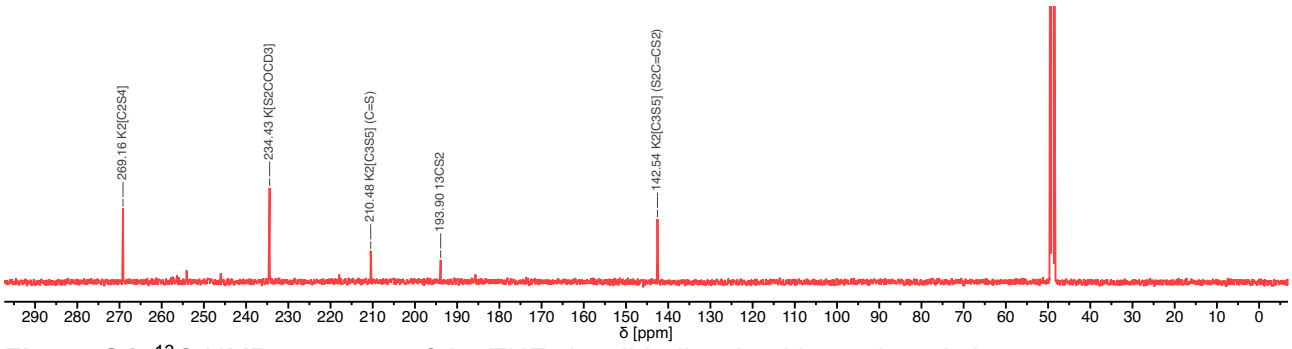

Figure S4: ^{13}C NMR spectrum of the THF-d_8 solid, dissolved in methanol-d_4.

3.2.2 In the Presence of 18-Crown-6

In a 5 mL scintillation vial, 0.2 M stock solution $^{13}CS_2$ (110 μL, 0.022 mmol, 1.1 equiv.) in THF-d_8 was diluted with THF-d_8 (0.4 mL). A solution of K[Mo($^{t\text{Bu}}$diket)$_3$] (13.7 mg, 0.020 mmol, 1.0 equiv.) and 18-crown-6 (5.3 mg, 0.020 mmol, 1.0 equiv.) in THF-d_8 (0.4 mL) was added dropwise and the reaction was stirred for 20 min at ambient temperature. The color changed instantly from dark green to brown/red and a solid precipitated. The reaction mixture was filtered by centrifugation. Both, the filtrate and the solid (dissolved in methanol-d_4) were analyzed by NMR spectroscopy.
Clean formation of [Mo($^{t\text{Bu}}$diket)$_3$] is visible from the ^{1}H NMR spectrum of the filtrate (Figure S5). Besides the new peak assigned to 18-crown-6 in the ^{13}C NMR spectrum of the solid (in methanol-d_4), the same set of signals is present as observed for the reaction in absence of 18-crown-6 (Figure S6). However, the product distribution is markedly different with a high selectivity for potassium tetrathiooxalate ([K(18-crown-6)]$_2$[$^{13}C_2S_4$], δ_C = 269.9 ppm). Note the small change in chemical shift which is due to the presence of 18-crown-6.

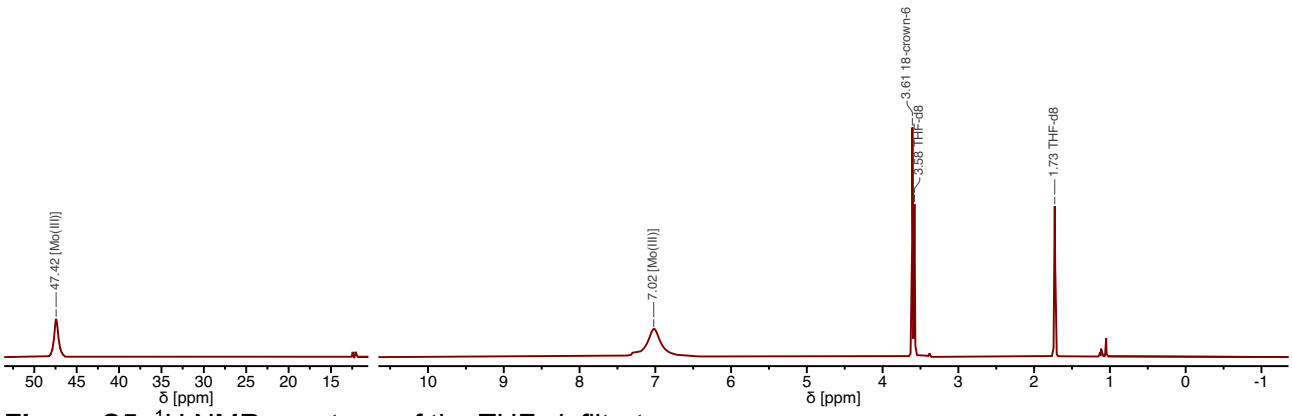

Figure S5: ^{1}H NMR spectrum of the THF-d_8 filtrate.

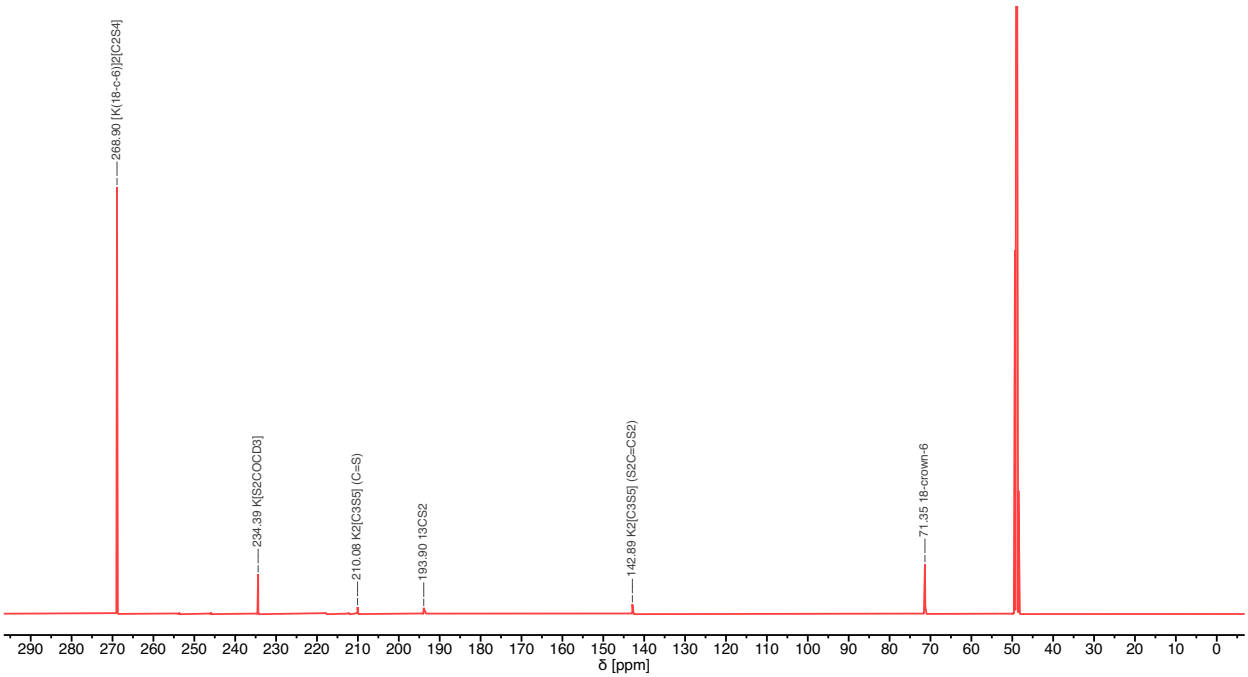

Figure S6: ^{13}C NMR spectrum of the THF-d_8 solid, dissolved in methanol-d_4.

3.3 Deuteration of [Mo(^{Me}diket)$_3$]

The terminal alpha-protons of the ^{Me}diket ligand of **1** were found to be easily exchanged both under basic and acidic conditions, as visible by a decreased integral (as well as minor change in chemical shift) of the corresponding terminal alpha-protons in ^{1}H NMR spectroscopy. Considerable deuteration of the ligand was observed when **1** was treated with [TBA]$_2$[oxalate] (in MeCN-d_3) or when it was stirred in methanol-d_4 for 24 h (Figure S7). Strikingly, the same effect of ligand deuteration was evident in reactivity tests of chemically reduced **1** (*e.g.* with KC_8) with CO_2 (see Section S3.1).

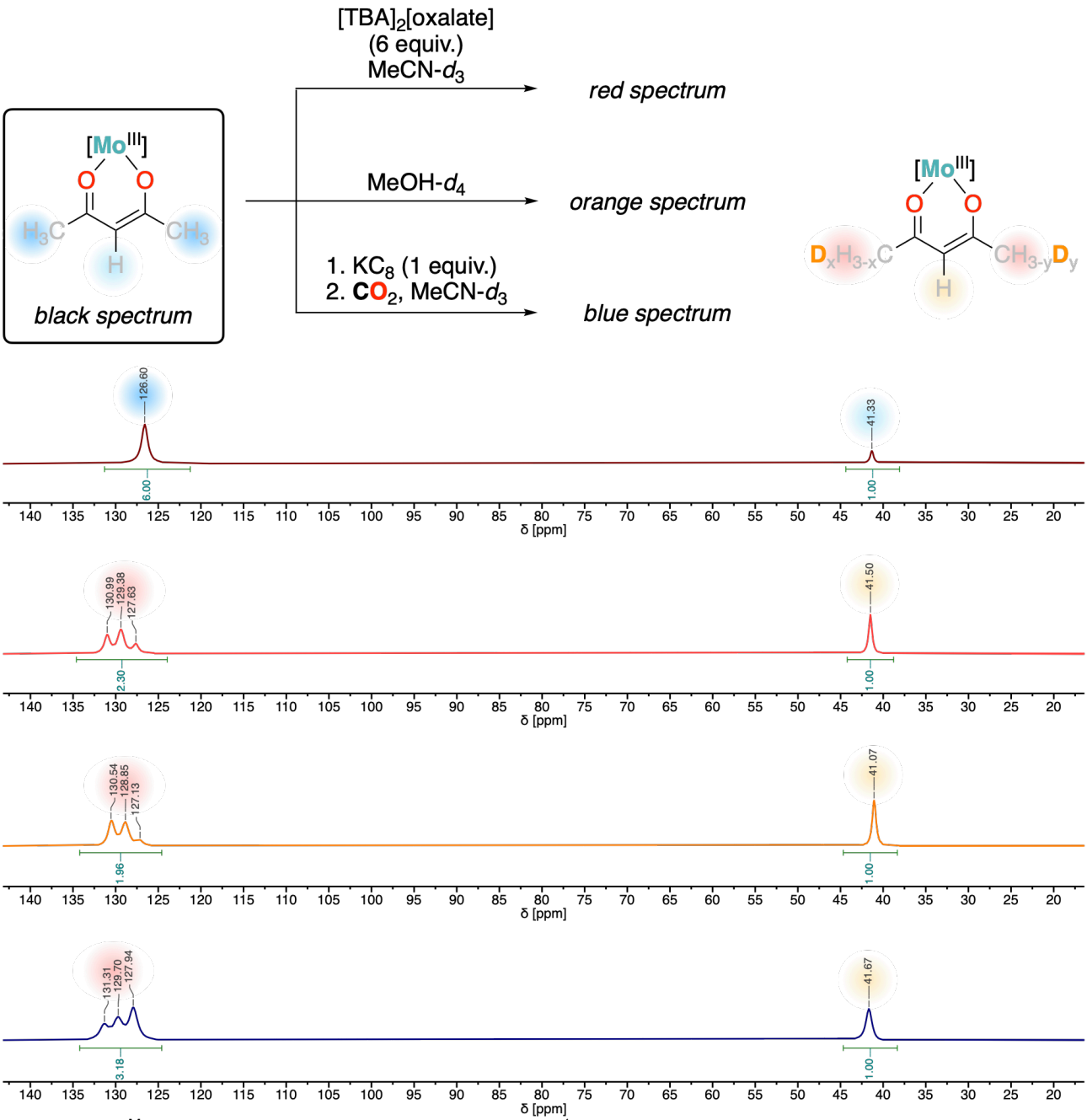

Figure S7: ^{Me}diket ligand deuteration monitored by ^{1}H NMR spectroscopy: **1** in MeCN-d_3 (*black*, *top*), **1** + [TBA]$_2$[oxalate] in MeCN-d$_3$ stirred for 24 h (*red*), **1** in methanol-d_4, stirred for 24 h (*orange*) and **1** reduced with KC_8 under CO_2 in MeCN-d_3 (*blue*).

3.4 Reactivity Studies of 6

In a series of reactivity studies, we have aimed at isolating the free carboxylated ligand [$^{t\text{Bu}}$diket·CO_2]$^-$. This turned out to be challenging, due to the known lability of the carboxyl group which is located in β-position to two carbonyls and thus prone to decarboxylation.[11] On the other hand, most reactivity tests of **6** resulted in the formation of **3** (as gauged by ^{1}H NMR), suggesting the feasibility of a closed synthetic cycle for CO_2 incorporation into a β-diketone ligand. Overall, we found that an oxidizing agent is required to induce de-coordination of the carboxylated ligand. For example, addition of $^{t\text{Bu}}$diketH to **$^{13\text{C}}$6**, cleanly afforded **3**, which can be isolated by extraction with ^{n}pentane (Scheme S1, *left* arrow). Compared to the completely ^{13}C NMR-silent **$^{13\text{C}}$6**, two signals of comparable intensity evolved at $\delta(^{13}\text{C})$ = 126 ppm and $\delta(^{13}\text{C})$ = 171.1 ppm over a period of 8 h (see Figure S27). While the first signal matches to free $^{13}CO_2$, the second one is tentatively assigned to the C_3-carboxylated $^{t\text{Bu}}$diket ligand. As a control experiment, exposure of independently prepared K[$^{t\text{Bu}}$diket] to $^{13}CO_2$ generates a signal in the ^{13}C NMR spectrum at the very same chemical shift ($\delta(^{13}\text{C})$ = 171.1 ppm, see Scheme S1 (*bottom left*) and Figure S28).

However, when dissolving **$^{13\text{C}}$6** in methanol-d_4, a single peak at δ = 161.5 ppm evolved (see Scheme S1, *right* arrow and Figure S29), reminiscent of the experimental outcome with the $^{\text{Me}}$diket-supported Mo-complex. This chemical shift is in very good agreement with literature, suggesting the formation of potassium methyl carbonate (K[OCO_2Me]).[12] The product identity was further evidenced by single crystal XRD: Crystals of K[OCO_2Me] were grown by slow by slow diffusion of diethyl ether into a saturated solution in methanol. In addition, no $^{13}CO_2$ evolution was observed, supporting the hypothesis above. While considerable amounts of **3** were observed by ^{1}H NMR, a new set of broad signals at δ = 42.27, 7.04, and 6.76 ppm appeared in the ^{1}H NMR spectrum (Figure S30). After two days, dark red crystals precipitated out of the methanol solution, which were identified as [Mo$^{\text{III}}$($^{t\text{Bu}}$diket)$_2$(μ-OMe)]$_2$ by single-crystal XRD. Stoichiometric amounts of H_2 were detected by GC-TCD analysis of the headspace. We therefore propose that methanol acts in two ways; first it displaces the carboxylate group attached to [$^{t\text{Bu}}$diket·CO_2]$^-$ under the formation of potassium methyl carbonate, while it also serves as an oxidizing agent generating H_2 and KOMe, which explains the formation of **3**. A slow reaction between **3** and KOMe further lead to the dimeric complex [Mo$^{\text{III}}$($^{t\text{Bu}}$diket)$_2$(μ-OMe)]$_2$ and K[$^{t\text{Bu}}$diket]. Independent reactivity tests of **3** + KOMe led to identical ^{1}H NMR traces.

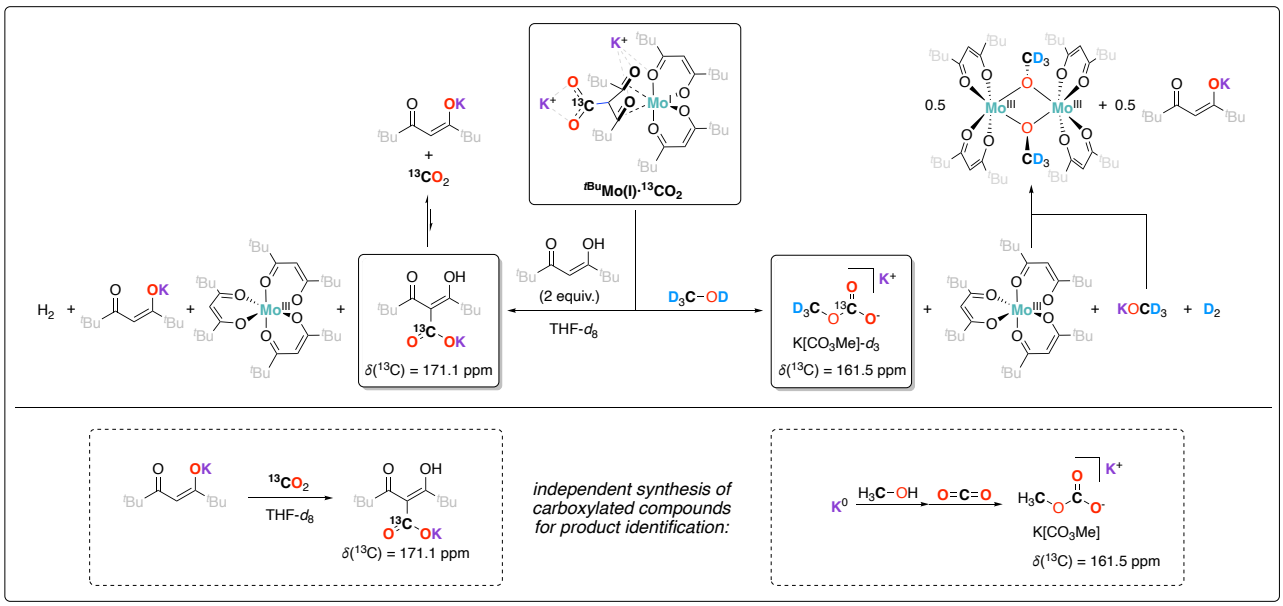

Scheme S1: Attempts to isolate and valorize the carboxylated ligand [$^{t\text{Bu}}$diket·CO_2]$^-$ of **6**.

3.5 Reactivity of K[$^{t\text{Bu}}$diket] with CS_2

Analogously to the reactivity with CO_2, thiocarboxylation of K[$^{t\text{Bu}}$diket] upon addition of excess $^{13}CS_2$ was observed by ^{13}C NMR spectroscopy (K[$^{t\text{Bu}}$diket·$^{13}CS_2$], δ_C = 249.3 ppm, Figure S8). However, it is noteworthy that such a signal has never been observed in any reaction of reduced molybdenum complex with CS_2, likely due to its lower stability and shorter lifetime.

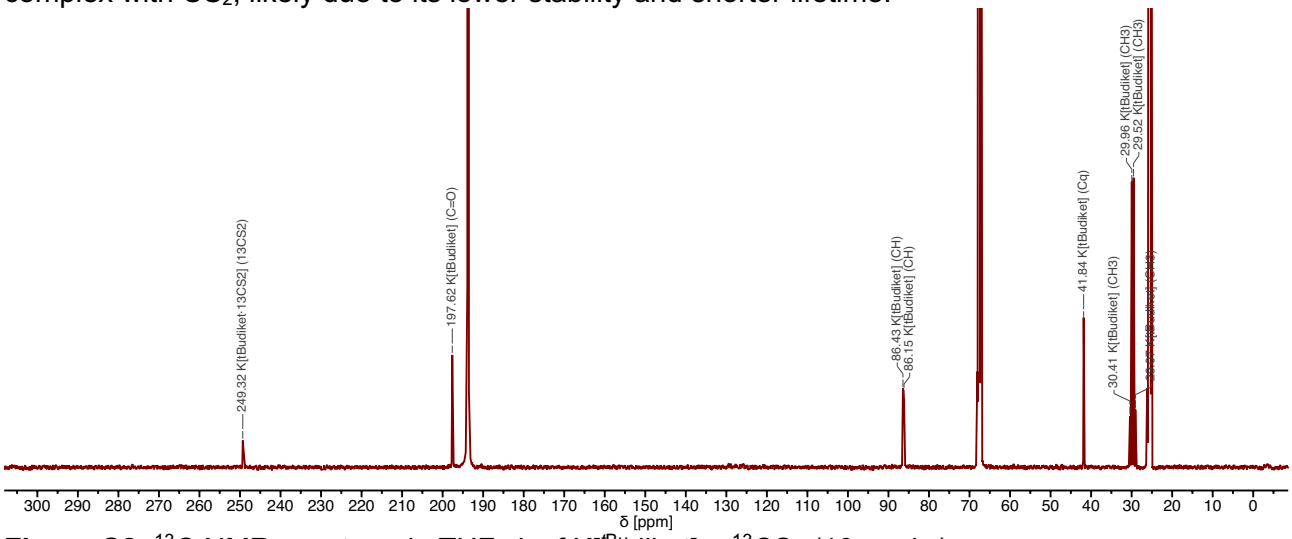

Figure S8: ^{13}C NMR spectrum in THF-d_8 of K[$^{t\text{Bu}}$diket] + $^{13}CS_2$ (10 equiv.).

Of important note here, is that addition of methanol-d_4 led to the disappearance of the signal at δ_C = 249.3 ppm, and the emergence of a strong resonance at δ_C = 233.8 ppm, assigned to potassium methylxanthate-d_3 (K[$^{13}CS_2OCD_3$], Figure S9).

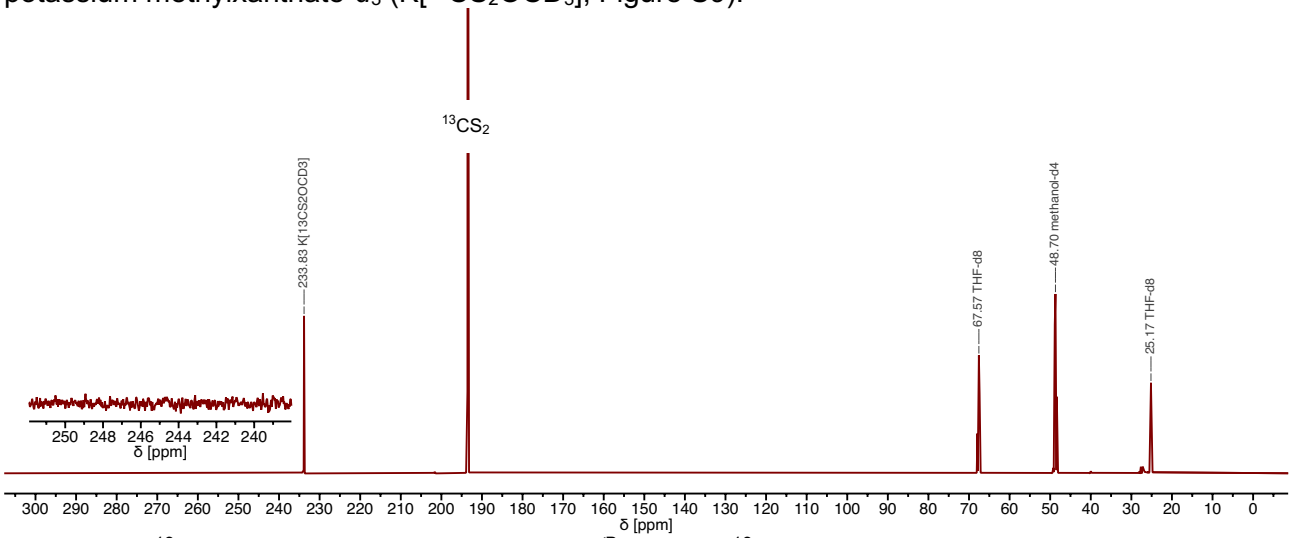

Figure S9: ^{13}C NMR spectrum in THF-d_8 of K[$^{t\text{Bu}}$diket] + $^{13}CS_2$ (10 equiv.) after addition of methanol-d_4.

3.5.1 Procedure

In a 5 mL scintillation vial, K[$^{t\text{Bu}}$diket] (6.0 mg, 0.02 mmol, 1.0 equiv.) was dissolved in THF-d_8 (600 μL). $^{13}CS_2$ (12 μL, 0.20 mmol, 10 equiv.) was added and the resulting colorless reaction mixture was stirred for 1 h at ambient temperature. The solution was transferred to an NMR tube and analyzed by ^{13}C NMR spectroscopy (Figure S8). Methanol-d_4 (600 μL) was added and the sample was again analyzed by ^{13}C NMR spectroscopy (Figure S9).

4. XRD Data

4.1 General Procedure

Single crystals of structurally characterized compounds were grown as described in Section S2. Suitable crystals were selected under the atmosphere of an argon filled glove box and tip-mounted on a Rigaku R-AXIS SPIDER IP or Bruker APEX-II CCD diffractometer. The crystals were kept at 100 K during data collection. Using Olex2,[13] the structure was solved with the ShelXT[14] structure solution program using Intrinsic Phasing and refined with the SHELXL[15] refinement package using Least Squares minimization.

4.2 Refinement Details

Table S5: Refinement details of crystal structures of ligand potassium salt.

Compound	**K(thf)[^{tBu}diket]**
Empirical formula	$C_{90}H_{161.64}K_6O_{18}$
Formula weight	1766.42
Temperature [K]	100.15
Crystal system	triclinic
Space group	P-1
a [Å]	20.6538(2)
b [Å]	25.2668(2)
c [Å]	25.4854(2)
α [°]	119.0280(10)
β [°]	90.1910(10)
γ [°]	112.3480(10)
Volume [Å^3]	10461.43(19)
Z	4
ρ_{calc}g [cm^3]	1.122
μ [mm^{-1}]	2.679
F(000)	3839.0
Crystal size [mm^3]	0.471 × 0.164 × 0.079
Radiation	Cu Kα (λ = 1.54184)
2Θ range for data collection [°]	4.446 to 136.502
Index ranges	-24 ≤ h ≤ 24, -30 ≤ k ≤ 30, -26 ≤ l ≤ 30
Reflections collected	142028
Independent reflections	38218 [R_{int} = 0.0780, R_{sigma} = 0.0603]
Data/restraints/parameters	38218/3048/2670
Goodness-of-fit on F^2	1.063
Final R indexes [I>=2σ (I)]	R_1 = 0.0950, wR_2 = 0.2753
Final R indexes [all data]	R_1 = 0.1187, wR_2 = 0.3002
Largest diff. peak/hole [e Å^{-3}]	1.28/-0.96

Table S6: Refinement details of crystal structures of Mo(IV) complexes .

Compound	$[Mo(^{Me}diket)_3]PF_6$	$[Mo(^{tBu}diket)_3]PF_6$
Empirical formula	$C_{30}H_{42}F_{12}Mo_2O_{12}P_2$	$C_{33}H_{57}O_6F_6PMo$
Formula weight	1076.45	790.69
Temperature [K]	100.00	100.00
Crystal system	trigonal	monoclinic
Space group	P-31c	$P2_1/n$
a [Å]	10.6761(3)	19.1980(7)
b [Å]	10.6761(3)	9.9251(3)
c [Å]	10.3685(4)	21.1389(7)
α [°]	90	90
β [°]	90	99.950(2)
γ [°]	120	90
Volume [$Å^3$]	1023.46(7)	3967.3(2)
Z	1	4
$\rho_{calc}g$ [cm^3]	1.747	1.324
μ [mm^{-1}]	0.801	0.436
F(000)	540.0	1656.0
Crystal size [mm^3]	0.964 × 0.246 × 0.245	0.444 × 0.153 × 0.122
Radiation	MoKα (λ = 0.71073)	MoKα (λ = 0.71073)
2Θ range for data collection [°]	5.904 to 52.732	4.546 to 50.668
Index ranges	-12 ≤ h ≤ 13, -13 ≤ k ≤ 11, -12 ≤ l ≤ 11	-23 ≤ h ≤ 23, -11 ≤ k ≤ 11, -25 ≤ l ≤ 25
Reflections collected	4046	61479
Independent reflections	703 [R_{int} = 0.0138, R_{sigma} = 0.0095]	7234 [R_{int} = 0.0546, R_{sigma} = 0.0285]
Data/restraints/ parameters	703/19/76	7234/0/442
Goodness-of-fit on F^2	1.076	1.019
Final R indexes [I>=2σ (I)]	R_1 = 0.0161, wR_2 = 0.0373	R_1 = 0.0364, wR_2 = 0.1179
Final R indexes [all data]	R_1 = 0.0183, wR_2 = 0.0396	R_1 = 0.0473, wR_2 = 0.1293
Largest diff. peak/hole [e $Å^{-3}$]	0.20/-0.31	1.30/-0.78

Table S7: Refinement details of crystal structures of Mo(III) complexes.

Compound	**[Mo(^{tBu}diket)$_3$]**	**[Mo(^{tBu}diket)$_2$(μ^2-OMe)]$_2$**
Empirical formula	$C_{33}H_{57}MoO_6$	$C_{46}H_{82}Mo_2O_{10}$
Formula weight	645.72	986.99
Temperature [K]	100	100.00
Crystal system	monoclinic	monoclinic
Space group	C2/c	$P2_1/n$
a [Å]	20.0596(9)	15.4923(5)
b [Å]	17.5220(8)	10.7879(4)
c [Å]	23.4507(11)	16.4481(5)
α [°]	90	90
β [°]	112.0991(12)	111.4060(10)
γ [°]	90	90
Volume [Å^3]	7637.0(6)	2559.33(15)
Z	8	2
ρ_{calc}g [cm^3]	1.123	1.281
μ [mm^{-1}]	0.378	0.540
F(000)	2760.0	1044.0
Crystal size [mm^3]	0.314 × 0.145 × 0.116	0.15 × 0.11 × 0.08
Radiation	MoKα (λ = 0.71073)	MoKα (λ = 0.71073)
2Θ range for data collection [°]	3.194 to 52.744	4.532 to 52.762
Index ranges	-25 ≤ h ≤ 25, -21 ≤ k ≤ 21, -29 ≤ l ≤ 29	-19 ≤ h ≤ 19, -13 ≤ k ≤ 13, -20 ≤ l ≤ 20
Reflections collected	66874	66144
Independent reflections	7831 [R_{int} = 0.0510, R_{sigma} = 0.0291]	5247 [R_{int} = 0.0422, R_{sigma} = 0.0171]
Data/restraints/ parameters	7831/528/481	5247/30/275
Goodness-of-fit on F^2	1.004	1.075
Final R indexes [I>=2σ (I)]	R_1 = 0.0336, wR_2 = 0.0784	R_1 = 0.0528, wR_2 = 0.1326
Final R indexes [all data]	R_1 = 0.0696, wR_2 = 0.0931	R_1 = 0.0635, wR_2 = 0.1458
Largest diff. peak/hole [e Å^{-3}]	0.24/-0.28	1.58/-0.65

Table S8: Refinement details of crystal structures of bis(^{R}diket) Mo(II) complexes.

Compound	**[Mo(^{Me}diket)$_2$(py)$_2$]**	**[Mo(^{Me}diket)$_2$(PEt$_3$)$_2$]**	**[Mo(^{tBu}diket)$_2$(py)$_2$]**	**[Mo(^{tBu}diket)$_2$(PEt$_3$)$_2$]**
Empirical formula	$C_{20}H_{24}MoN_2O_4$	$C_{22}H_{44}MoO_4P_2$	$C_{32}H_{48}MoN_2O_4$	$C_{34}H_{68}MoO_4P_2$
Formula weight	452.35	530.45	620.66	698.76
Temperature [K]	100.00	100.00	100.01(10)	100.01
Crystal system	monoclinic	monoclinic	triclinic	monoclinic
Space group	$P2_1/c$	$P2_1/n$	P-1	$P2_1/c$
a [Å]	7.92030(10)	11.1689(7)	9.6659(4)	9.9377(16)
b [Å]	14.2390(2)	9.9499(7)	9.8520(6)	11.7816(19)
c [Å]	9.1048(2)	12.3849(8)	10.9941(8)	16.636(3)
α [°]	90	90	115.997(7)	90
β [°]	110.561(2)	102.858(2)	102.344(5)	106.552(2)
γ [°]	90	90	104.827(4)	90
Volume [Å^3]	961.40(3)	1341.81(15)	843.25(10)	1867.1(5)
Z	2	2	1	2
ρ_{calc}g [cm^3]	1.563	1.313	1.222	1.243
μ [mm^{-1}]	0.710	0.631	0.423	0.470
F(000)	464.0	560.0	328.0	752.0
Crystal size [mm^3]	0.291 × 0.211 × 0.172	0.979 × 0.762 × 0.516	0.4 × 0.258 × 0.12	0.241 × 0.168 × 0.148
Radiation	MoKα (λ = 0.71073)	MoKα (λ = 0.71073)	Mo Kα (λ = 0.71073)	MoKα (λ = 0.71073)
2Θ range for data collection [°]	5.494 to 65.292	6.044 to 61.012	4.446 to 50.7	4.276 to 50.692
Index ranges	-10 ≤ h ≤ 11, -20 ≤ k ≤ 21, -13 ≤ l ≤ 12	-15 ≤ h ≤ 12, -14 ≤ k ≤ 14, -17 ≤ l ≤ 17	-11 ≤ h ≤ 11, -11 ≤ k ≤ 10, 0 ≤ l ≤ 13	-11 ≤ h ≤ 11, -13 ≤ k ≤ 13, -19 ≤ l ≤ 20
Reflections collected	5918	27173	3100	8132
Independent reflections	3175 [R_{int} = 0.0180, R_{sigma} = 0.0276]	4044 [R_{int} = 0.0175, R_{sigma} = 0.0134]	3100 [R_{int} = ?, R_{sigma} = 0.0387]	3341 [R_{int} = 0.0660, R_{sigma} = 0.0867]
Data/restraints/ parameters	3175/0/172	4044/0/221	3100/0/185	3341/0/196
Goodness-of-fit on F^2	1.062	1.166	1.129	0.996
Final R indexes [I>=2σ (I)]	R_1 = 0.0231, wR_2 = 0.0543	R_1 = 0.0197, wR_2 = 0.0461	R_1 = 0.0391, wR_2 = 0.1027	R_1 = 0.0462, wR_2 = 0.0940
Final R indexes [all data]	R_1 = 0.0273, wR_2 = 0.0561	R_1 = 0.0210, wR_2 = 0.0474	R_1 = 0.0403, wR_2 = 0.1035	R_1 = 0.0717, wR_2 = 0.1041
Largest diff. peak/hole [e Å^{-3}]	0.48/-0.61	0.44/-0.57	2.15/-0.85	0.72/-0.50

Table S9: Refinement details of crystal structures of reduced $^{t\text{Bu}}$diket-supported complexes. [a] 0.5 C_6H_6 and 2 ^{n}pentane molecules co-crystallized. [b] 4 THF molecules co-crystallized.

Compound	$K(MeCN)_2[Mo(^{tBu}diket)_3]$	$K(^{tBu}diket)[Mo(^{tBu}diket)_3]$	$K(15\text{-}c\text{-}5)[Mo(^{tBu}diket)_3]$	$K(18\text{-}c\text{-}6)[Mo(^{tBu}diket)_3]$[b]
Empirical formula	$C_{37}H_{63}KMoN_2O_6$	$C_{44}H_{76}K_2MoO_8$	$C_{94}H_{165}K_2Mo_2O_{22}$	$C_{94}H_{169}K_2Mo_2O_{22}$
Formula weight	766.93	907.18	1917.33	1921.36
Temperature [K]	100.00	100.00(10)	100.00(10)	100.0
Crystal system	monoclinic	monoclinic	monoclinic	monoclinic
Space group	C2/c	$P2_1/n$	I2/a	$P2_1/n$
a [Å]	19.8789(10)	20.7616(8)	42.1214(5)	12.6846(5)
b [Å]	19.2756(9)	11.3642(4)	17.67080(10)	34.4038(13)
c [Å]	21.7938(9)	21.1142(8)	32.4322(4)	24.7112(10)
α [°]	90	90	90	90
β [°]	98.043(2)	90.651(3)	112.111(2)	102.3150(10)
γ [°]	90	90	90	90
Volume [Å^3]	8268.8(7)	4981.3(3)	22364.6(5)	10535.8(7)
Z	8	4	8	4
ρ_{calc}g [cm^3]	1.232	1.210	1.139	1.211
μ [mm^{-1}]	0.459	0.475	2.978	0.380
F(000)	3264.0	1936.0	8216.0	4124.0
Crystal size [mm^3]	0.774 × 0.278 × 0.136	0.31 × 0.148 × 0.069	0.219 × 0.114 × 0.075	0.348 × 0.32 × 0.19
Radiation	MoKα (λ = 0.71073)	Mo Kα (λ = 0.71073)	Cu Kα (λ = 1.54184)	MoKα (λ = 0.71073)
2Θ range for data collection [°]	4.562 to 52.746	3.924 to 50.698	5.802 to 160.832	4.65 to 52.746
Index ranges	-24 ≤ h ≤ 24, -24 ≤ k ≤ 24, -27 ≤ l ≤ 24	-25 ≤ h ≤ 25, -13 ≤ k ≤ 13, -25 ≤ l ≤ 25	-51 ≤ h ≤ 53, -13 ≤ k ≤ 22, -40 ≤ l ≤ 41	-15 ≤ h ≤ 15, -43 ≤ k ≤ 43, -30 ≤ l ≤ 30
Reflections collected	73569	61816	85319	159478
Independent reflections	8461 [R_{int} = 0.0255, R_{sigma} = 0.0141]	9111 [R_{int} = 0.0759, R_{sigma} = 0.0650]	23757 [R_{int} = 0.0366, R_{sigma} = 0.0342]	21530 [R_{int} = 0.0606, R_{sigma} = 0.0330]
Data/restraints/ parameters	8461/0/466	9111/112/573	23757/253/1121	21530/355/1130
Goodness-of-fit on F^2	1.048	1.052	1.029	1.113
Final R indexes [I>=2σ (I)]	R_1 = 0.0200, wR_2 = 0.0493	R_1 = 0.0539, wR_2 = 0.1040	R_1 = 0.0572, wR_2 = 0.1602	R_1 = 0.0632, wR_2 = 0.1496
Final R indexes [all data]	R_1 = 0.0231, wR_2 = 0.0507	R_1 = 0.0665, wR_2 = 0.1110	R_1 = 0.0670, wR_2 = 0.1674	R_1 = 0.0778, wR_2 = 0.1587
Largest diff. peak/hole [e Å^{-3}]	0.62/-0.63	1.50/-0.86	1.41/-1.14	1.60/-1.04

Table S10: Refinement details of crystal structures of formal Mo(I) complexes.

Compound	$K(thf)_x[Mo(^{tBu}diket)_2(^{tBu}diket{\cdot}CO_2)]$	$K_2(dme)[Mo(^{tBu}diket)_2(^{tBu}diket{\cdot}CO_2)]$	$K[Mo(^{tBu}diket)_2(^{tBu}diket{\cdot}H)]$
Empirical formula	$C_{90}H_{156}K_4Mo_2O_{21.5}$	$C_{38}H_{66}K_2MoO_{10}$	$C_{33}H_{58}KMoO_6$
Formula weight	1930.42	857.04	685.83
Temperature [K]	100.00(10)	100.00(10)	100.00(10)
Crystal system	triclinic	triclinic	monoclinic
Space group	P-1	P-1	$P2_1/c$
a [Å]	14.7678(7)	20.3517(4)	22.9432(2)
b [Å]	18.5557(8)	21.0677(3)	24.0368(2)
c [Å]	20.0580(12)	21.2065(4)	20.9977(2)
α [°]	99.741(4)	78.2300(10)	90
β [°]	106.208(5)	83.745(2)	111.0590(10)
γ [°]	94.304(4)	87.352(2)	90
Volume [$Å^3$]	5158.3(5)	8845.7(3)	10806.42(18)
Z	2	8	12
ρ_{calc}g [cm^3]	1.243	1.287	1.265
μ [mm^{-1}]	3.937	4.513	4.312
F(000)	2056.0	3632.0	4380.0
Crystal size [mm^3]	0.11 × 0.1 × 0.08	0.13 × 0.09 × 0.03	0.154 × 0.1 × 0.064
Radiation	Cu Kα (λ = 1.54184)	Cu Kα (λ = 1.54184)	Cu Kα (λ = 1.54184)
2Θ range for data collection [°]	6.286 to 136.502	4.37 to 136.5	5.82 to 160.892
Index ranges	-17 ≤ h ≤ 17, -20 ≤ k ≤ 22, -24 ≤ l ≤ 24	-24 ≤ h ≤ 24, -25 ≤ k ≤ 22, -25 ≤ l ≤ 25	-14 ≤ h ≤ 28, -30 ≤ k ≤ 30, -26 ≤ l ≤ 26
Reflections collected	55359	125820	106958
Independent reflections	18580 [R_{int} = 0.1290, R_{sigma} = 0.1176]	32365 [R_{int} = 0.1038, R_{sigma} = 0.0809]	23142 [R_{int} = 0.0407, R_{sigma} = 0.0348]
Data/restraints/ parameters	18580/173/1109	32365/671/1839	23142/18/1247
Goodness-of-fit on F^2	1.034	1.049	1.072
Final R indexes [I>=2σ (I)]	R_1 = 0.1055, wR_2 = 0.2685	R_1 = 0.0955, wR_2 = 0.2431	R_1 = 0.0529, wR_2 = 0.1406
Final R indexes [all data]	R_1 = 0.1476, wR_2 = 0.2990	R_1 = 0.1253, wR_2 = 0.2623	R_1 = 0.0603, wR_2 = 0.1453
Largest diff. peak/hole [e $Å^{-3}$]	1.32/-1.67	1.80/-1.58	0.62/-1.35

5. NMR Spectroscopy

5.1 NMR Spectra of Isolated Metal Complexes

5.1.1 Mo(IV) Complexes

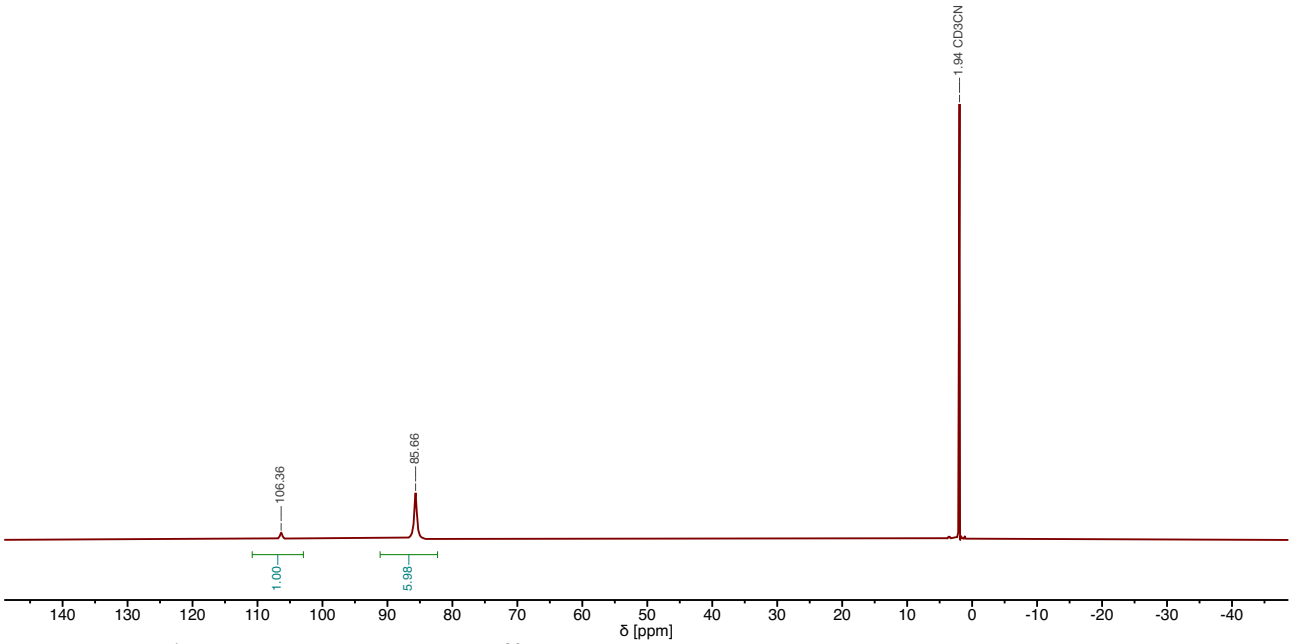

Figure S10: ^{1}H NMR spectrum of [Mo(^{Me}diket)$_3$]PF$_6$ in MeCN-d_3.

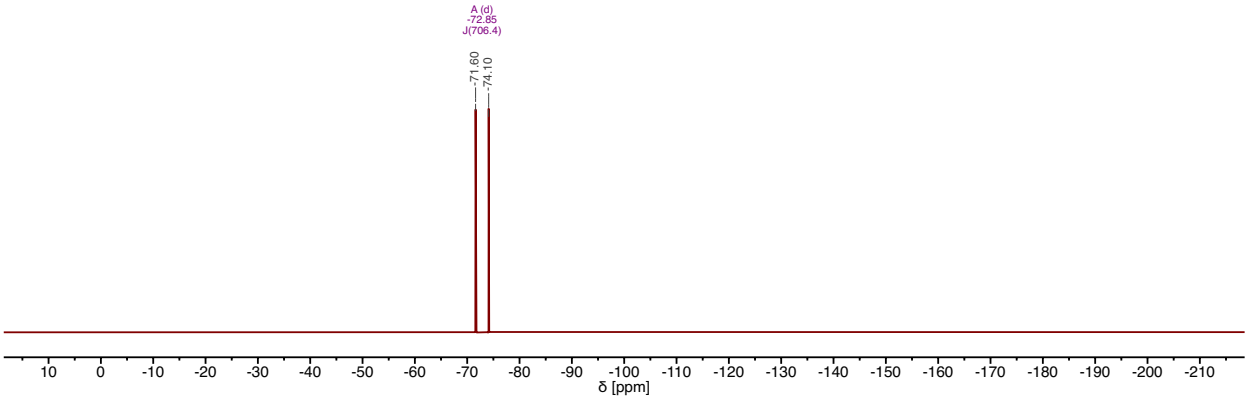

Figure S11: ^{19}F NMR spectrum of [Mo(^{Me}diket)$_3$]PF$_6$ in MeCN-d_3.

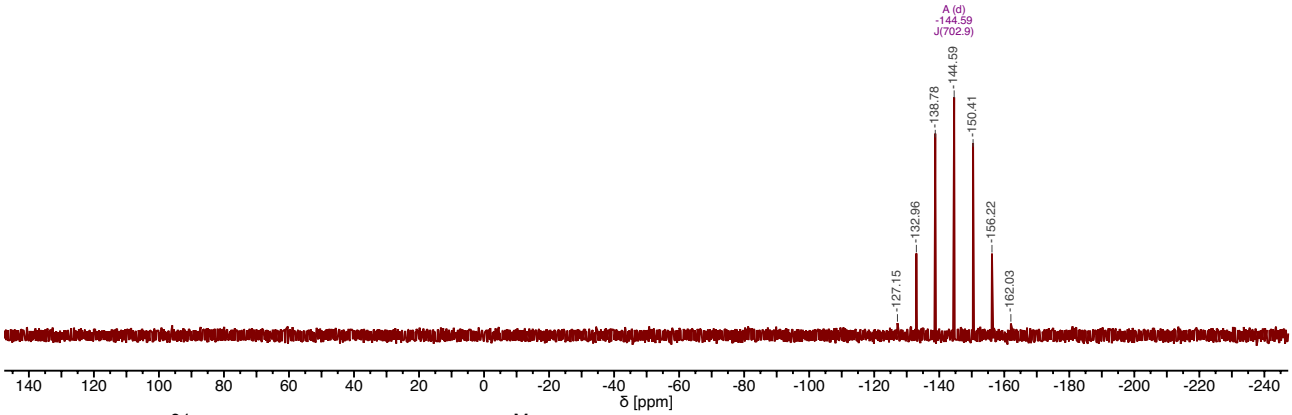

Figure S12: ^{31}P NMR spectrum of [Mo(^{Me}diket)$_3$]PF$_6$ in MeCN-d_3.

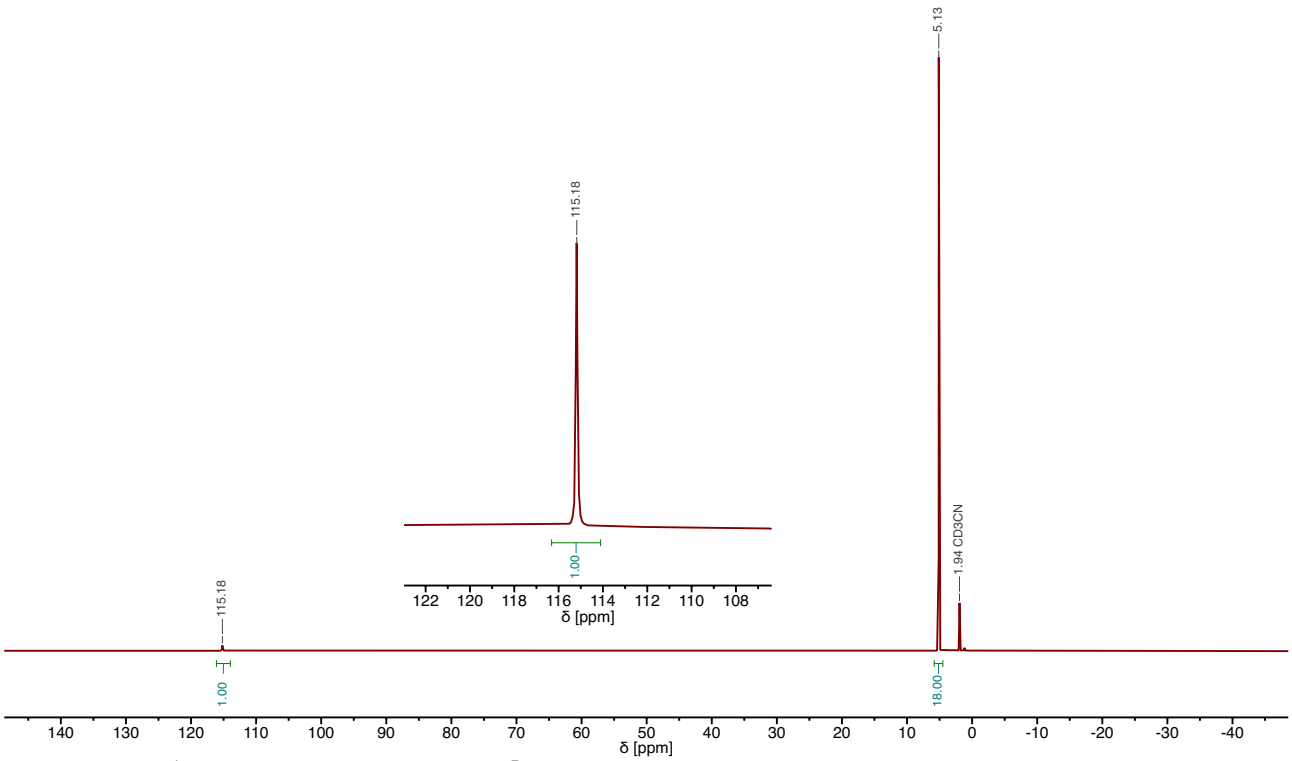

Figure S13: ^{1}H NMR spectrum of [Mo($^{t\text{Bu}}$diket)$_3$]PF_6 in MeCN-d_3.

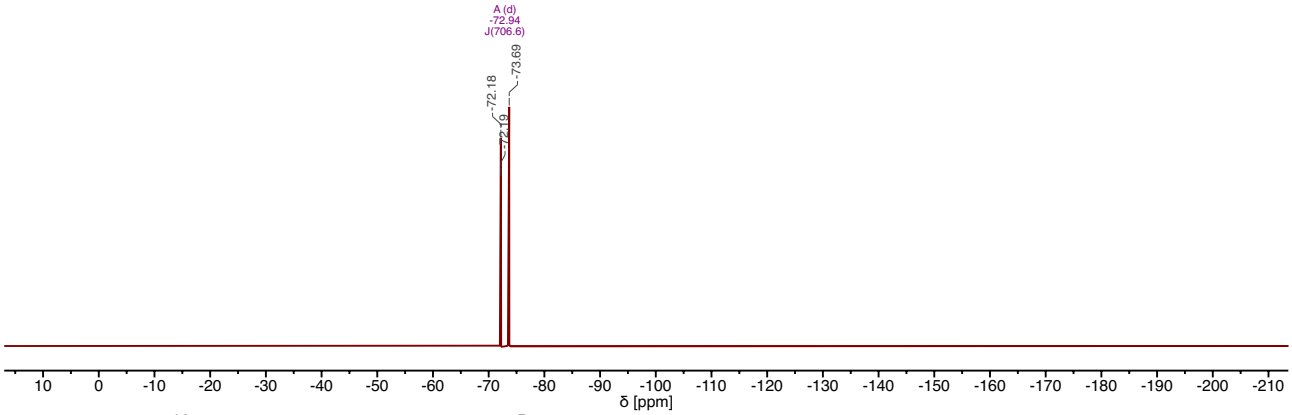

Figure S14: ^{19}F NMR spectrum of [Mo($^{t\text{Bu}}$diket)$_3$]PF_6 in MeCN-d_3.

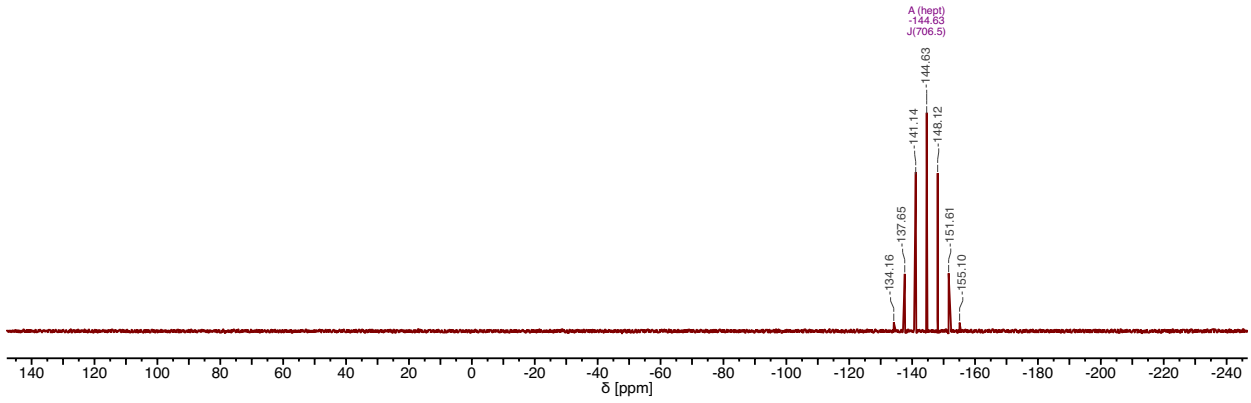

Figure S15: ^{31}P NMR spectrum of [Mo($^{t\text{Bu}}$diket)$_3$]PF_6 in MeCN-d_3.

5.1.2 Mo(III) Complexes

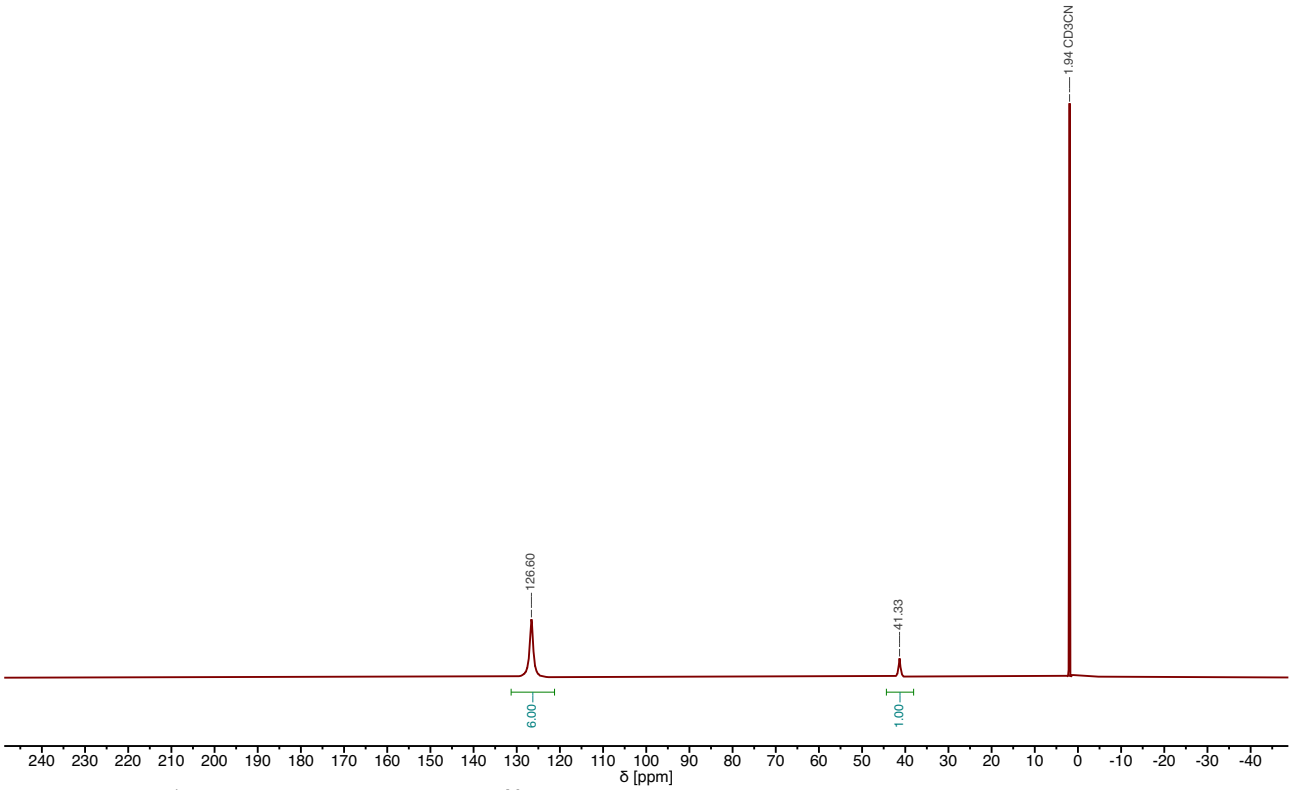

Figure S16: ^{1}H NMR spectrum of [Mo(^{Me}diket)$_3$] in MeCN-d_3.

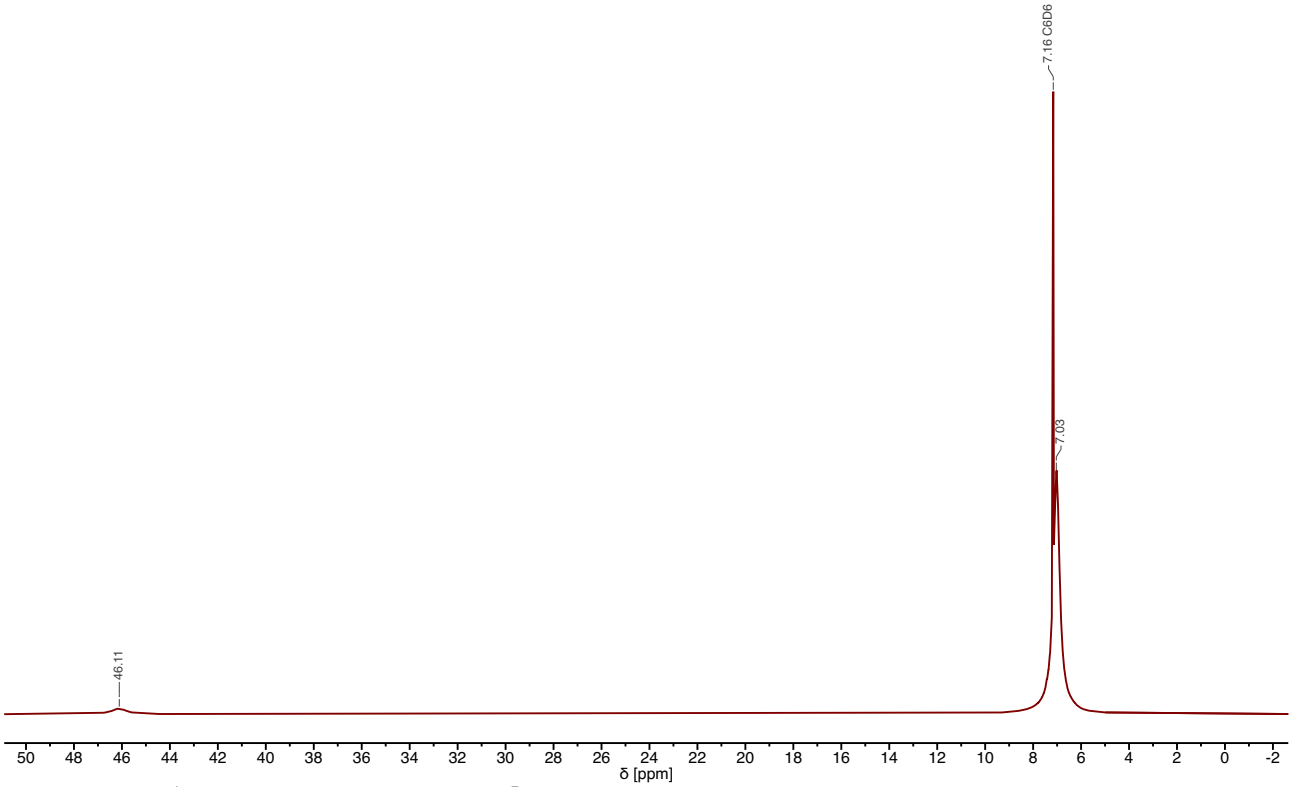

Figure S17: ^{1}H NMR spectrum of [Mo(^{tBu}diket)$_3$] in benzene-d_6.

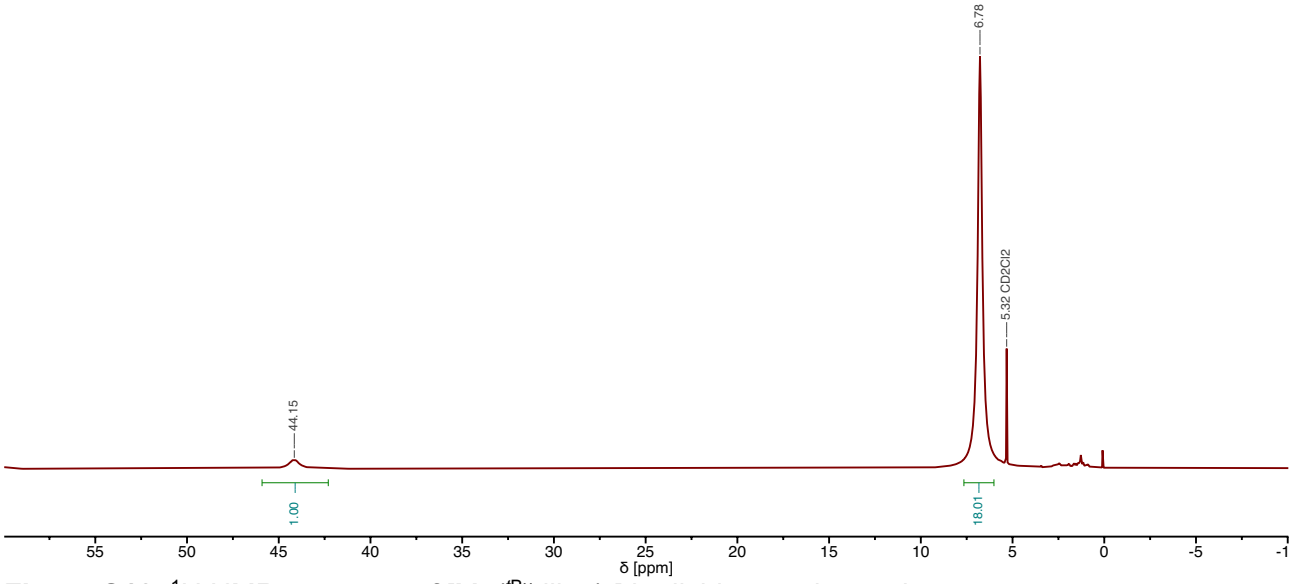

Figure S18: ^{1}H NMR spectrum of [Mo($^{t\text{Bu}}$diket)$_3$] in dichloromethane-d_2.

5.1.3 Mo(II) Complexes

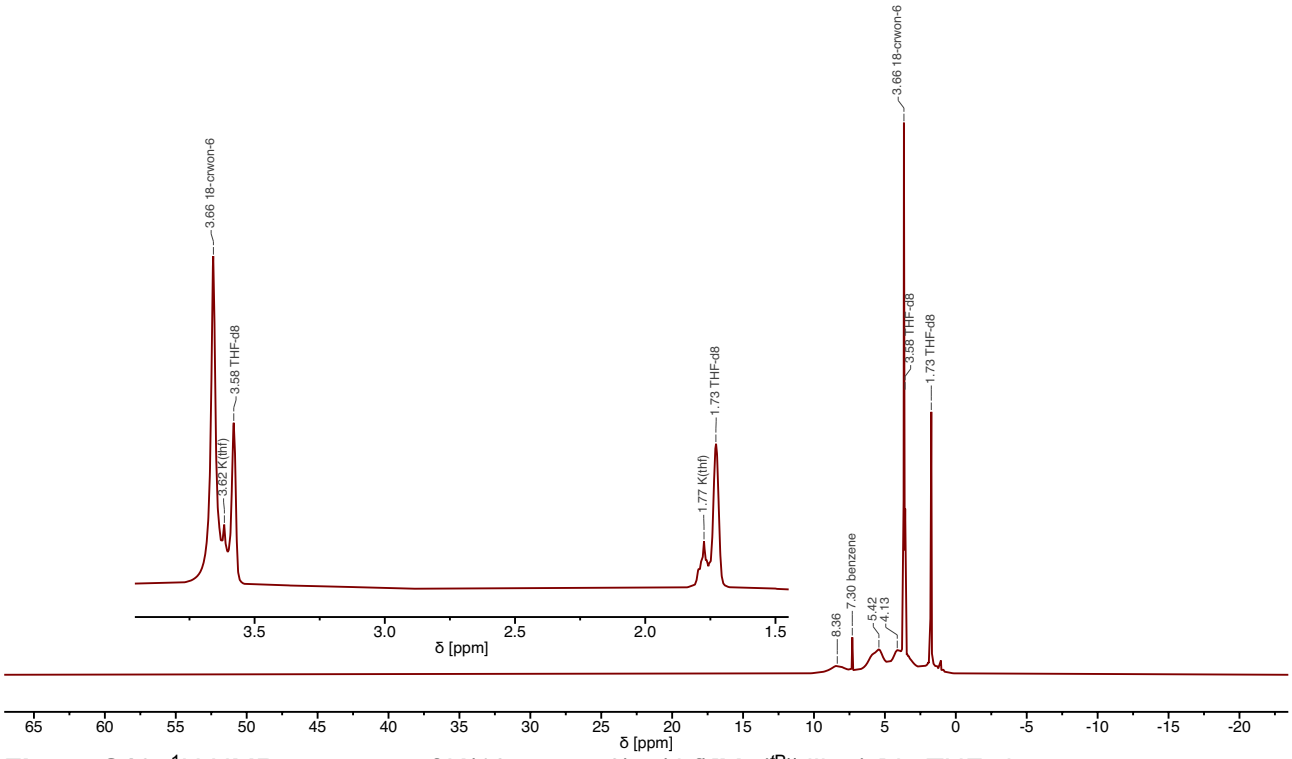

Figure S19: ^{1}H NMR spectrum of K(18-crown-6)$_{0.5}$(thf)[Mo($^{t\text{Bu}}$diket)$_3$] in THF-d_8.

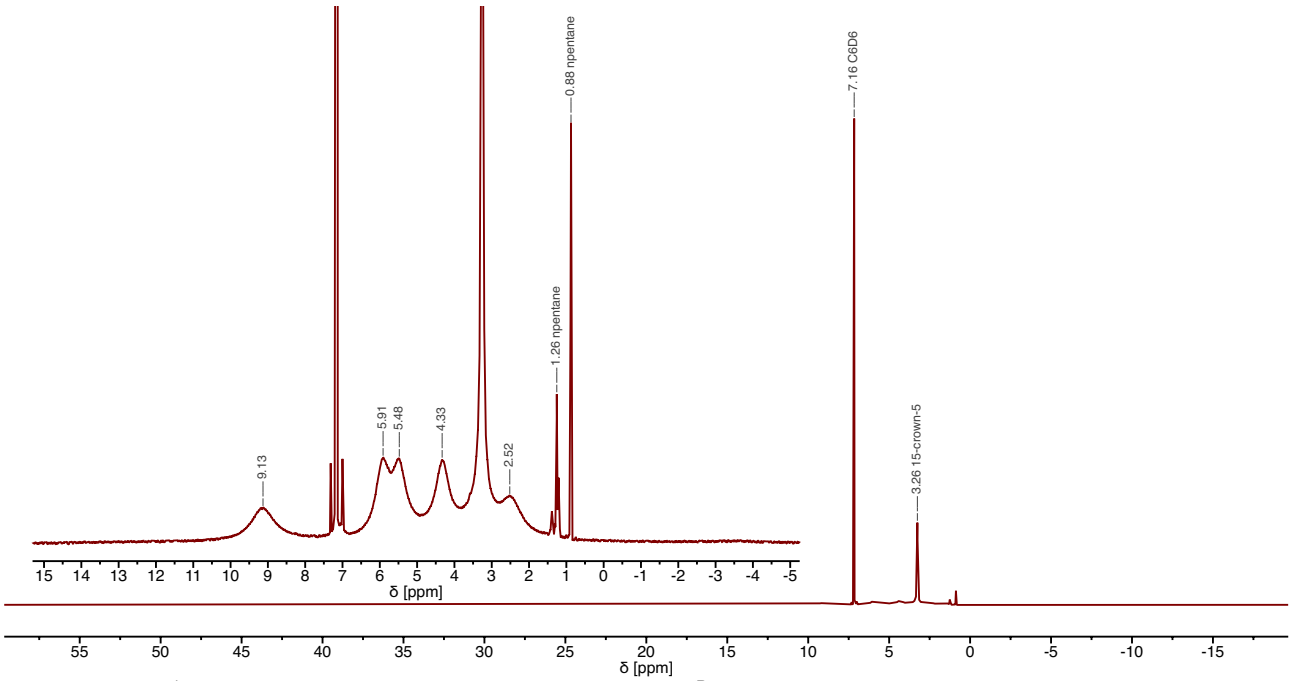

Figure S20: ^{1}H NMR spectrum of K(15-crown-5)[Mo($^{t\text{Bu}}$diket)$_3$] in benzene-d_6.

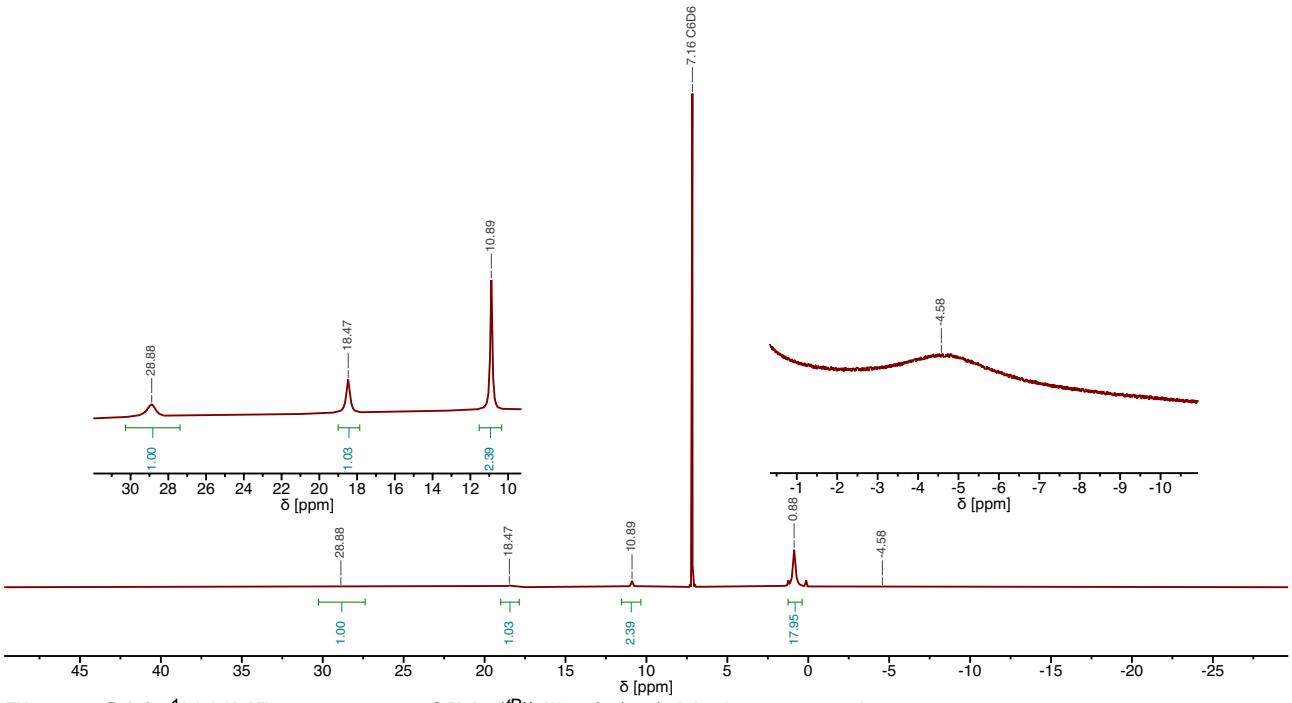

Figure S21: ^{1}H NMR spectrum of [Mo($^{t\text{Bu}}$diket)$_2$(py)$_2$] in benzene-d_6.

5.2 NMR Spectra of Reaction with CO_2

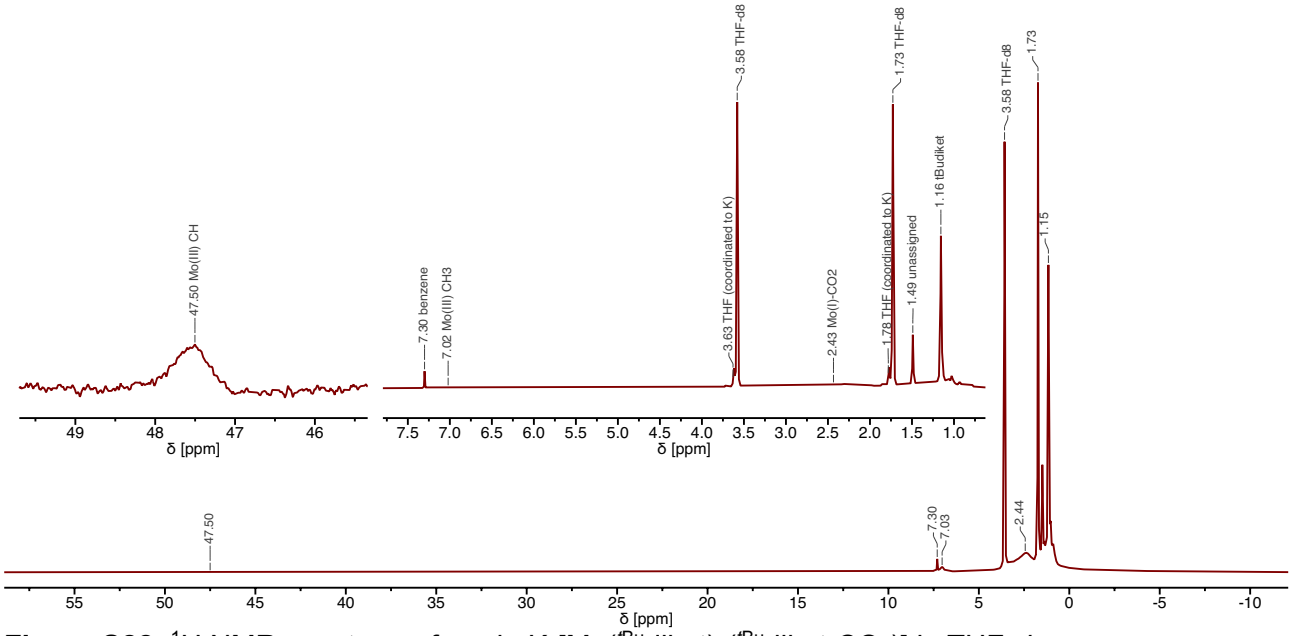

Figure S22: ^{1}H NMR spectrum of crude $K_2[Mo(^{tBu}diket)_2(^{tBu}diket{\cdot}CO_2)]$ in THF-d_8.

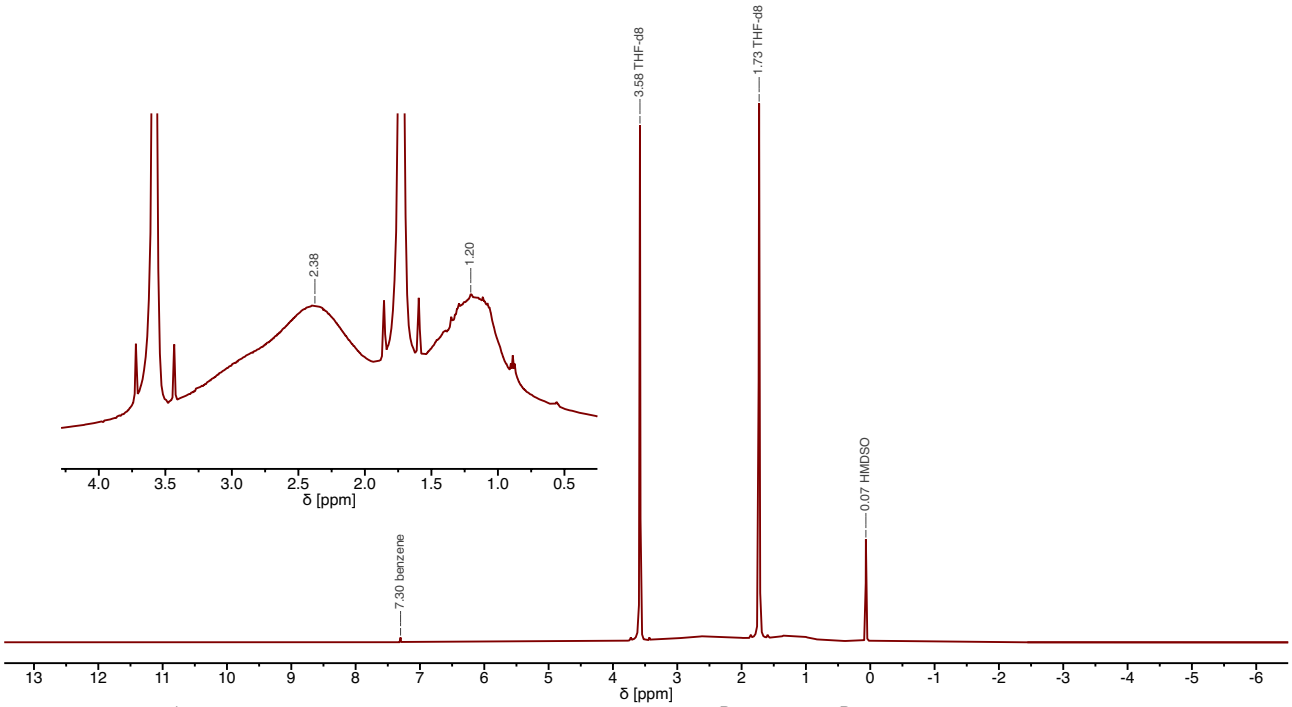

Figure S23: ^{1}H NMR spectrum of recrystallized $K_2[Mo(^{tBu}diket)_2(^{tBu}diket{\cdot}CO_2)]$ in THF-d_8.

5.3 NMR Spectra of Reaction with CS_2

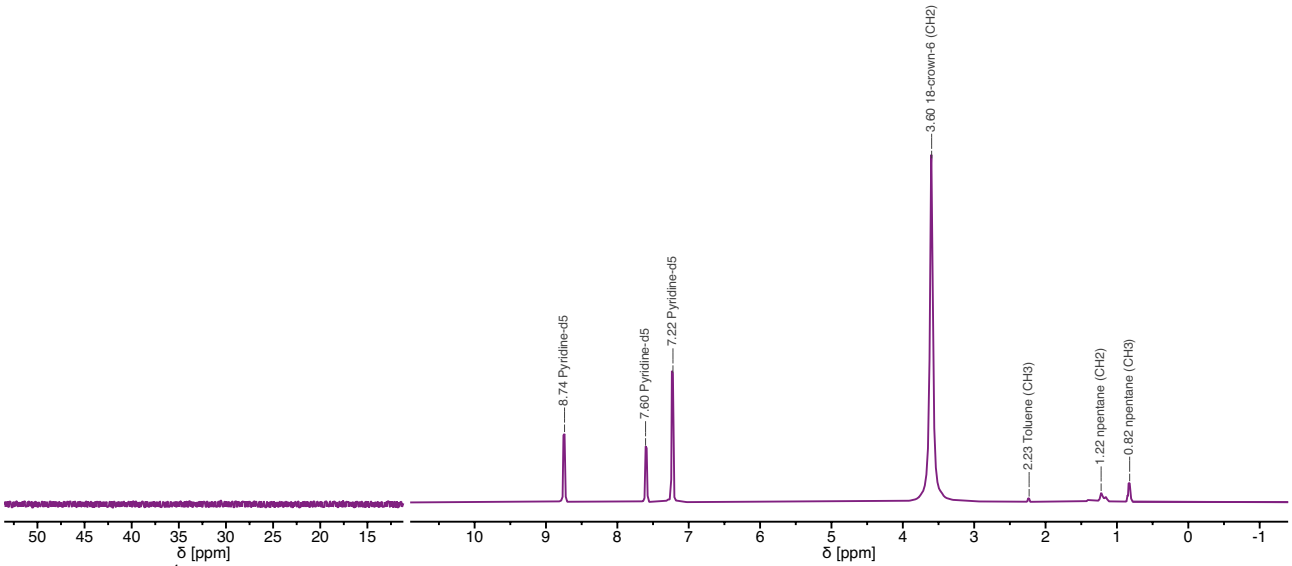

Figure S24: ^{1}H NMR spectrum of recrystallized $[K(18\text{-crown-6})]_2[C_2S_4]$ in Py-d_5.

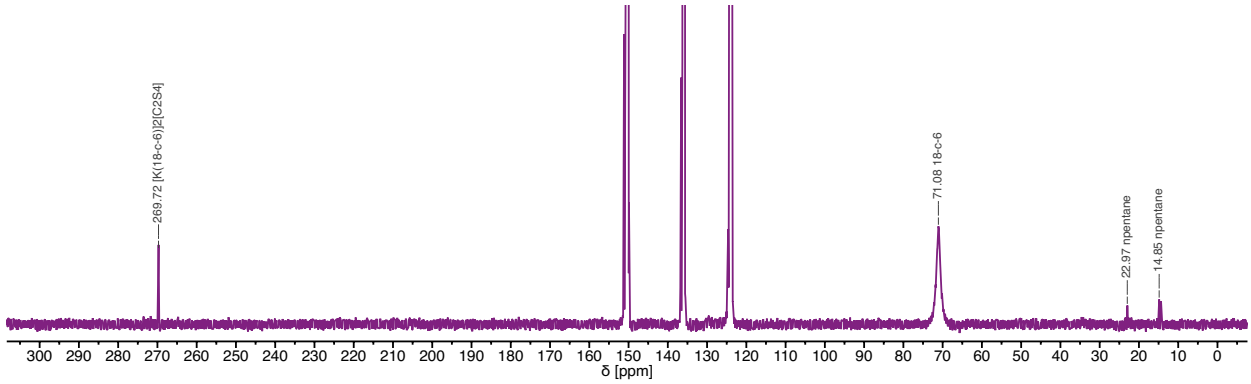

Figure S25: ^{13}C NMR spectrum of recrystallized $[K(18\text{-crown-6})]_2[C_2S_4]$ in Py-d_5.

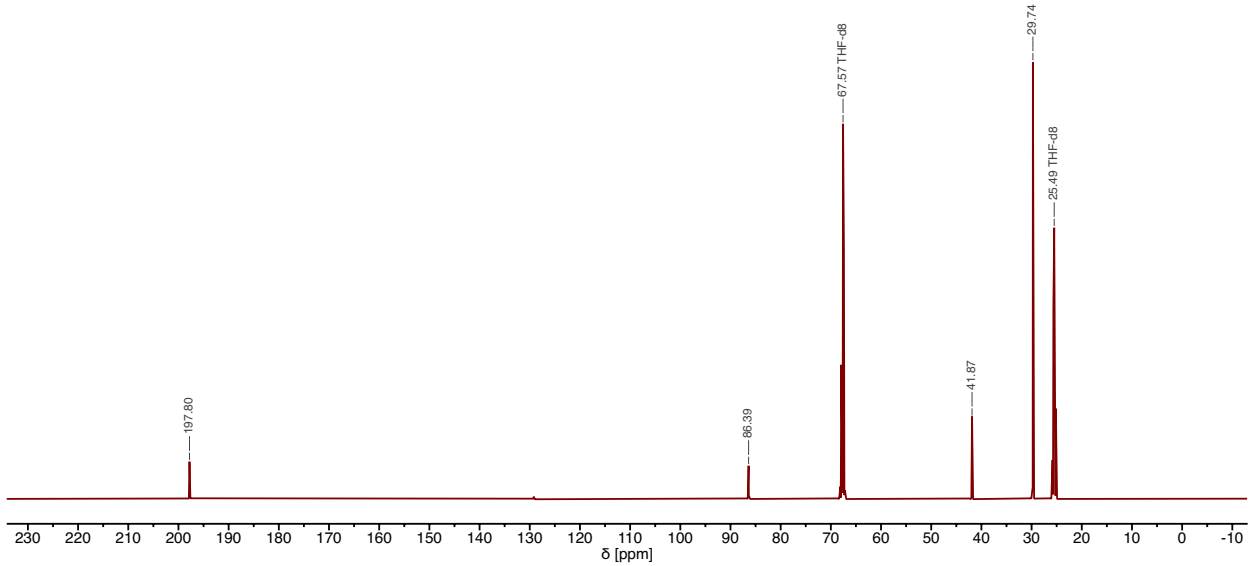

Figure S26: ^{13}C NMR spectrum of K[$^{t\text{Bu}}$diket] in THF-d_8.

5.4 Reactivity Studies

5.4.1 ^{13C}6 + $^{t\text{Bu}}$diketH

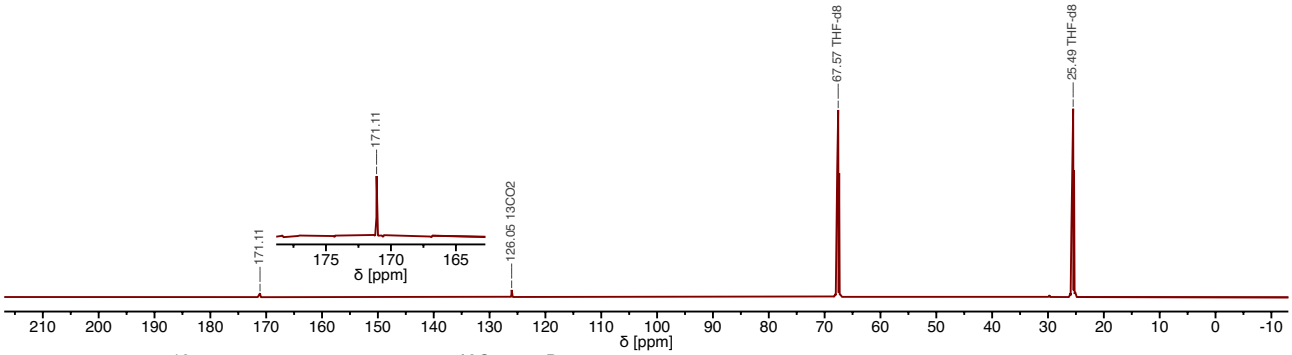

Figure S27: ^{13}C NMR spectrum of **^{13C}6** + $^{t\text{Bu}}$diketH in THF-d_8 after 8 h at ambient temperature.

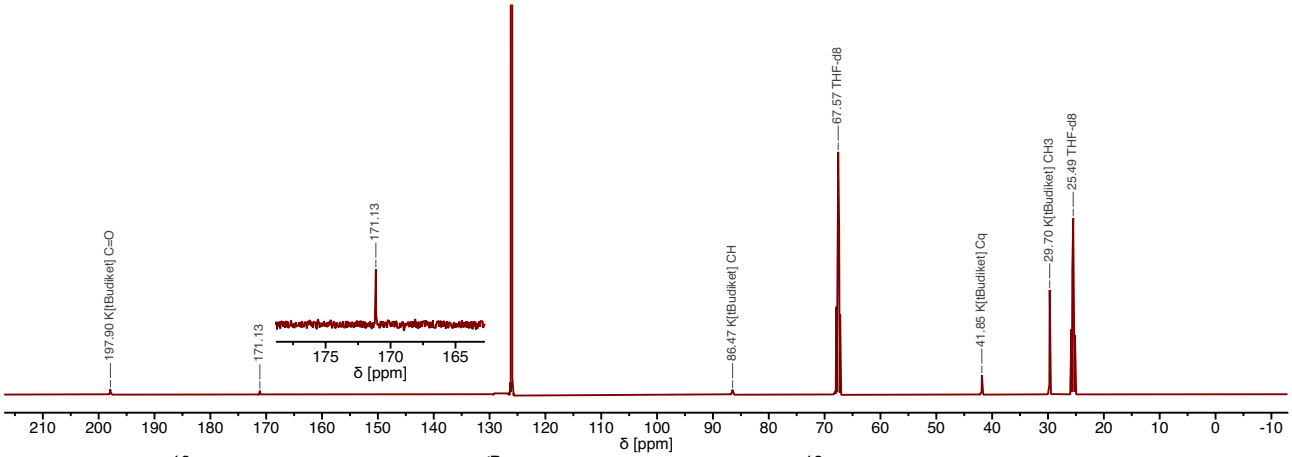

Figure S28: ^{13}C NMR spectrum of K[$^{t\text{Bu}}$diket] in THF-d_8 under $^{13}CO_2$ (1 atm).

5.4.2 ^{13C}6 in Methanol-d_4

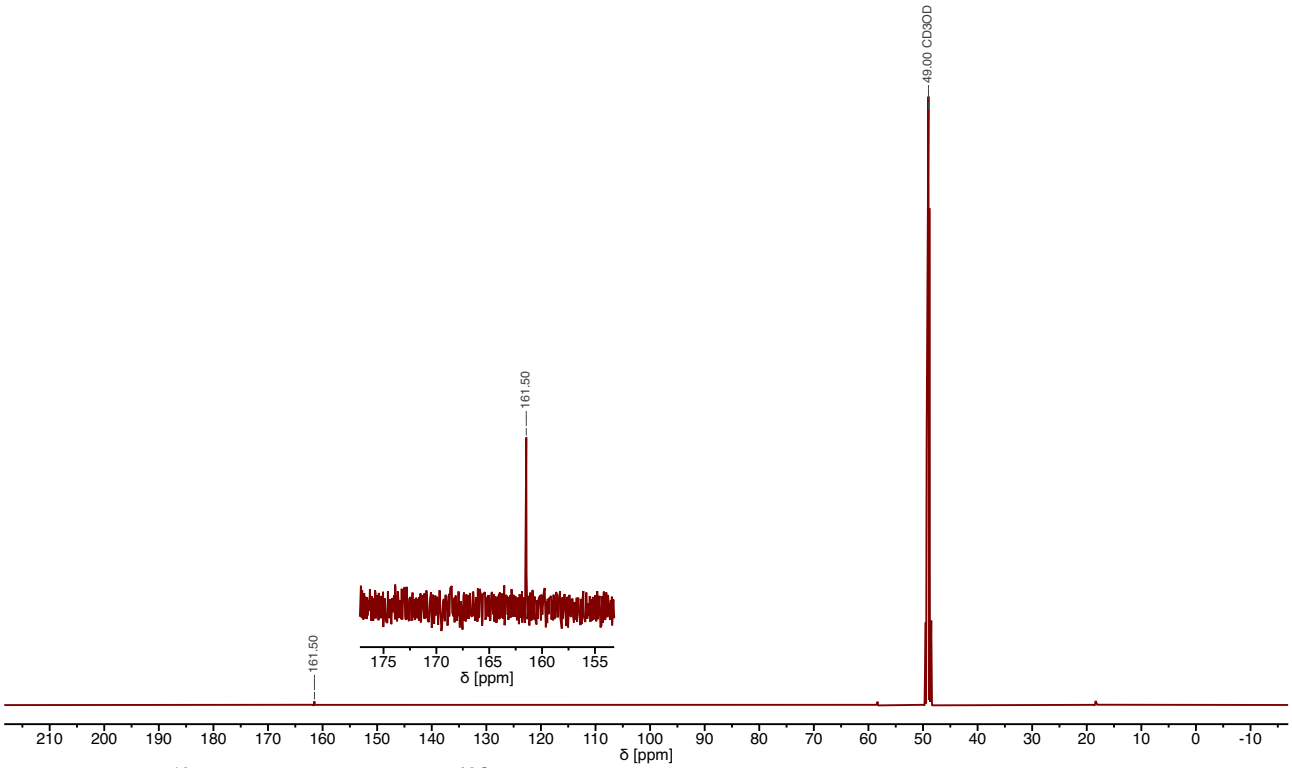

Figure S29: ^{13}C NMR spectrum of **^{13C}6** in methanol-d_4 after 8 h at ambient temperature.

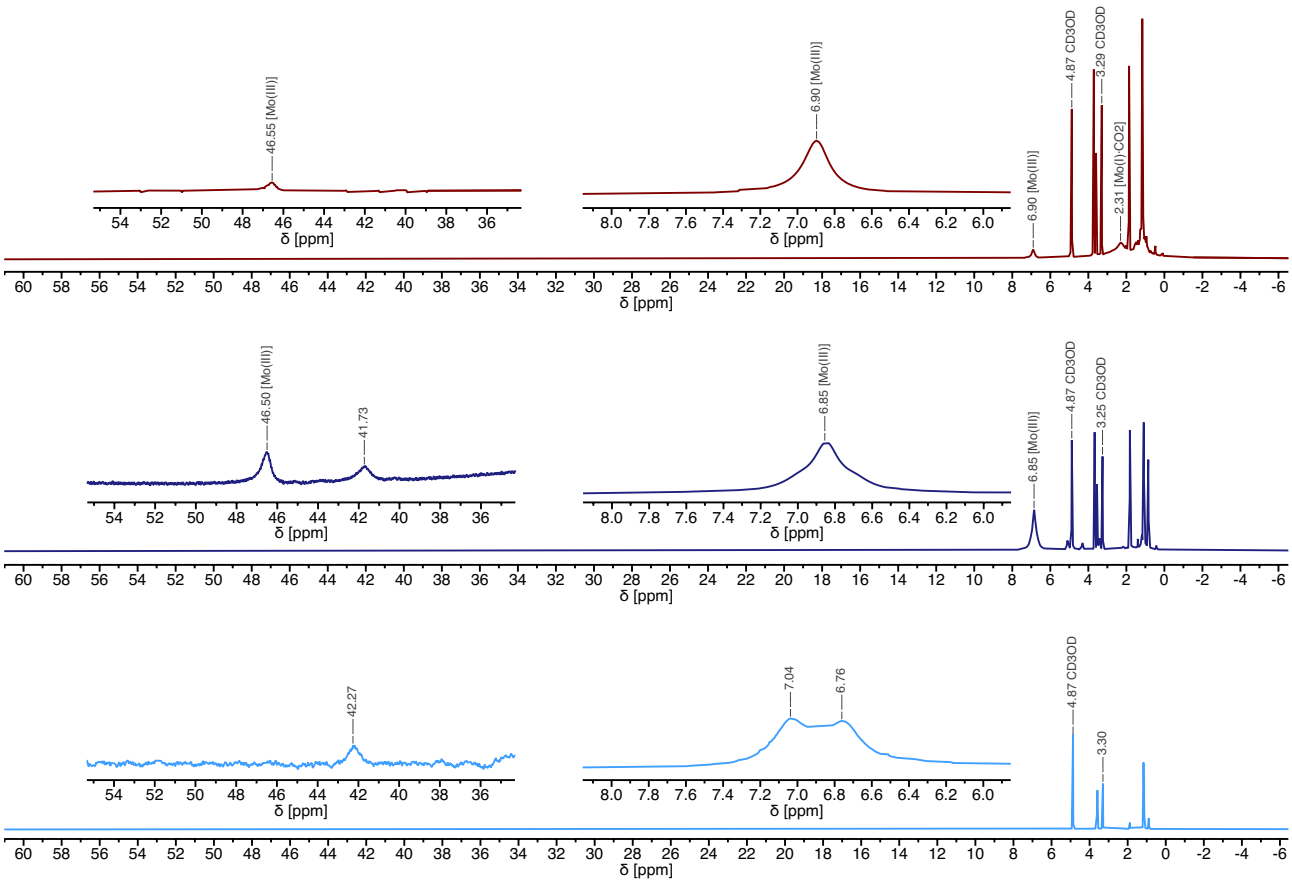

Figure S30: ^{1}H NMR spectrum of **^{13C}6** in methanol-d_4 after 10 min (*maroon*, *top* trace), after 8 h (*dark blue*, *middle* trace) at ambient temperature, and after washing with ^{n}pentane (*light blue*, *bottom* trace).

5.4.3 ^{13C}6 in D_2O

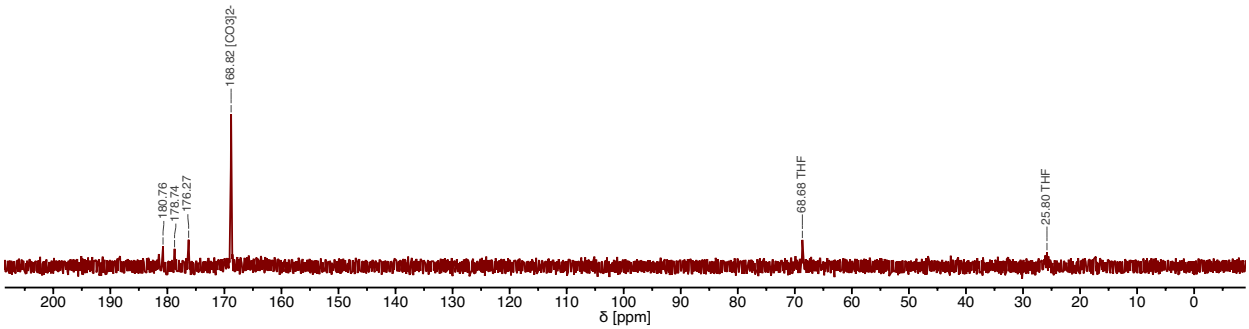

Figure S31: ^{13}C NMR spectrum of **^{13C}6** suspended in D_2O (without filtration). The chemical shift was reference using the residual THF signals.

5.4.4 1 + KC_8 under CO_2

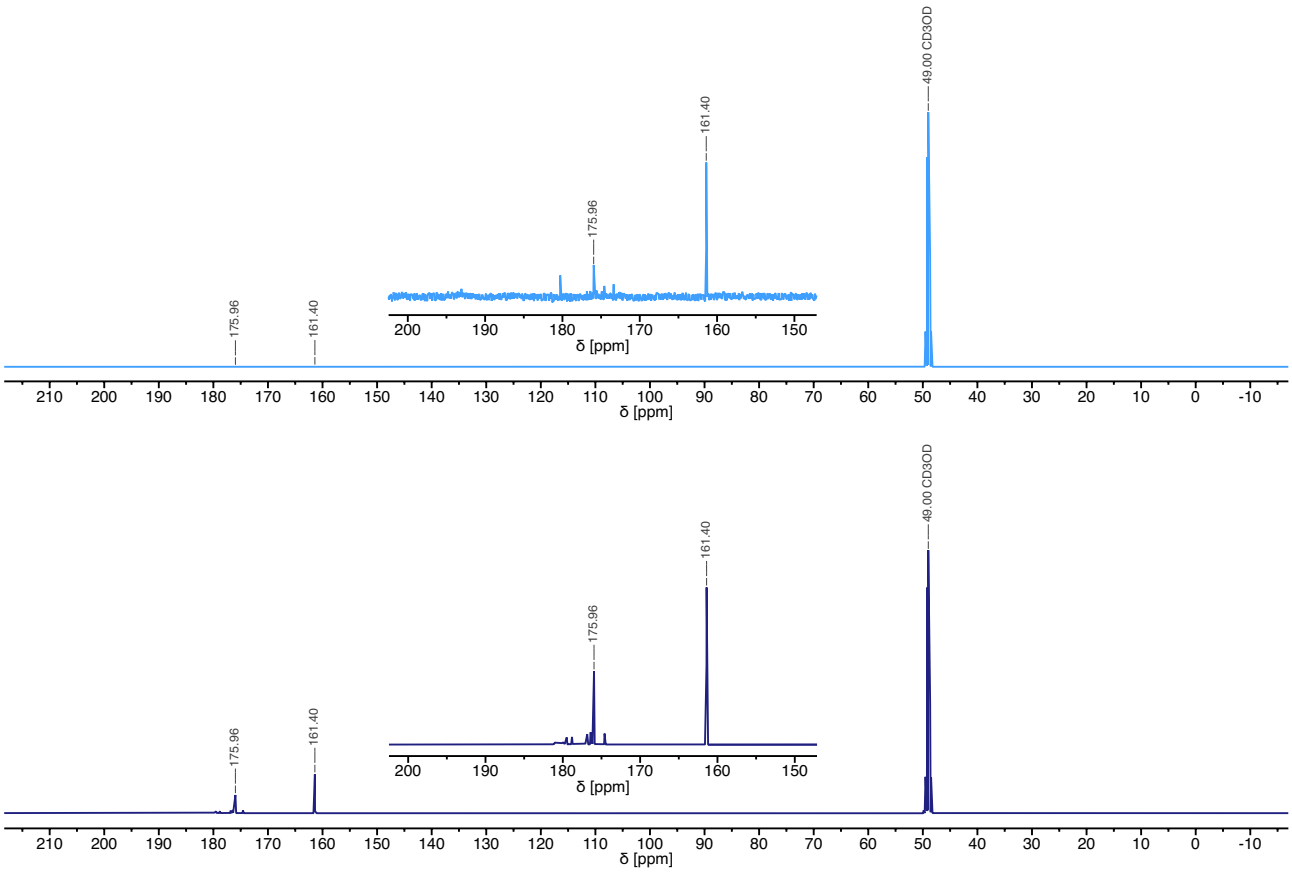

Figure S32: ^{13}C NMR spectra of **1** + KC_8 (1 equiv.) in methanol-d_4 under $^{12}CO_2$ (1 atm, *light blue*, *top* trace) and $^{13}CO_2$ (1 atm, *dark blue*, *bottom* trace).

5.5 Additional Spectra

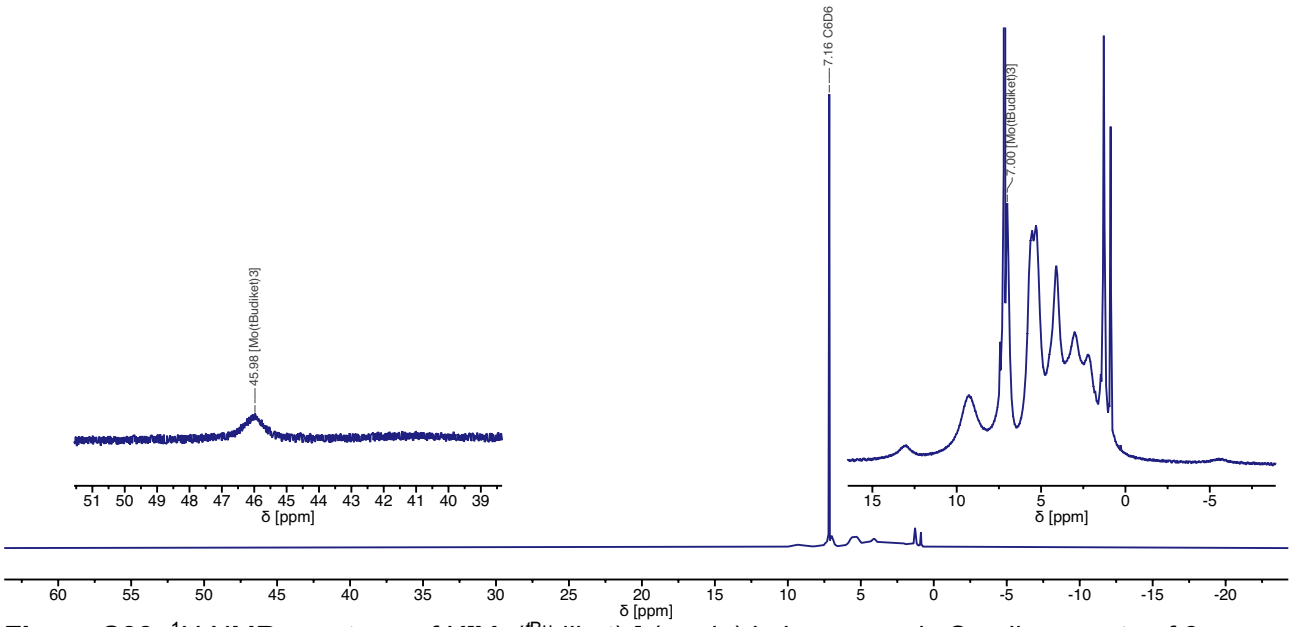

Figure S33: ^{1}H NMR spectrum of K[Mo($^{t\text{Bu}}$diket)$_3$] (crude) in benzene-d_6. Small amounts of **3** (indicated within the spectrum) could be removed by treatment with crown ether (18-crown-6 or 15-crown-5) which allowed for purification by recrystallization (see Figure S19 and Figure S20).

6. UV-Vis Spectra

6.1 ^{Me}diket Supported Complexes

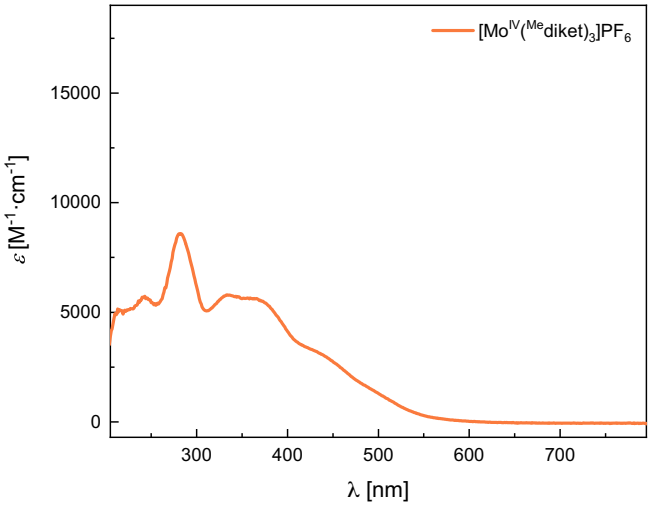

Figure S34: UV-Vis spectrum of [Mo(^{Me}diket)$_3$]PF$_6$ in MeCN (d = 2 mm).

6.2 $^{t\text{Bu}}$diket Supported Complexes

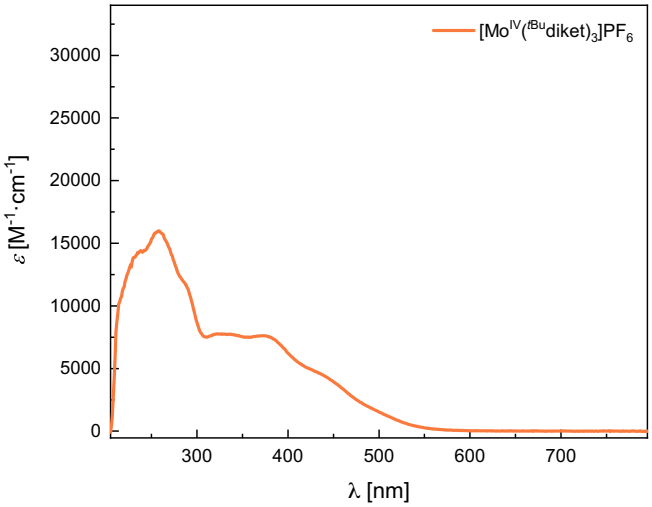

Figure S35: UV-Vis spectrum of [Mo($^{t\text{Bu}}$diket)$_3$]PF$_6$ in THF (d = 2 mm).

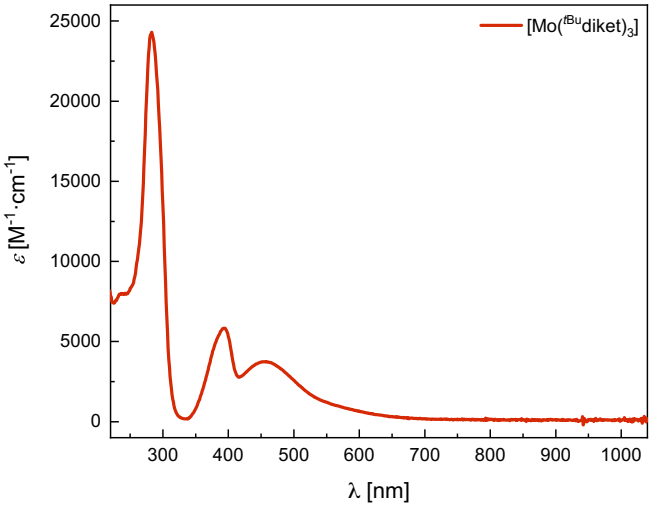

Figure S36: UV-Vis spectrum of [Mo($^{t\text{Bu}}$diket)$_3$] in THF (d = 2 mm).

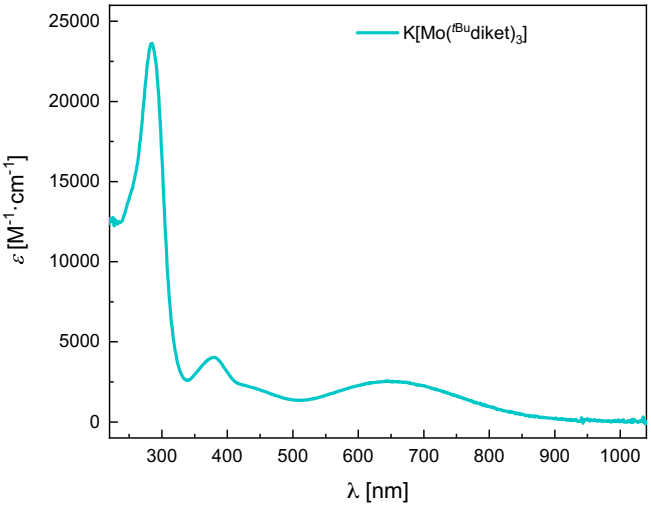

Figure S37: UV-Vis spectrum of K[Mo($^{t\text{Bu}}$diket)$_3$] in THF (*d* = 2 mm).

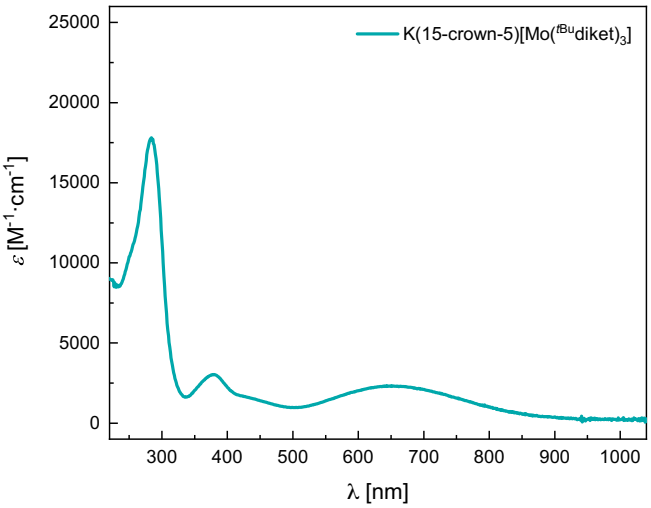

Figure S38: UV-Vis spectrum of K(15-crown-5)[Mo($^{t\text{Bu}}$diket)$_3$] in THF (*d* = 2 mm).

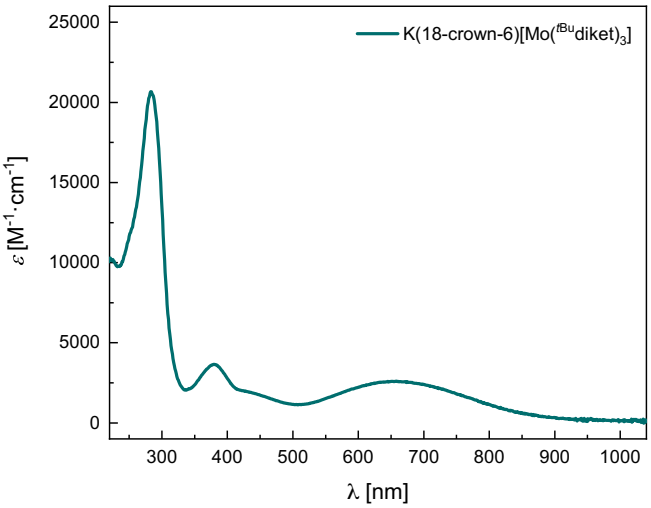

Figure S39: UV-Vis spectrum of K(18-crown-6)[Mo($^{t\text{Bu}}$diket)$_3$] in THF (*d* = 2 mm).

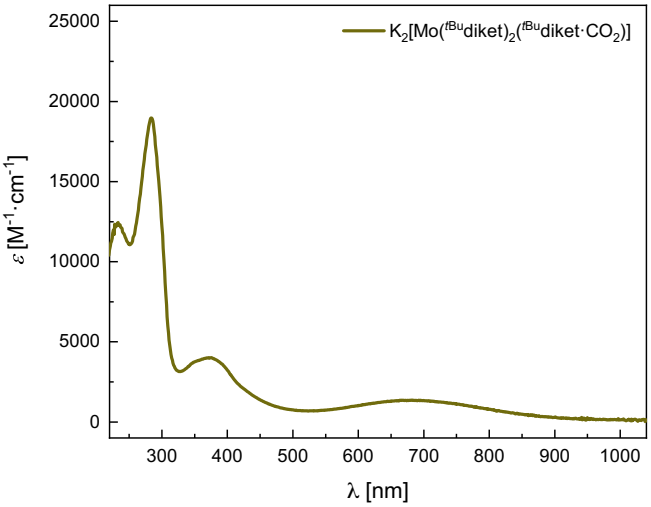

Figure S40: UV-Vis spectrum of $K_2[Mo(^{t\text{Bu}}\text{diket})_2(^{t\text{Bu}}\text{diket}\cdot CO_2)]$ in THF (d = 2 mm).

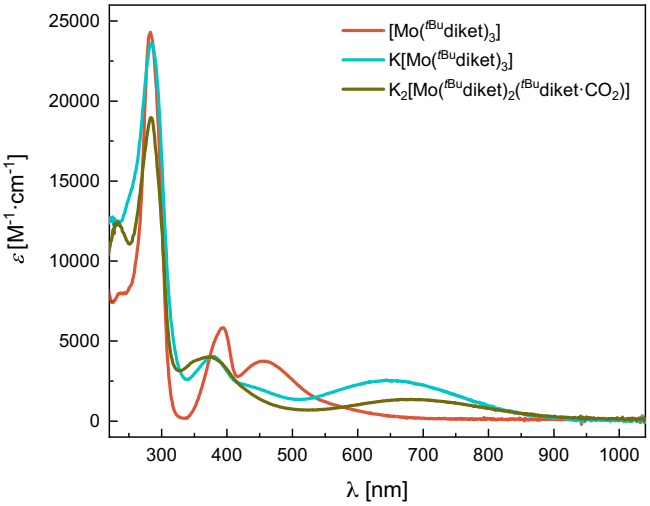

Figure S41: Overlayed UV-Vis spectra of $[Mo(^{t\text{Bu}}\text{diket})_3]$, $K[Mo(^{t\text{Bu}}\text{diket})_3]$ and $K_2[Mo(^{t\text{Bu}}\text{diket})_2(^{t\text{Bu}}\text{diket}\cdot CO_2)]$, respectively, in THF ($d$ = 2 mm).

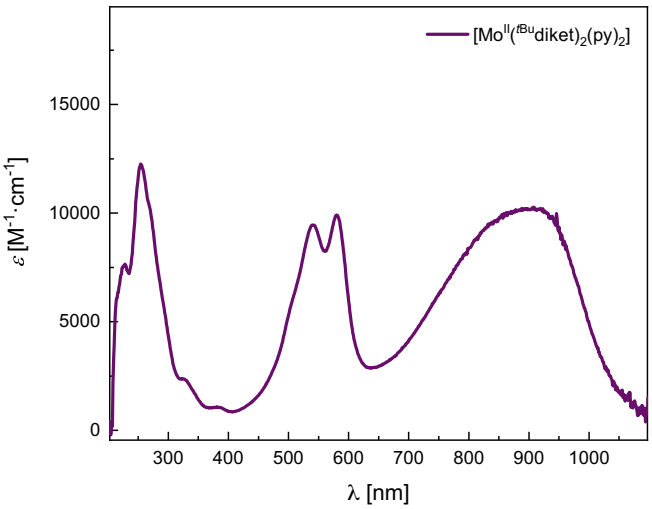

Figure S42: UV-Vis spectrum of $[Mo(^{t\text{Bu}}\text{diket})_2(py)_2]$ in THF (d = 2 mm).

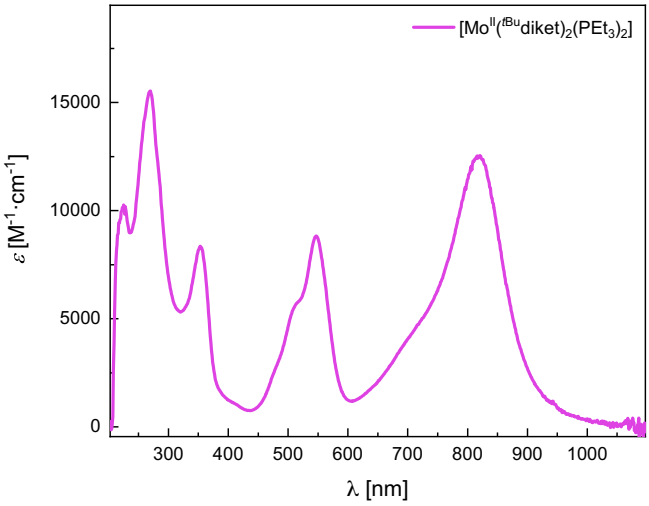

Figure S43: UV-Vis spectrum of [Mo($^{t\text{Bu}}$diket)$_2$(PEt$_3$)$_2$] in THF (*d* = 2 mm).

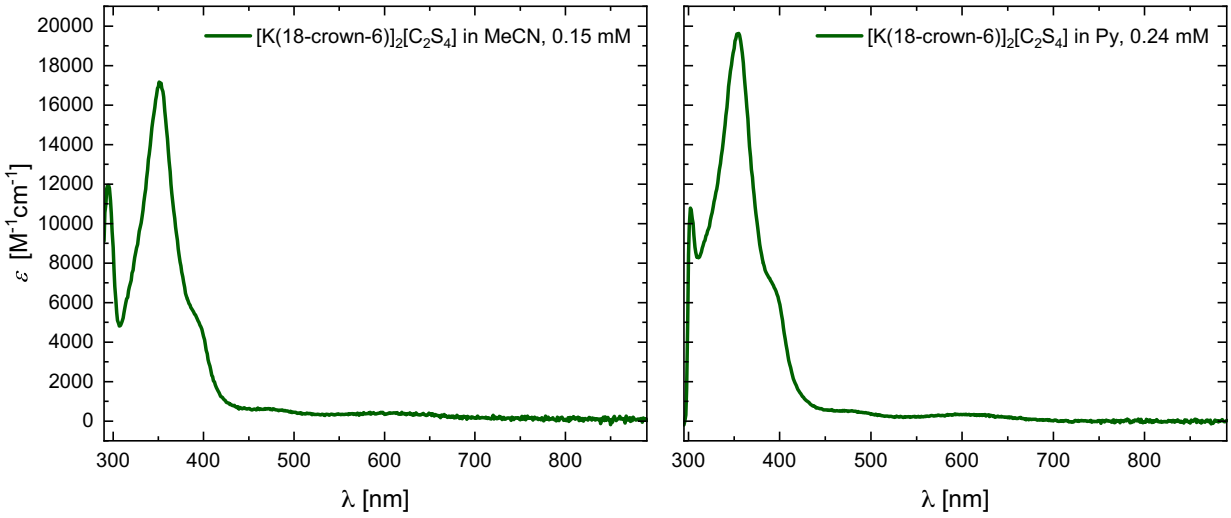

Figure S44: UV-Vis spectrum of [K(18-crown-6)$_2$] in MeCN (*left*) and pyridine (*right*) (*d* = 2 mm).

7. Infrared (IR) Spectroscopy

7.1 Reactivity of 5 with $^{12/13}CO_2$

7.1.1 Spectra

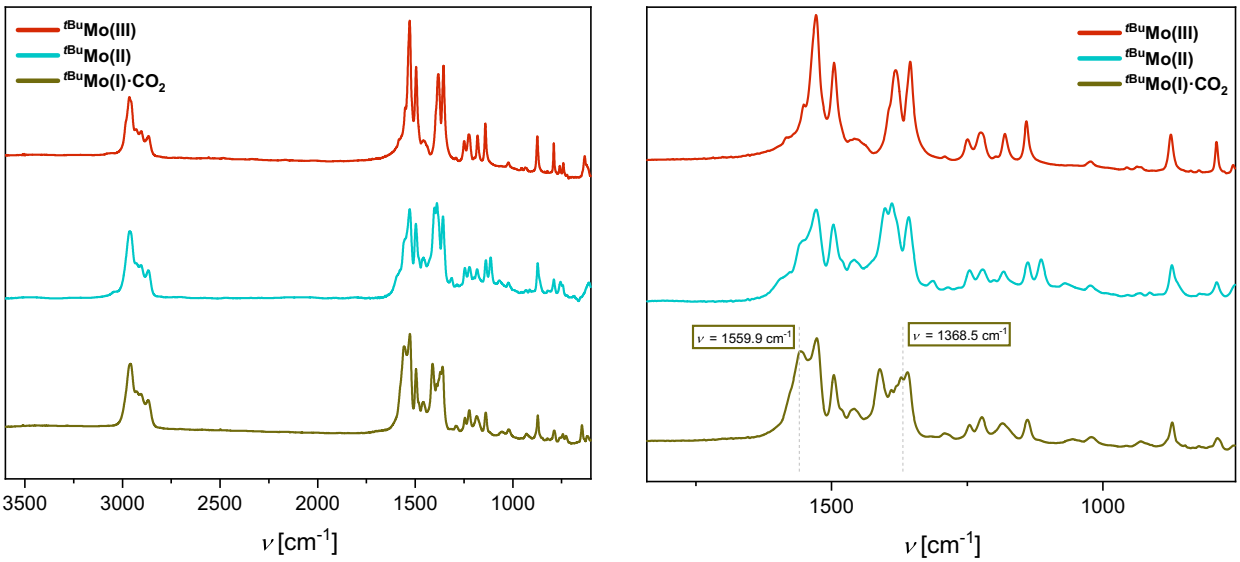

Figure S45: IR spectra of [Mo($^{t\text{Bu}}$diket)$_3$] (*top*, *red*), K[Mo($^{t\text{Bu}}$diket)$_3$] (*middle*, *light turquoise*), and K$_2$[Mo($^{t\text{Bu}}$diket)$_2$($^{t\text{Bu}}$diket·$^{12}CO_2$)] (*bottom*, *green*).

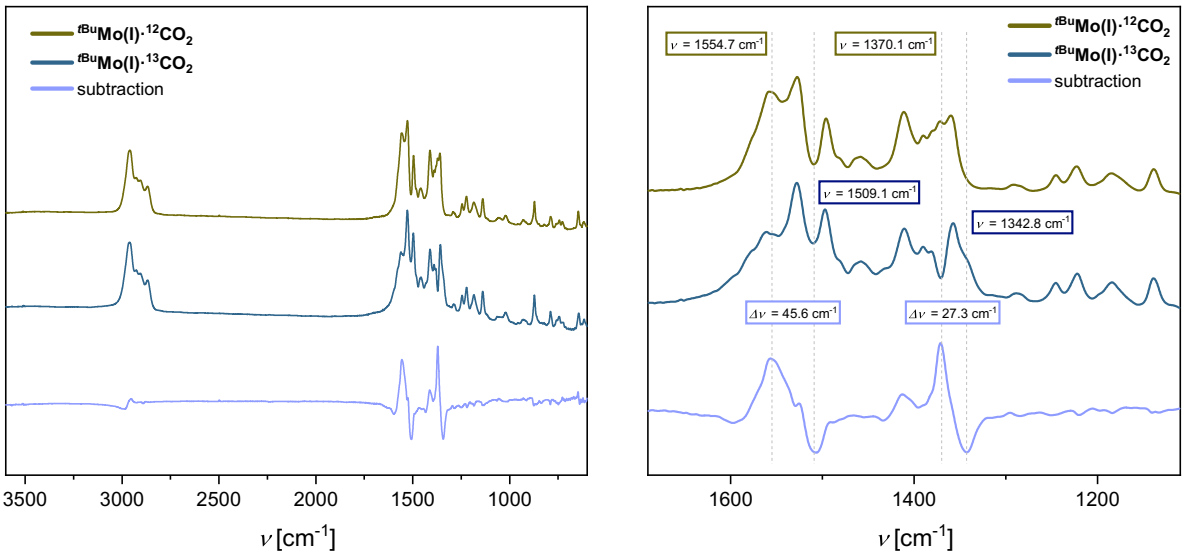

Figure S46: IR spectra of K$_2$[Mo($^{t\text{Bu}}$diket)$_2$($^{t\text{Bu}}$diket·$^{12}CO_2$)] (*top*, *green*), and K$_2$[Mo($^{t\text{Bu}}$diket)$_2$($^{t\text{Bu}}$diket·$^{13}CO_2$)] (*middle*, *turquoise*). The subtraction of the two spectra is displayed below (*light blue*).

The observed shift in IR vibration upon ^{13}C labelling was predicted by Hook's law (Equation 1):

$$\tilde{\nu} = \frac{1}{2\pi c}\sqrt{\frac{f(m_1+m_2)}{m_1 m_2}} \quad \text{(Equation 1)}$$

Table S11: Measured and predicted shift of IR vibrations upon ^{13}C labelling of **6**.

vibration	ν meas (^{12}C) [cm^{-1}]	ν meas (^{13}C) [cm^{-1}]	$\Delta\nu_{meas}$ [cm^{-1}]	$\Delta\nu_{predicted}$ [cm^{-1}]
C-O	1554.7	1509.1	45.6	34.5
C-C	1370.1	1342.8	27.3	26.6

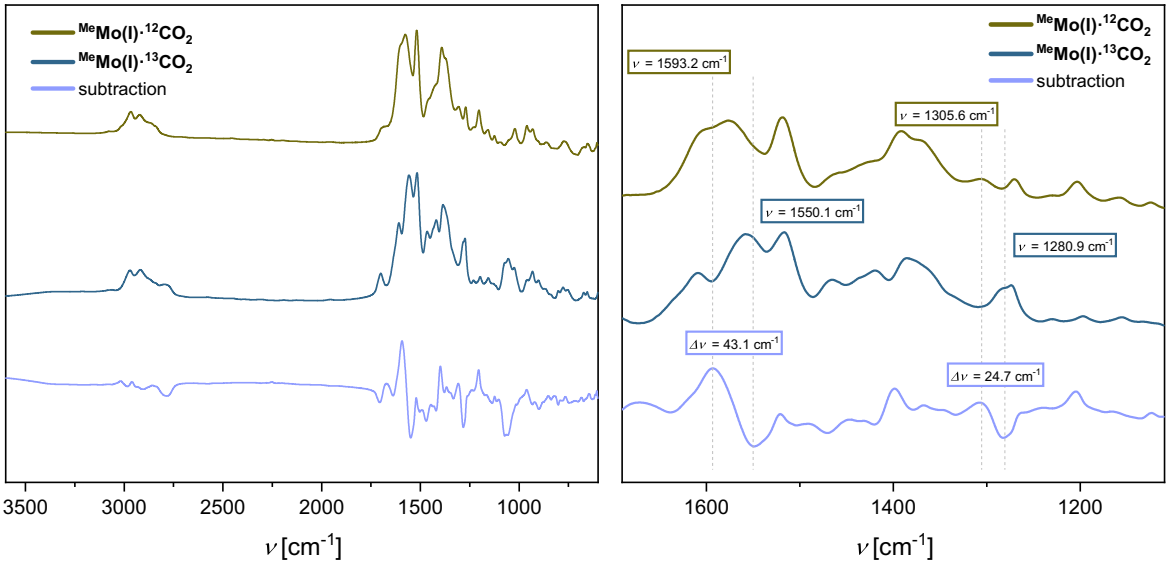

Figure S47: IR spectra of chemically reduced **1** exposed to $^{12}CO_2$ (*top*, *green*), and $^{13}CO_2$ (*middle*, *turquoise*). The subtraction of the two spectra is displayed below (*light blue*).

Table S12: Measured and predicted shift of IR vibrations upon ^{13}C labelling.

vibration	ν meas (^{12}C) [cm^{-1}]	ν meas (^{13}C) [cm^{-1}]	$\Delta\nu_{meas}$ [cm^{-1}]	$\Delta\nu_{predicted}$ [cm^{-1}]
C-O	1593.2	1550.2	43.0	35.4
C-C	1305.6	1280.9	24.7	25.4

7.2 Reactivity of 5 with $^{12/13}CS_2$

7.2.1 Procedure

To a solution of K[Mo($^{t\text{Bu}}$diket)$_3$] (14 mg, 0.020 mmol) in THF was added a 0.1 M stock solution of $^{12}CS_2$ (or $^{13}CS_2$) in THF (220 μL, 0.022 mmol, 1.1 equiv.). After an instantly occurring color change from dark green to red/brown, all volatiles were removed under reduced pressure. The remaining dark brown residue was diluted with KBr, pressed into a pellet, and analyzed by FT-IR spectroscopy.

7.2.2 Spectra

The recorded IR spectra are displayed in Figure S48. Upon addition of CS_2 to K[Mo($^{t\text{Bu}}$diket)$_3$] (*yellow* spectrum), [Mo($^{t\text{Bu}}$diket)$_3$] is formed as the main product (compare with *red* spectrum). The subtraction (*light blue* spectrum) of spectra obtained from reactivity with either $^{12}CS_2$ (*yellow* spectrum) or $^{13}CS_2$ (*orange* spectrum) reveals the red shift of mainly one single band from 990 cm^{-1} to 962 cm^{-1}. This band is assigned to the asymmetric CS_2 vibration of the $[C_2S_4]^{2-}$ dianion, based on the comparison with isolated [K(18-crown-6)]$_2$[C_2S_4] (*green* spectrum), and in agreement with literature.[16-19]

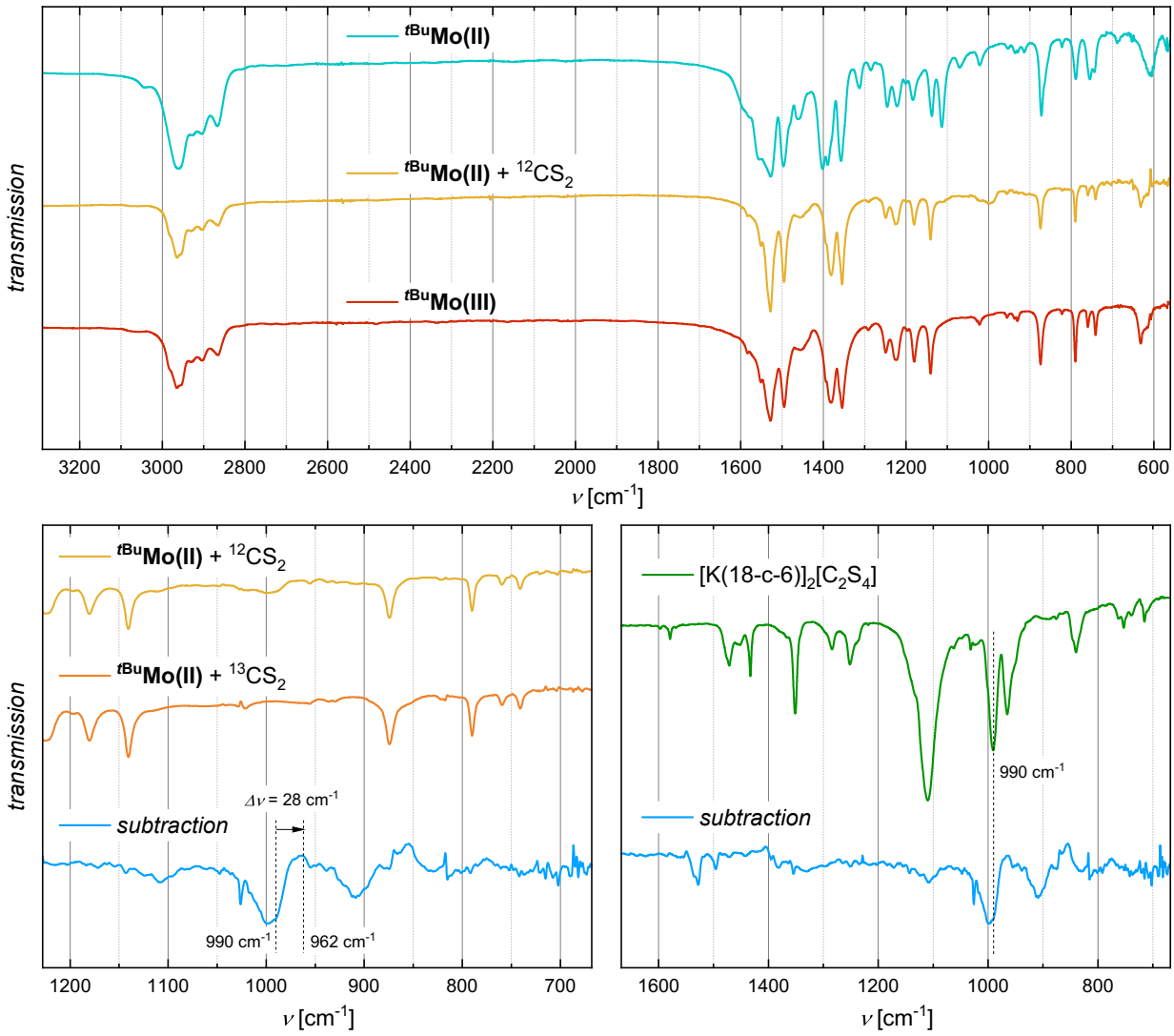

Figure S48: FT-IR spectra of reactivity studies with $^{12/13}CS_2$ (KBr pellet). The spectrum in *light blue* corresponds to the subtraction of the spectra obtained from K[Mo($^{t\text{Bu}}$diket)$_3$] + $^{12}CS_2$ (*yellow*) and K[Mo($^{t\text{Bu}}$diket)$_3$] + $^{13}CS_2$ (*orange*). The spectra of K[Mo($^{t\text{Bu}}$diket)$_3$] (*turquoise*), [Mo($^{t\text{Bu}}$diket)$_3$] (*red*) and [K(18-crown-6)]$_2$[C_2S_4] were obtained from independently isolated compounds. More details are given in the text above.

Table S13: Measured and predicted shift of IR vibrations for the reaction of **5** with $^{12/13}CS_2$.

vibration	ν meas (^{12}C) [cm^{-1}]	ν meas (^{13}C) [cm^{-1}]	$\Delta\nu_{meas}$ [cm^{-1}]	$\Delta\nu_{predicted}$ [cm^{-1}]
C-C	990	962	28	19

8. EPR Spectroscopy

8.1 EPR Spectrum of 6

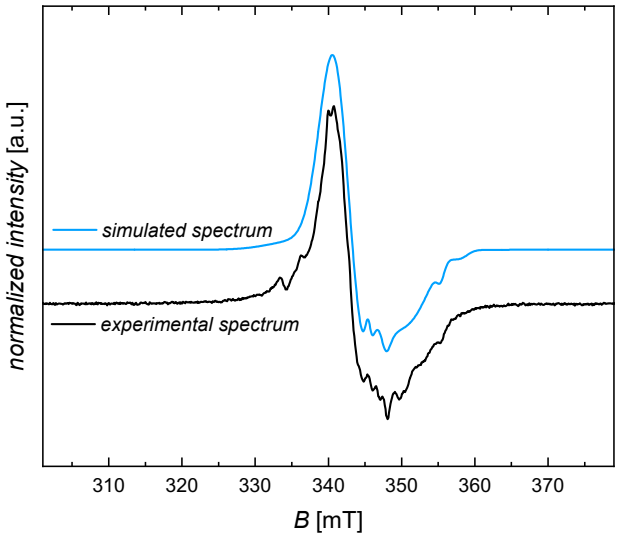

Figure S49: X-Band EPR spectrum of K_2[Mo($^{t\text{Bu}}$diket)$_2$($^{t\text{Bu}}$diket·CO_2)] (*black*) and its simulated spectrum (*blue*). Collection parameters: *c* = 2 mM (in 2-MeTHF), *T* = 20 K, microwave frequency 9.5 GHz. Simulation parameters: *S* = 1/2, *g* = (1.994, 1.979, 1.932), *A*($^{95/97}$Mo)=(63.6, 48.8, 73.3) with *g*-strains of (0.026, 0.023, 0.035) and *A*-strains of (37.4, 59.4, 94.9).

9. Theoretical Calculation of 6

9.1 Method

Density functional theory (DFT) calculations were performed with the Gaussian program package.[20] Geometry optimization and single point calculation (frequency analysis) were carried out with the unrestricted pbe functional. The sdd basis set was used for Mo and the Def2SVP basis set used for all light atoms (C, H, O). For simplicity, the potassium counter cation was omitted, and the calculation was run on a charged complex (2x negatively charged). The graphics containing the molecular orbitals and spin density (difference between α and β spins) were generated using the ChemCraft software (Version 1.8).[21]

9.2 Spin Density Plot

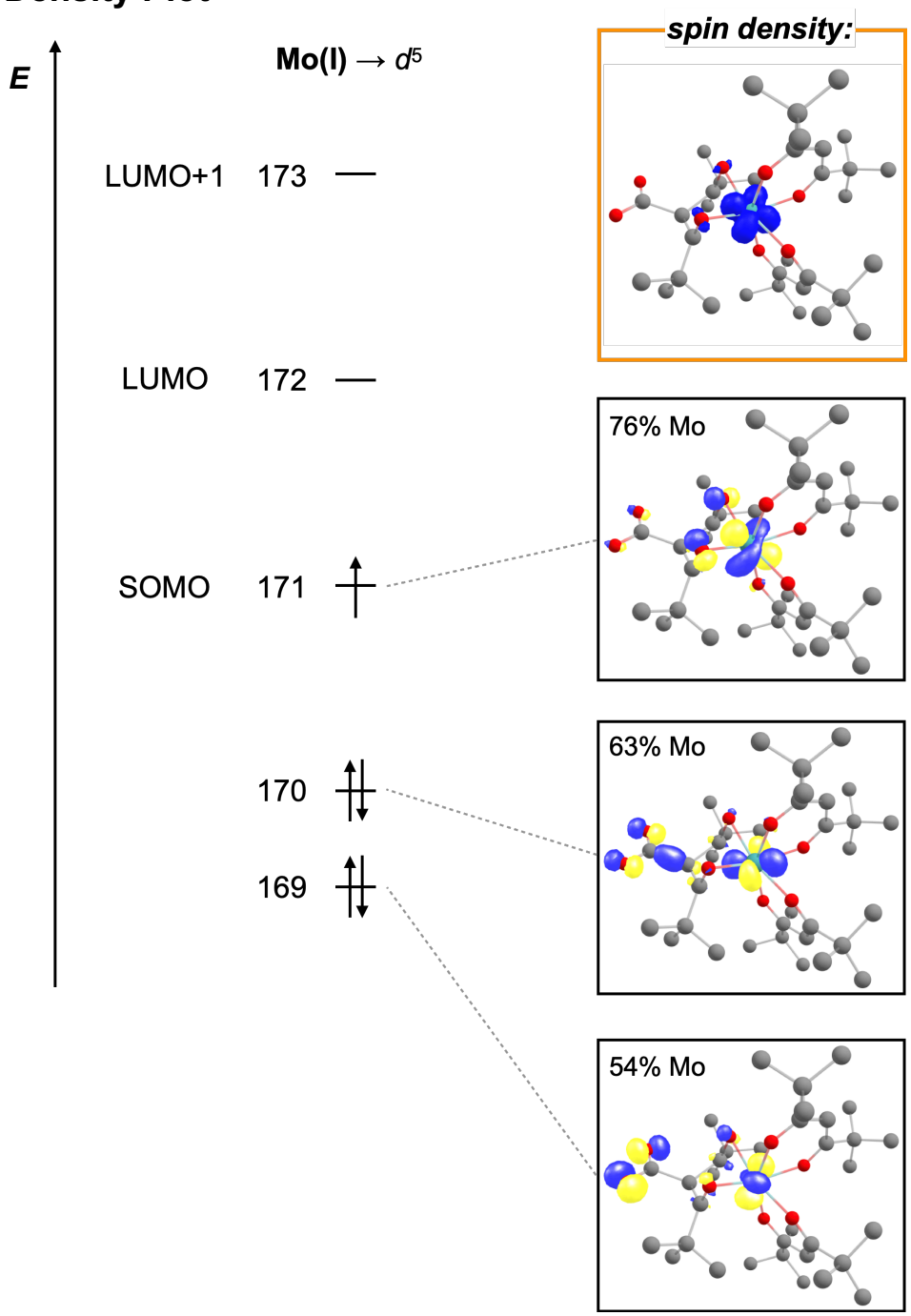

Figure S50: Qualitative molecular orbital diagram of $[Mo(^{tBu}diket)_2(^{tBu}diket{\cdot}CO_2)]^{2-}$ with the most relevant molybdenum-based molecular orbitals (*black* boxes) and the spin density (*orange* box).

9.3 Coordinates of Optimized Geometry

Mo	-0.2008756	-0.4445510	-0.2217436
O	1.3334619	-1.7590220	-0.9613730
O	-0.7009813	-2.2350173	0.6490181
O	1.3009256	0.0828204	1.2333021
O	-4.3958831	-2.5748971	-1.4334865
O	-1.1403358	-1.3285750	-1.8187484
O	0.9147205	0.9832195	-1.3773226
O	-4.2859572	-3.0675015	0.7468799
O	-1.0337807	1.4117098	0.5840125
C	4.6235116	-3.4113989	-0.7646298
C	3.4092061	-0.8598364	3.6705219
C	2.3610382	-4.3672203	-1.2467596
C	3.2252774	-3.0999415	-1.2953293
C	4.6561225	0.6674139	2.1178189
C	3.0573389	-1.4001150	0.6303728
C	3.2664718	0.2136295	2.5816463
C	3.3270352	-2.6089874	-2.7451162
C	2.4676385	-2.0122797	-0.4960842
C	2.4568542	-0.3853133	1.4025563
C	2.5186627	1.4165086	3.1560192
C	-0.8546106	-0.7702703	3.2444762
C	-2.2265077	-2.8250440	2.9807802
C	-2.0290499	-1.3820412	2.4821796
C	-1.7304061	-1.4616172	0.9586992
C	3.4992715	2.1766960	-1.7716504
C	-3.3064088	-0.5950559	2.7768644
C	-3.9263937	-2.4546520	-0.2827836
C	-2.8670868	-1.3123013	-0.0663184
C	1.0719984	2.2294308	-1.2835202
C	-1.1146148	3.2650388	2.8251148
C	-2.1531545	-0.6949591	-1.2728369
C	2.1663835	2.7932517	-2.2183708
C	-0.6557205	2.6052464	0.4641061
C	1.8460201	2.3288318	-3.6444918
C	0.3592979	3.0645267	-0.4072480
C	-1.4154270	3.6152460	1.3625014
C	2.2796991	4.3166086	-2.1966407
C	-2.9024733	0.2534028	-2.2504057
C	-1.0330137	5.0751345	1.1151482
C	-2.0064032	1.4080634	-2.7006660
C	-3.2656472	-0.5882474	-3.4874810
C	-2.9157263	3.4434447	1.1006701
C	-4.1975485	0.8000814	-1.6505805
H	5.0935402	-4.1926366	-1.3863693
H	4.5916921	-3.7846433	0.2709992
H	3.9644036	-1.7360634	3.3022617

H	5.2781122	-2.5254354	-0.7891894
H	3.9462565	-0.4541327	4.5463762
H	2.4190843	-1.2068381	4.0035498
H	5.2590821	-0.1686087	1.7336161
H	2.7928660	-5.1567797	-1.8864873
H	4.0574611	-1.7167046	0.9178532
H	2.2880820	-4.7540365	-0.2179228
H	5.2090198	1.1235519	2.9579173
H	3.7719138	-3.3868749	-3.3898280
H	3.9554266	-1.7052220	-2.8126692
H	4.5768421	1.4164233	1.3145085
H	1.3405081	-4.1378406	-1.5849193
H	-1.3046441	-3.4041337	2.8155052
H	0.0593024	-1.3512612	3.0525970
H	-1.0550404	-0.7815707	4.3321834
H	3.0919269	1.8532791	3.9919380
H	1.5245394	1.1240783	3.5191414
H	-2.4583894	-2.8298146	4.0634977
H	2.3261515	-2.3559108	-3.1223131
H	-0.6605559	0.2618767	2.9225993
H	-3.0474842	-3.2852484	2.4084983
H	2.3638082	2.1884648	2.3875703
H	3.4150312	1.0811561	-1.7258722
H	3.7784688	2.5328467	-0.7667270
H	-3.4798270	-0.5483868	3.8677900
H	4.3101099	2.4478559	-2.4702314
H	-0.0423327	3.3835746	3.0481694
H	-4.1646975	-1.1005352	2.3079262
H	-1.3891922	2.2226506	3.0354578
H	-3.2401554	0.4381711	2.3996357
H	1.7349887	1.2359167	-3.6673031
H	-3.4841607	-0.4940299	0.3337131
H	-1.6843454	3.9229464	3.5043611
H	2.6501554	2.6263333	-4.3397925
H	0.5834118	4.1258225	-0.4176107
H	2.5476578	4.6937471	-1.1972301
H	0.0291121	5.2651762	1.3356212
H	0.9002098	2.7685187	-3.9990685
H	-1.0525749	1.0171136	-3.0831863
H	3.0669247	4.6433742	-2.8974852
H	-2.3473073	-0.9533377	-3.9722180
H	-3.8606131	-1.4545120	-3.1587583
H	-3.2113671	2.3975819	1.2588750
H	-1.7810078	2.1017116	-1.8780897
H	-4.0089900	1.3880028	-0.7391294
H	1.3368791	4.7972152	-2.5013630
H	-1.6307998	5.7296420	1.7721238
H	-4.8762689	-0.0314708	-1.4080755

H	-1.2270464	5.3772707	0.0741208
H	-3.5031790	4.0866056	1.7782718
H	-3.1711968	3.7097753	0.0628598
H	-2.4980796	1.9800294	-3.5097193
H	-3.8325838	0.0241471	-4.2147072
H	-4.7015209	1.4607692	-2.3796732

10. Electrochemistry

10.1 CV Studies

All CV experiments were performed in an argon-filled glovebox (Vigor) using a conventional three electrode single-compartment cell, connected to a SP300 Bio-Logic potentiostat (Bio-Logic Science Instruments SAS). A $Ag/AgNO_3$ (10 mM $AgNO_3$ in 0.1 M $TBAPF_6$ in CH_3CN) reference electrode was used which was protected by a guard compartment separated by a Vycor® frit. All potentials were referenced to an internal ferrocene/ferrocenium standard, added in the last step of each experiment. A 3 mm diameter glassy carbon electrode (GCE, BASi) was used as the working electrode. Electrodes were polished on wet polishing cloth using a 1 µm diamond suspension and a 0.05 µm alumina slurry before each set of experiments. The scan rate was 100 $mV \cdot s^{-1}$ unless otherwise noted. The half-wave potentials ($E_{1/2}$) were defined as the weighing average of the corresponding cathodic peak potential (E_c) and anodic peak potential (E_a) for reversible processes. In all CV studies, 1 mM solutions of compound in CH_3CN or THF containing 0.1 M $TBAPF_6$ as supporting electrolyte were used, unless otherwise noted. For CV experiments under CO_2, the electrolyte solution was purged with purified CO_2 for 20 min (10 $mL \cdot min^{-1}$) prior to the measurement.

10.1.1 CV of 1

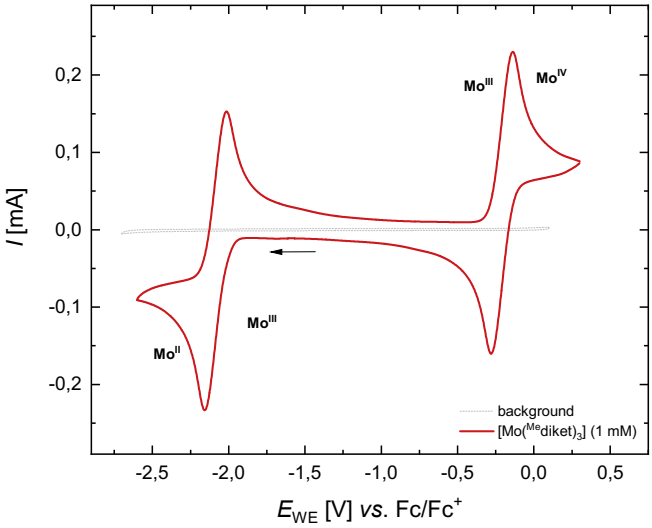

Figure S51: CV (scan rate ν = 100 $mV \cdot s^{-1}$, 2nd scan) of [Mo(^{Me}diket)$_3$] (1 mM) in $TBAPF_6$/MeCN (0.1 M). A $TBAPF_6$/MeCN (0.1 M) background measurement is displayed as a grey dotted line, formal Mo oxidation states are indicated in black.

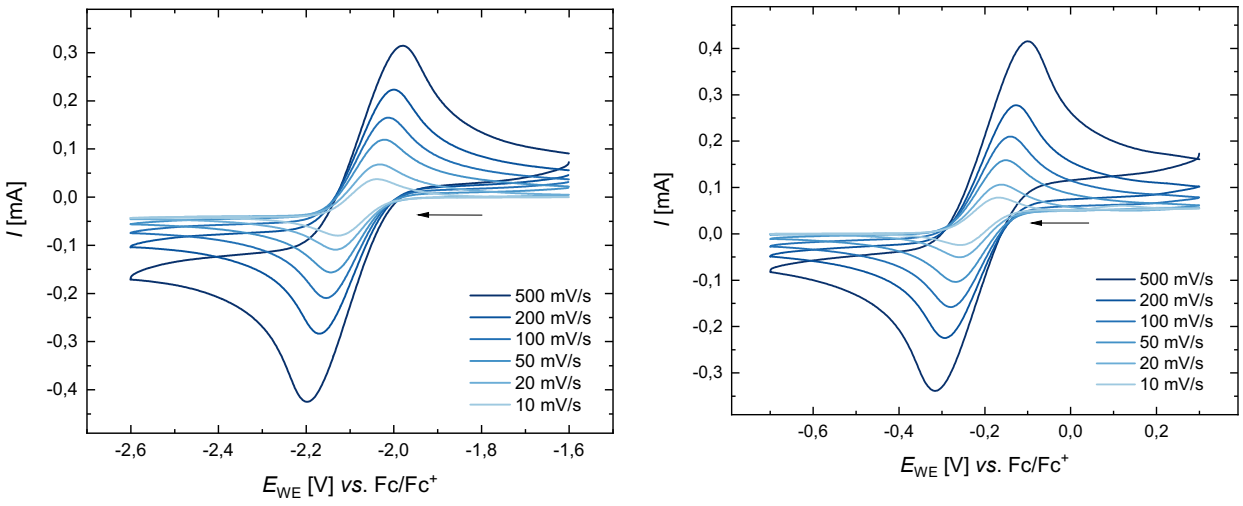

Figure S52: CV of [Mo(^{Me}diket)$_3$] (1 mM) in $TBAPF_6$/MeCN (0.1 M) with varying scan rate ν (see Figure legend) of the Mo(III)/Mo(II) (*left*) and of the Mo(III)/Mo(IV) redox couple (*right*).

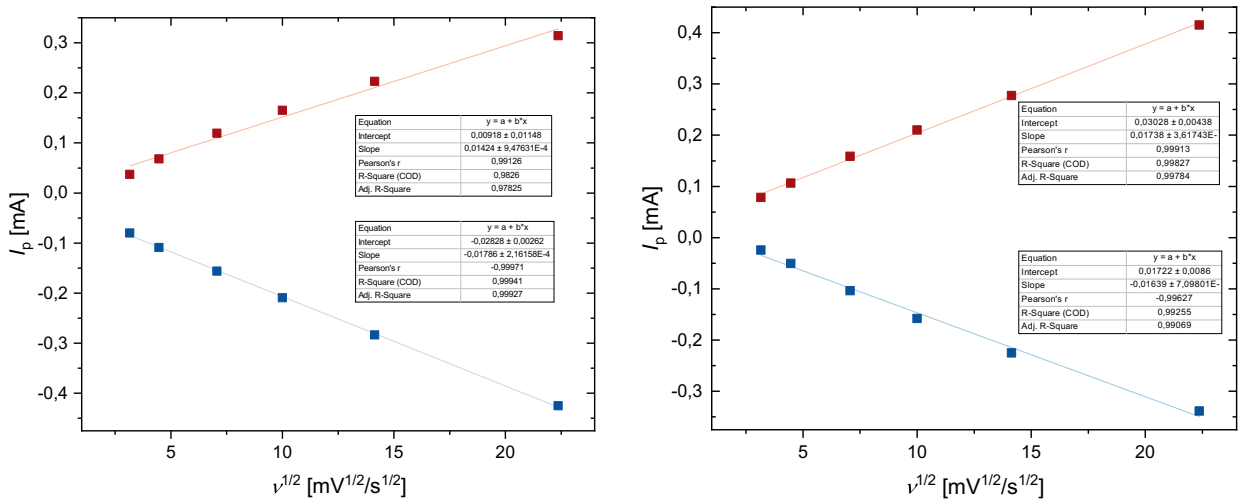

Figure S53: Randles-Ševčík plot of [Mo(^{Me}diket)$_3$] (1 mM) in TBAPF$_6$/MeCN (0.1 M) of the Mo(III)/Mo(II) (*left*) and of the Mo(III)/Mo(IV) redox couple (*right*).

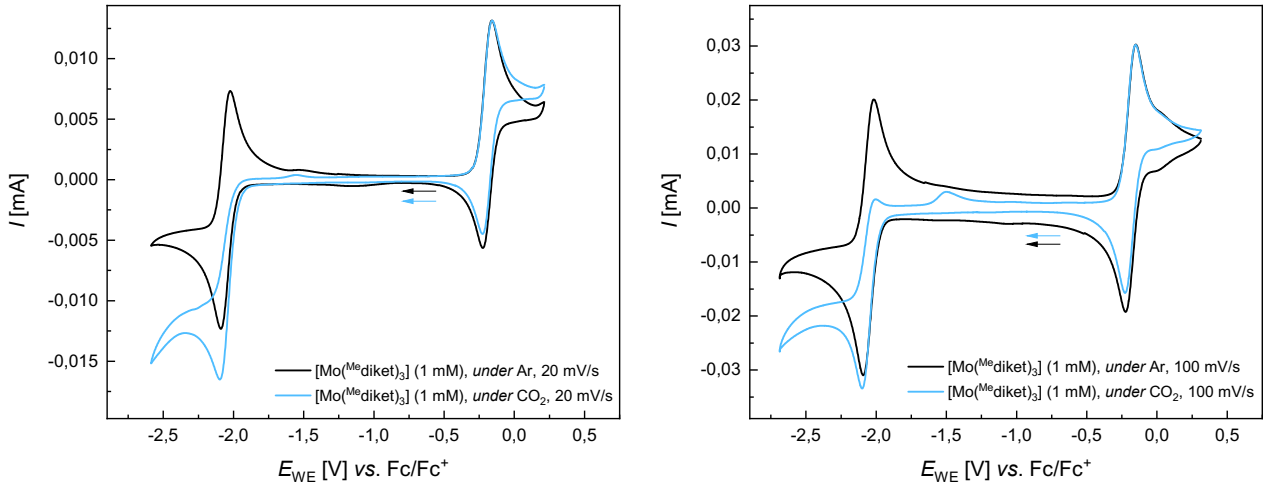

Figure S54: CV (2nd scan) of [Mo(^{Me}diket)$_3$] (1 mM) in TBAPF$_6$/MeCN (0.1 M) under argon (*black* trace) and under CO$_2$ (*light blue* trace) at ν = 20 mV·s^{-1} (*left*) and ν = 100 mV·s^{-1} (*right*).

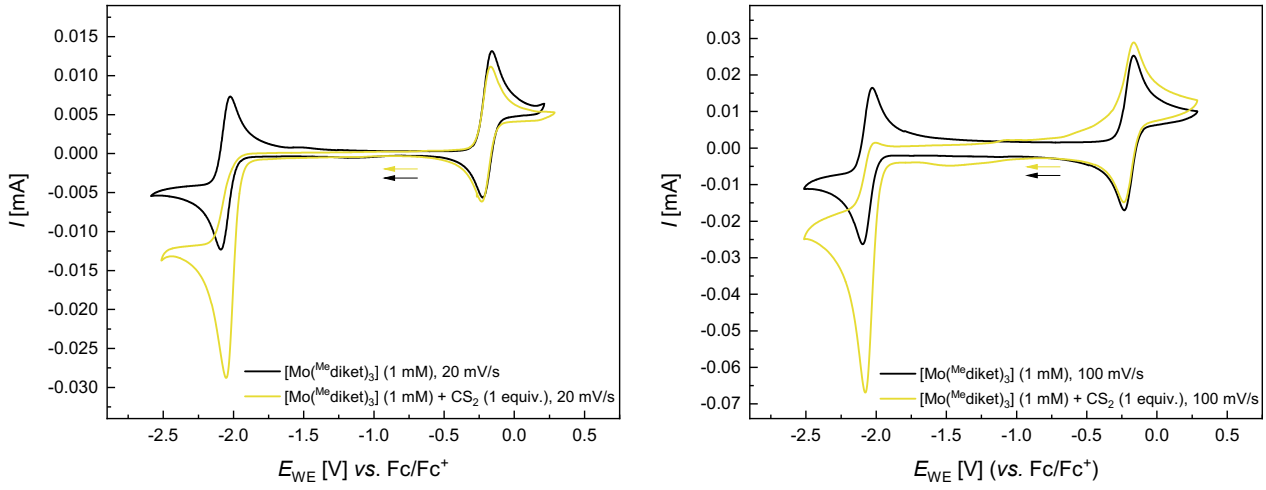

Figure S55: CV (2nd scan) of [Mo(^{Me}diket)$_3$] (1 mM) in TBAPF$_6$/MeCN (0.1 M) under argon (*black* trace) and in presence of 1 equiv. of CS_2 (*yellow* trace) at ν = 20 mV·s^{-1} (*left*) and ν = 100 mV·s^{-1} (*right*).

10.1.2 CV of 2

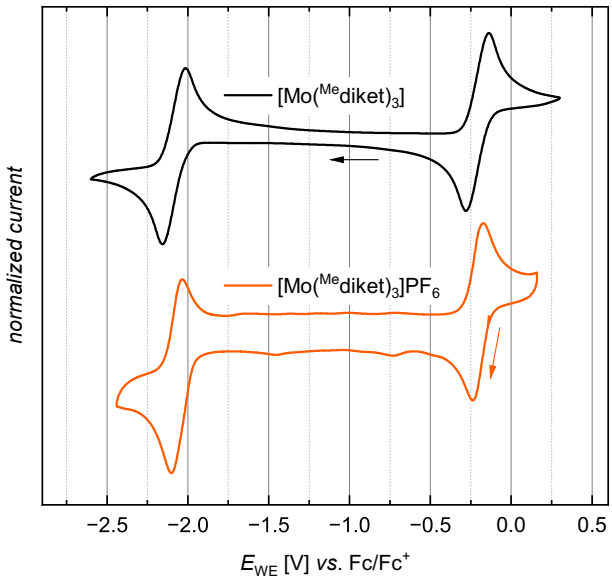

Figure S56: CV of [Mo^{III}(^{Me}diket)$_3$] (*black* trace) and [Mo^{VI}(^{Me}diket)$_3$]PF$_6$ (*orange* trace) at a scan rate ν = 100 mV·s^{-1} in TBAPF$_6$/MeCN (0.1 M).

10.1.3 CV of 3

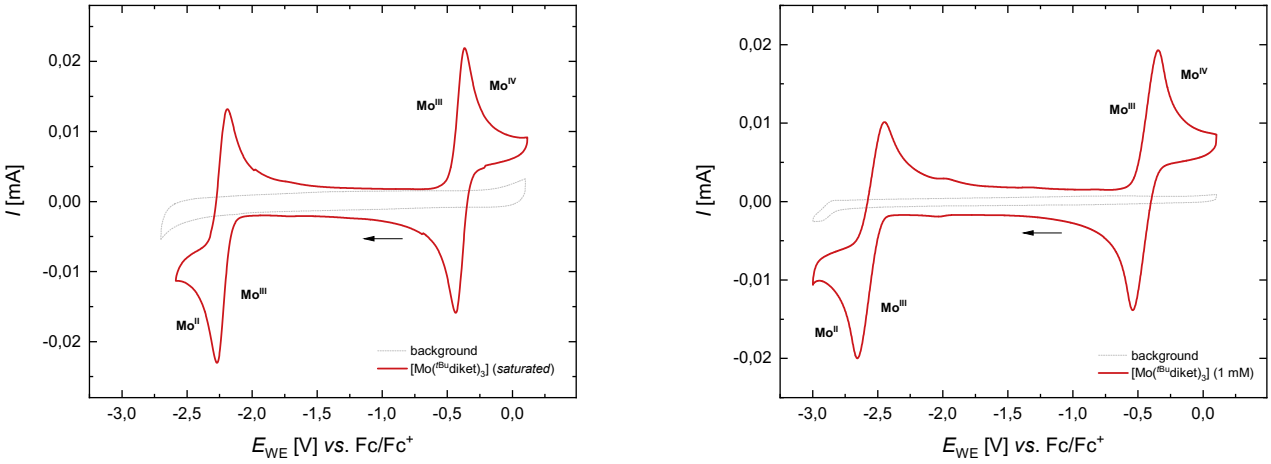

Figure S57: CV (scan rate ν = 100 mV·s^{-1}, 2nd scan) of [Mo($^{t\text{Bu}}$diket)$_3$] in TBAPF$_6$/MeCN (0.1 M) (*left*) TBAPF$_6$/THF (0.1 M) (*right*). A TBAPF$_6$/MeCN (0.1 M) and TBAPF$_6$/THF (0.1 M) background measurement is displayed as a grey dotted line, formal Mo oxidation states are indicated in black. Note that the solubility of [Mo($^{t\text{Bu}}$diket)$_3$] in TBAPF$_6$/MeCN (0.1 M) is < 1 mM.

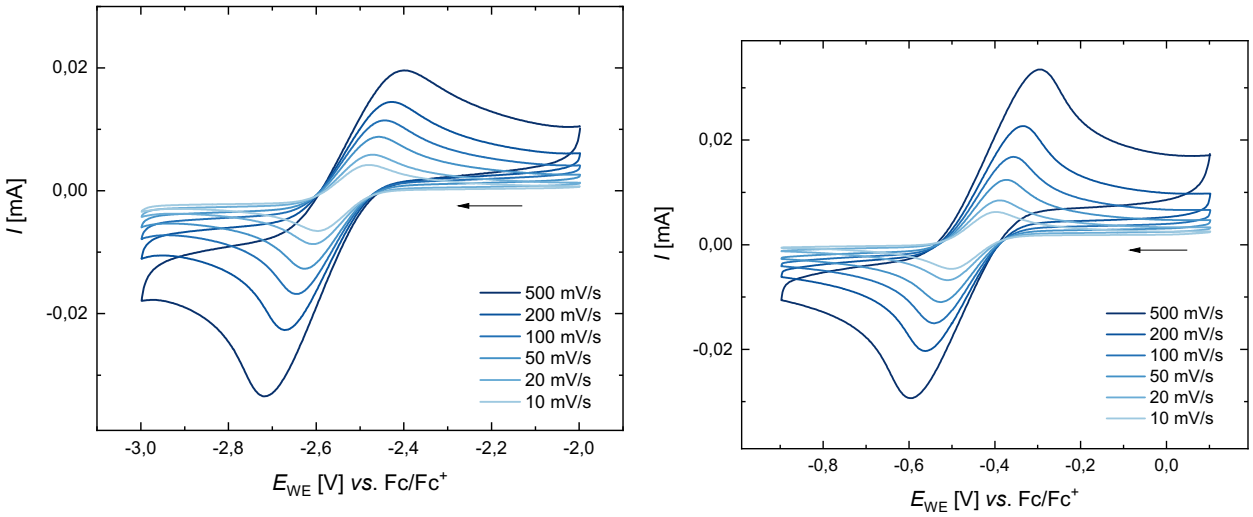

Figure S58: CV of [Mo($^{t\text{Bu}}$diket)$_3$] (1 mM) in TBAPF$_6$/THF (0.1 M) with varying scan rate ν (see Figure legend) of the Mo(III)/Mo(II) (*left*) and of the Mo(III)/Mo(IV) redox couple (*right*).

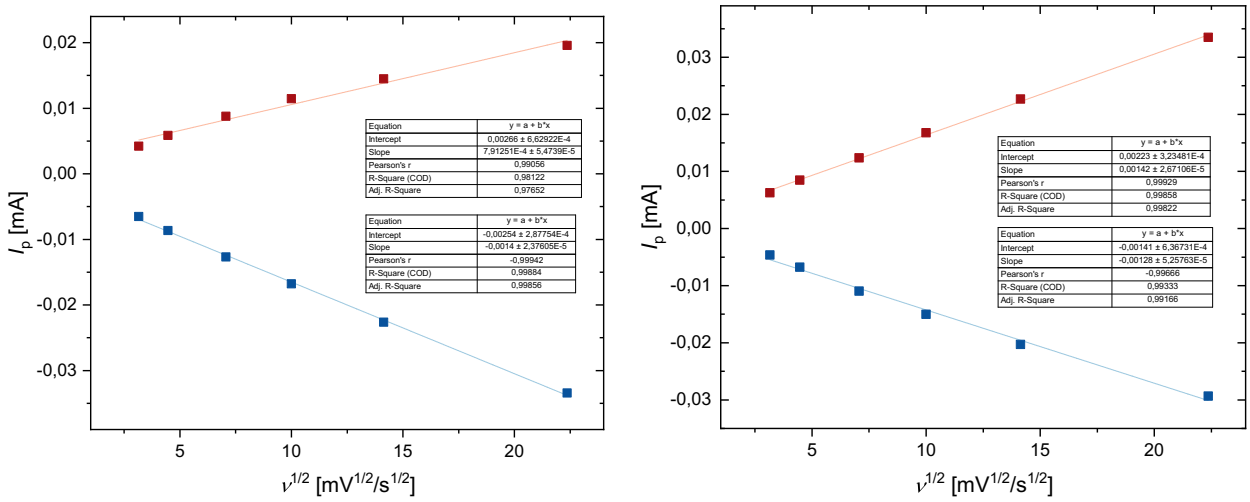

Figure S59: Randles-Ševčík plot of [Mo($^{t\text{Bu}}$diket)$_3$] (1 mM) in TBAPF$_6$/THF (0.1 M) of the Mo(III)/Mo(II) (*left*) and of the Mo(III)/Mo(IV) redox couple (*right*).

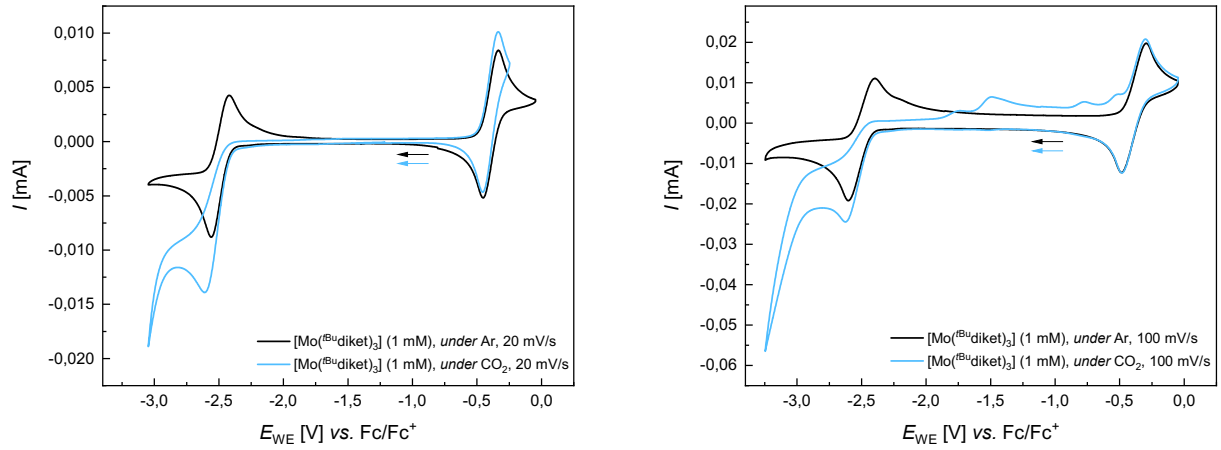

Figure S60: CV (2nd scan) of [Mo($^{t\text{Bu}}$diket)$_3$] (1 mM) in TBAPF$_6$/THF (0.1 M) under argon (*black* trace) and under CO_2 (*light blue* trace) at ν = 20 mV·s^{-1} (*left*) and ν = 100 mV·s^{-1} (*right*).

10.1.4 CV of 6

$K_2[Mo(^{tBu}diket)_2(^{tBu}diket{\cdot}CO_2)]$ (**6**) was analyzed by cyclic voltammetry in $TBAPF_6$/THF (0.1 M). Two irreversible oxidations are observed at E_{ox} = -1.80 V and -1.54 V (*vs.* Fc/Fc^+). The further signals are assigned to *in-situ* formed **3** based on the perfect overlap of corresponding redox potentials.

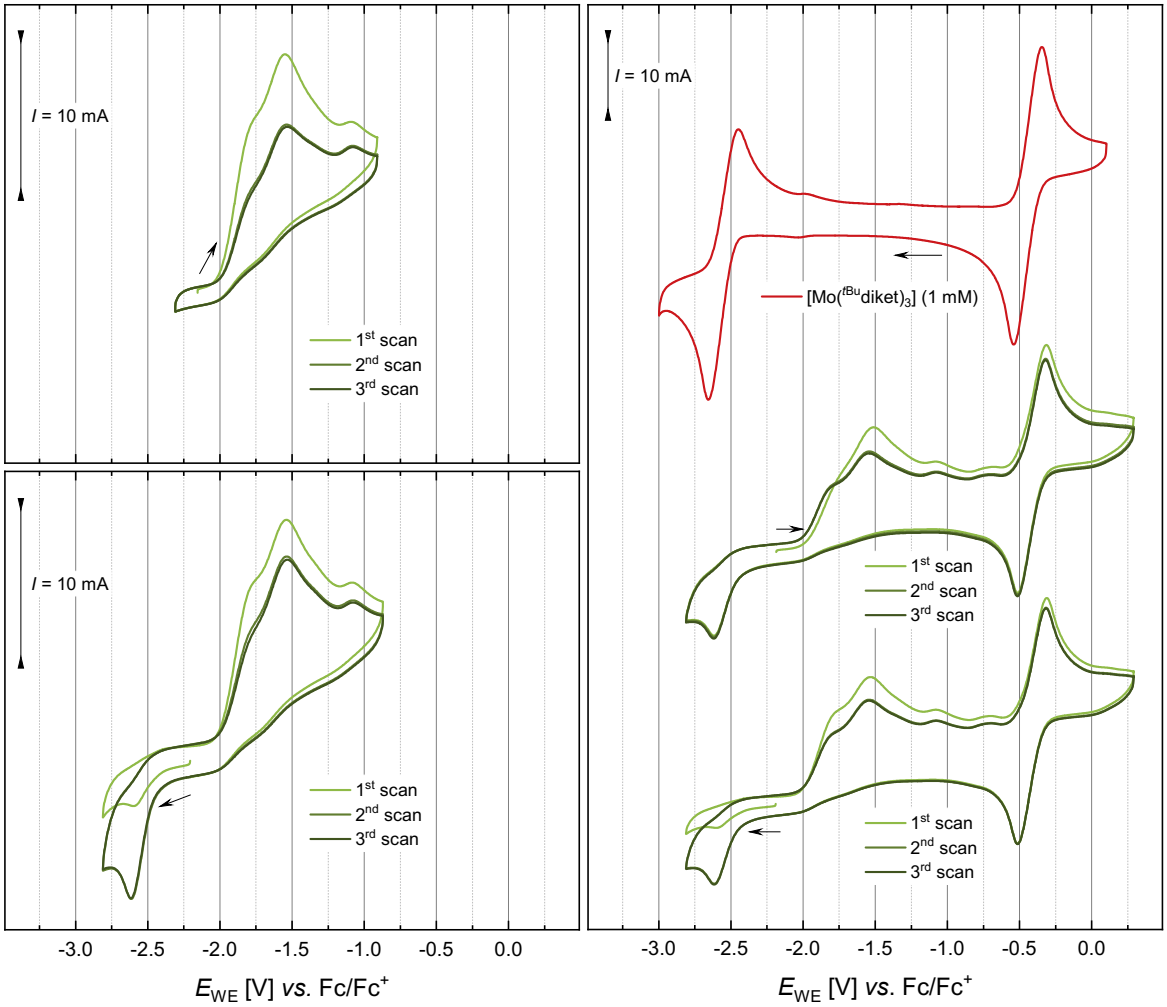

Figure S61: *left:* CV of $K_2[Mo(^{tBu}diket)_2(^{tBu}diket{\cdot}CO_2)]$ (1 mM) in $TBAPF_6$/THF (0.1 M) at a scan rate of ν = 100 mV·s^{-1} in anodic (*top*) and cathodic (*bottom*) scan direction. *right:* Comparison of CV of $[Mo(^{tBu}diket)_3]$ (1 mM) and $K_2[Mo(^{tBu}diket)_2(^{tBu}diket{\cdot}CO_2)]$ (1 mM) in $TBAPF_6$/THF (0.1 M) at a scan rate of ν = 100 mV·s^{-1}.

10.2 Controlled Potential Electrolysis (CPE) under CO_2

CPE experiments were performed in an argon-filled glovebox (Vigor) using a custom-built two compartment H-type cell. The two compartments were separated by two Ceramic-PVDF Composite membranes (16 µm thickness, Xuran). A 0.5 mm diameter platinum wire (10 cm length) was used as the counter electrode and placed in the anodic compartment. A glassy carbon plate electrode (A = 2 cm^2), cut connected via a tantalum wire was used as the working electrode in the cathodic compartment. A $Ag/AgNO_3$ (10 mM in 0.1 M $TBAPF_6$ in CH_3CN) reference electrode was used which was protected by a guard compartment separated by a Vycor® frit, also placed in the working compartment. Both compartments were filled with 6 mL of supporting electrolyte (0.1 M $TBAPF_6/CH_3CN$). Constant magnetic stirring of 300 rpm with a small Teflon-coated stir bar was applied in both compartments during electrolysis. The applied potentials are referenced *vs.* the $Ag/AgNO_3$ reference electrode and may vary slightly from experiment to experiment, owing to small variations of the reference electrode potential.

A 5 mM concentration of the substrate (*i.e.* 0.03 mmol) was used for all CPE experiments. For electrolyses under CO_2, both compartments were purged with purified CO_2 for 20 min (10 mL·min^{-1}).
A CV was recorded prior to CPE, in order to evaluate the optimal potential to be applied.
After all, a constant potential of -2.1 V (*vs.* Ag/$AgNO_3$) was applied for 2 h.

10.2.1 Attempted Product Identification

The strong paramagnetic nature of solutions combined with the presence of a 20-fold excess of supporting electrolyte hampered direct product identification by ^{13}C NMR; however, upon exposure of cathodic solutions to air after electrolysis, or alternatively extracting the reaction mixture taken to dryness with D_2O, allowed removing the paramagnetic components and recording ^{13}C NMR spectrum. In both cases, signals in the range of 180 - 190 ppm were observed (Figure S62, *light blue* trace) which hinted to the formation of oxalate ($C_2O_4^{2-}$). The use of $^{13}CO_2$ led to increased intensities of the latter signals (Figure S62, *dark blue* trace), however these results were hard to reproduce and did not allow to unambiguously assign the product to oxalate, nor was quantification possible. For comparison, Figure S8-3-1a shows the ^{13}C NMR spectrum after running an electrolysis under Ar and otherwise same conditions (Figure S62, *black* trace).

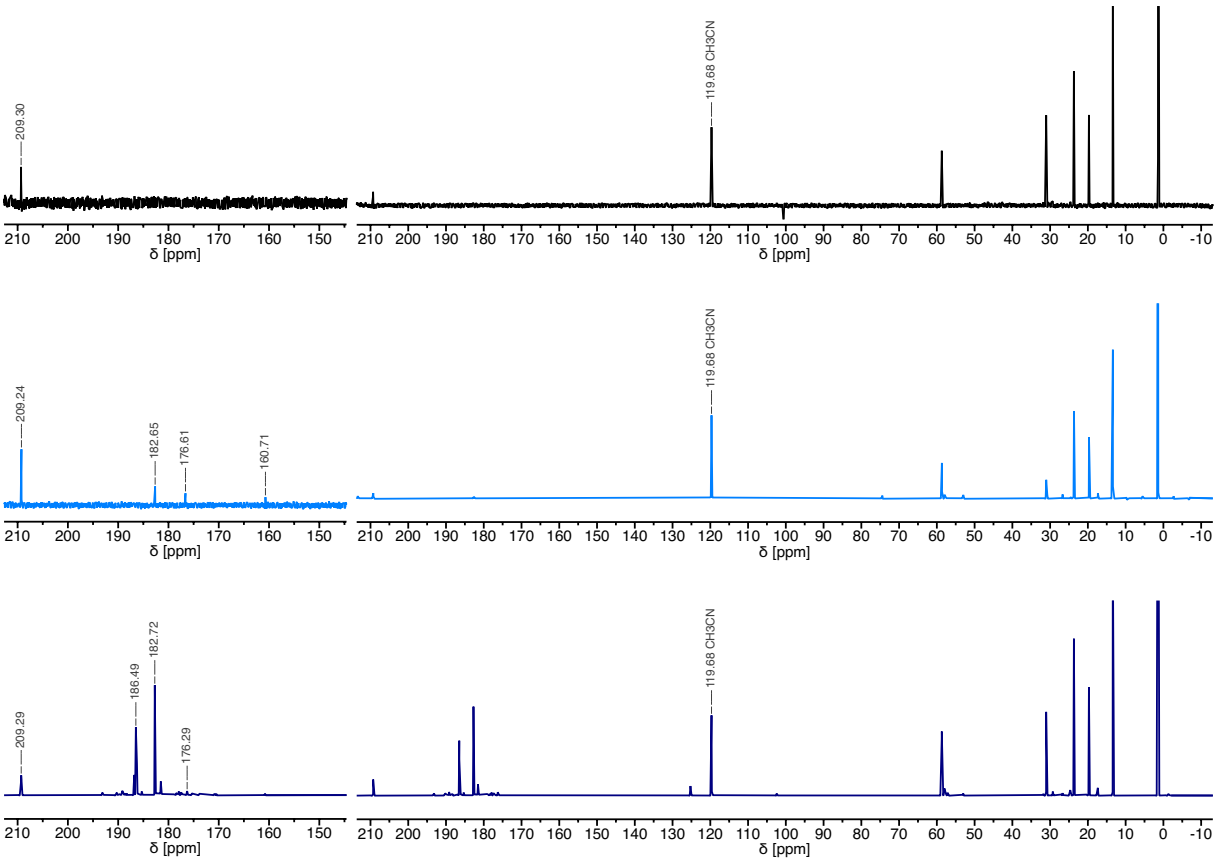

Figure S62: Analysis after CPE (under Ar (*black*), under CO_2 (*light blue*) and under $^{13}CO_2$ (*dark blue*) by ^{13}C NMR spectroscopy, after extraction with D_2O. On the left, a zoom on 210 ppm < δ < 150 ppm is displayed.

10.3 Controlled Potential Electrolysis (CPE) in Presence of CS_2

The same setup and procedure as described in Section S8.2 was employed with minor modifications. In order to avoid potential overload due to very high current, the electrode surface of the working electrode was reduced to 0.5 cm^2 (instead of 2.0 cm^2). In the case of CPE with $TEABF_4$/MeCN (0.1 M) as the supporting electrolyte, glassy carbon foam was employed as the working electrode to prevent the deposition of insoluble product onto the

electrode, which led to rapid current decrease. In addition, CS_2 (101 μL, 1.68 mmol, 56 equiv.) was added to both the working- and the counter compartment (instead of purging with CO_2). A constant potential of -2.0 V (*vs.* Ag/$AgNO_3$) was applied for 2 h.
If $TBAPF_6$/MeCN was employed as supporting electrolyte, the soluble product, $[TBA]_2[C_2S_4]$, remains in solution and undergoes further reaction with excess CS_2 , leading to decreased selectivity and lower overall yields for tetrathiooxalate. As recognized previously,[19, 22] use of tetraethyl ammonium (TEA) cations (*e.g.* $TEABF_4$/MeCN as supporting electrolyte) was reported to have a beneficial impact on the selectivity for tetrathiooxalate, because $[TEA]_2[C_2S_4]$ is insoluble in MeCN and precipitates.
We have investigated the electrocatalytic reduction of CS_2 in presence of **3** in both supporting electrolytes (*i.e.* $TBAPF_6$/MeCN or $TEABF_4$/MeCN). With $TBAPF_6$, unselective reduction of CS_2 was observed, leading to multiple products ($[TBA]_2[C_2S_4]$ ($\delta(^{13}C)$ = 268.4 ppm) and $[TBA]_2[C_3S_5]$ ($\delta(^{13}C)$ = 221.2 ppm, 149.1 ppm), among others). In $TEABF_4$, the electroreduction proved to be much more selective, generating $[TEA]_2[C_2S_4]$ as a partly insoluble yellow solid ($\delta(^{13}C)$ = 268.5 ppm).

10.3.1 Product Analysis

The solution of the working compartment was transferred to a 25 mL scintillation vial and all volatiles were removed under reduced pressure. The obtained dark solid was analyzed by NMR- and UV-Vis spectroscopy (Figure S63).
In case of CPE in $TEABF_4$, the yellow precipitate was directly analyzed by ^{13}C NMR spectroscopy in methanol-d_4 (Figure S64) and identified as analytically pure $[TEA]_2[C_2S_4]$. However, substantial amounts of tetrathiooxalate product remained in solution (^{13}C NMR, Figure S65, and UV-Vis spectroscopy). For quantification, the analytically pure deposit as well as the whole working compartment (taken to dryness) were analyzed by UV-Vis spectroscopy in methanol (λ_{max} = 345 nm, n_{tot} = 0.12 mmol) (Figure S66). Given the amount of charge passed during the 2 h electrolysis (ΔQ = 28 C), a faradaic efficiency of 42% was calculated.

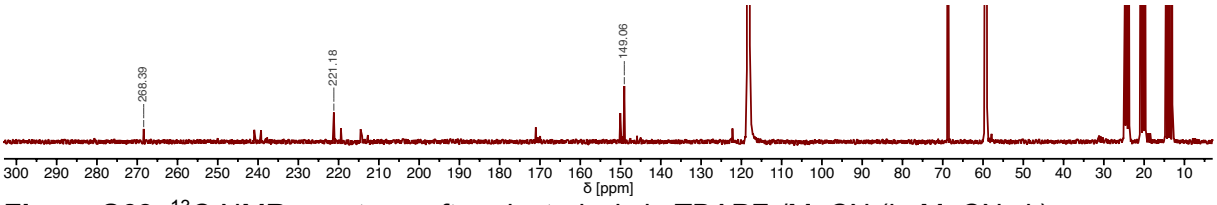

Figure S63: ^{13}C NMR spectrum after electrolysis in $TBAPF_6$/MeCN (in MeCN-d_3).

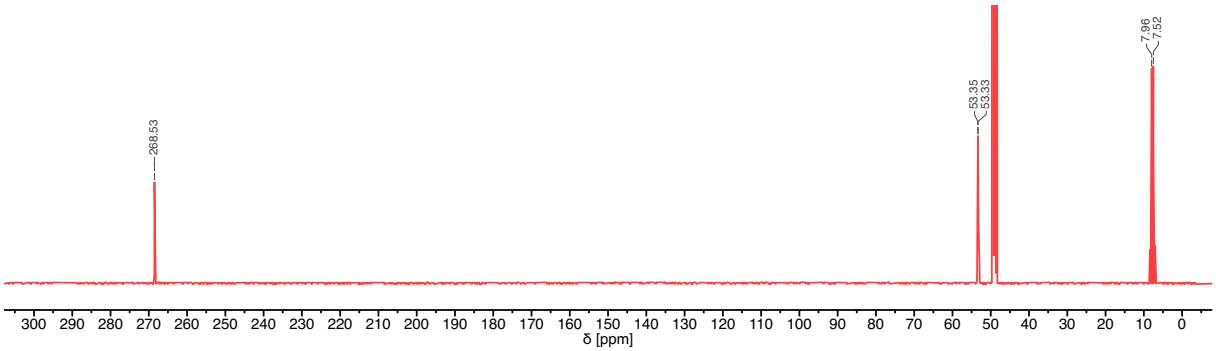

Figure S64: ^{13}C NMR spectrum of yellow precipitate formed after electrolysis in $TEABF_4$/MeCN (in methanol-d_4).

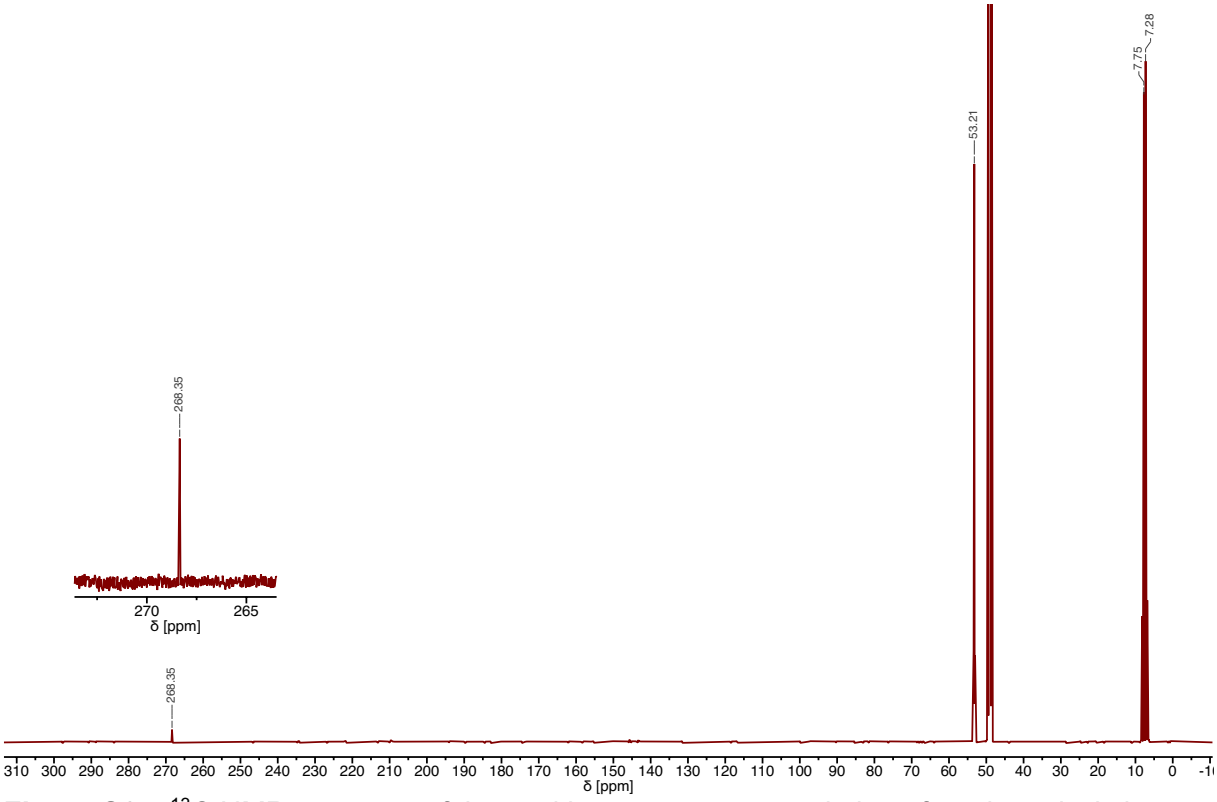

Figure S65: ^{13}C NMR spectrum of the working compartment solution after electrolysis in $TEABF_4$/MeCN (taken to dryness, in methanol-d_4).

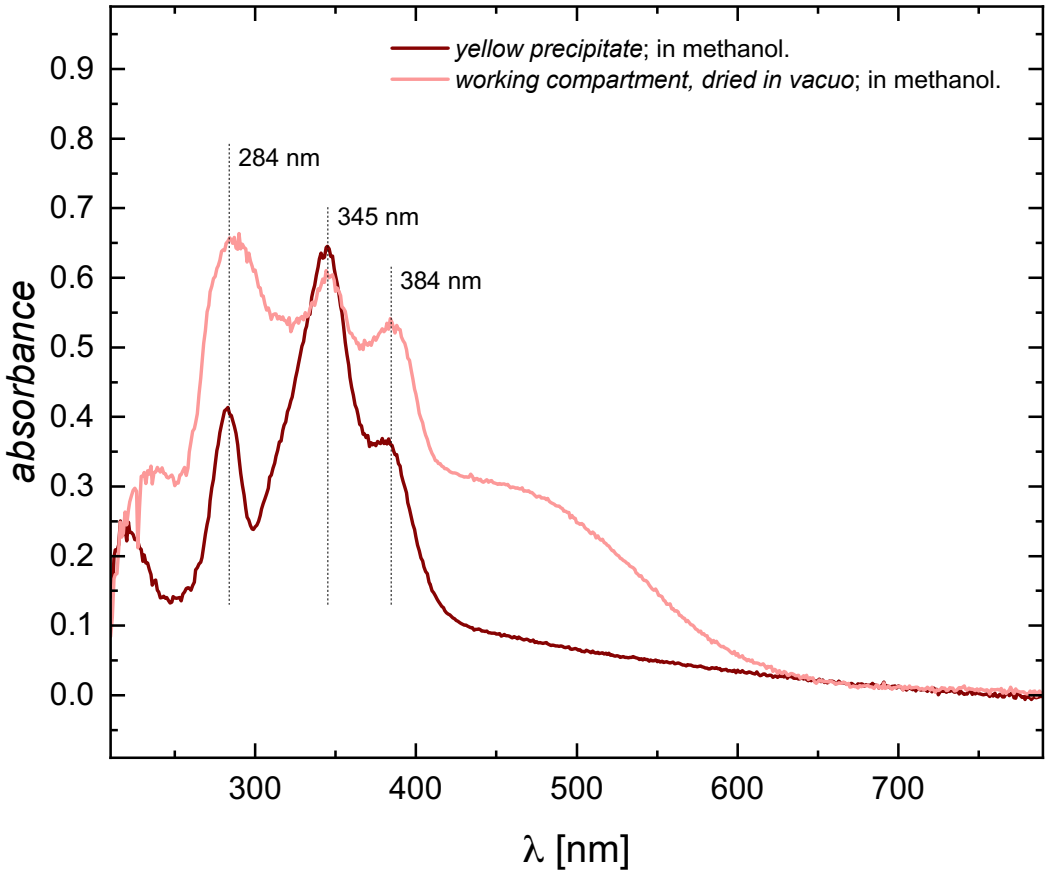

Figure S66: Product analysis after CPE (with $TEABF_4$ as supporting electrolyte) by UV-Vis spectroscopy in methanol.

11. Proposed Reaction Mechanism

Here, we propose two mechanisms for the reactivity of **5** with either CO_2 or CS_2 (Scheme S2). The proposals are based on the observed overall disproportionation reaction, that is induced by CO_2 which stands in stark contrast to the formation of potassium tetrathiooxalate in presence of CS_2. In both cases, a (not observed) CE_2-bound Mo(II) intermediate ([Mo($^{t\text{Bu}}$diket)$_2$($^{t\text{Bu}}$diket·CE_2)]$^{1-}$) is initially generated upon reaction of **5** with either CO_2 (E = O) or CS_2 (E = S). For E = O, we propose that this intermediate has a more anodic reduction potential (if compared to **5**) and hence undergoes a second reduction by another equivalent of **5**, leading to an overall formal disproportionation reaction. More facile reduction of [Mo($^{t\text{Bu}}$diket)$_2$($^{t\text{Bu}}$diket·CO_2)]$^{1-}$ is indicated by the CV of **6** (Figure S61), displaying two irreversible oxidation waves in its anodic scan at potentials of -1.80 V and -1.54 V (*vs.* Fc/Fc$^+$). These two oxidation events may be tentatively assigned to the oxidation of **6** to **3** via [Mo($^{t\text{Bu}}$diket)$_2$($^{t\text{Bu}}$diket·CO_2)]$^{1-}$**.** Overall, two equivalents of **5** are required for the generation of one equivalent of **6**.

A markedly different situation is encountered for E = S: in our proposed mechanism, the less electron withdrawing nature of the dithiocarboxylate group disfavors the further reduction to [Mo($^{t\text{Bu}}$diket)$_2$($^{t\text{Bu}}$diket·CS_2)]$^{2-}$. Instead, homolytic C-C bond scission leads to the release of **3** and a formal $CS_2^{\cdot-}$ radical anion, which readily dimerizes to the tetrathiooxalate dianion. Here, the intermediacy of [Mo($^{t\text{Bu}}$diket)$_2$($^{t\text{Bu}}$diket·CS_2)]$^{1-}$ is justified by reactivity studies of the free ligand anion [$^{t\text{Bu}}$diket]$^-$ with $^{13}CS_2$, where the formation of the dithiocarboxylated ligand is suggested by ^{13}C NMR spectroscopy (Section S3.5).

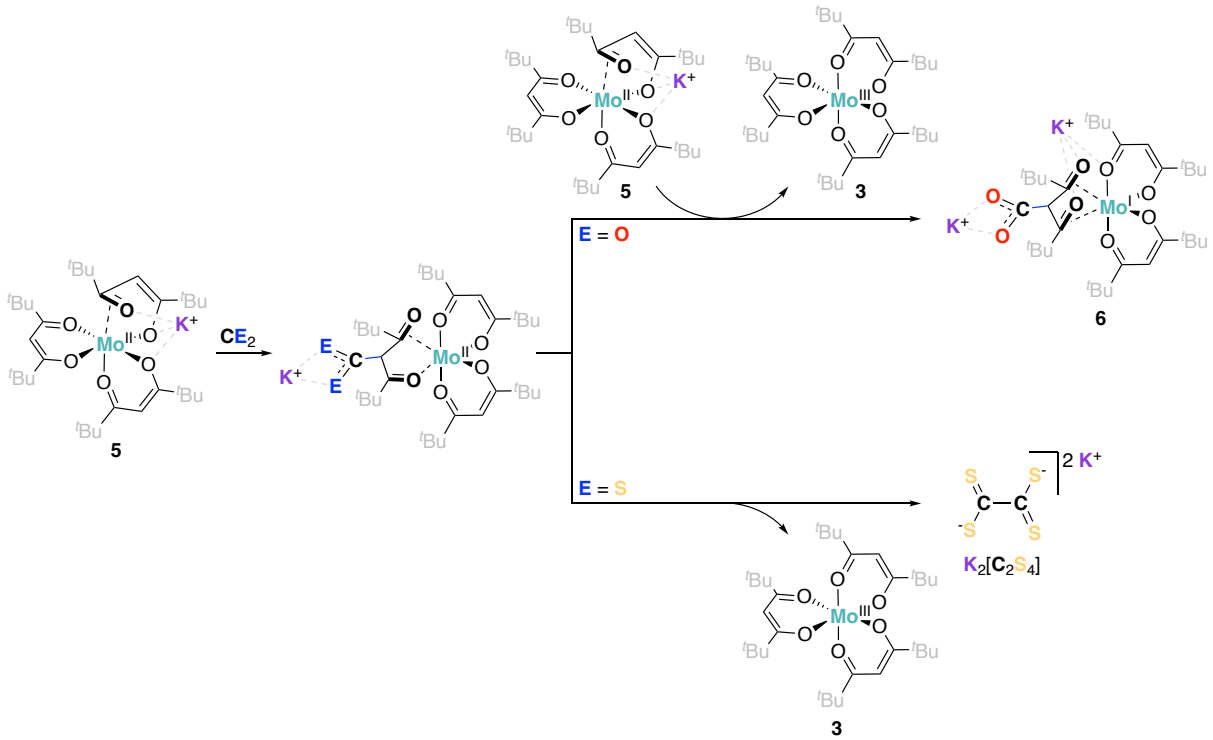

Scheme S2: Proposed mechanistic pathways for the formation of **6** *vs.* $K_2[C_2S_4]$.

12. References

(1) Evans, D. F. 400. The determination of the paramagnetic susceptibility of substances in solution by nuclear magnetic resonance. *Journal of the Chemical Society (Resumed)* **1959**. DOI: 10.1039/jr9590002003.

(2) Piguet, C. Paramagnetic Susceptibility by NMR: The "Solvent Correction" Removed for Large Paramagnetic Molecules. *Journal of Chemical Education* **1997**, *74* (7). DOI: 10.1021/ed074p815.

(3) Stoll, S.; Schweiger, A. EasySpin, a comprehensive software package for spectral simulation and analysis in EPR. *J Magn Reson* **2006**, *178* (1), 42-55. DOI: 10.1016/j.jmr.2005.08.013.

(4) Viculis, L. M.; Mack, J. J.; Mayer, O. M.; Hahn, H. T.; Kaner, R. B. Intercalation and exfoliation routes to graphite nanoplatelets. *J. Mater. Chem.* **2005**, *15* (9). DOI: 10.1039/b413029d.

(5) Shibahara, T.; Yamasaki, M. A New Syntheic Route to Hexachloromolybdate(III). An X-Ray Structure of $(NH_4)_3[MoCl_6]$. *Bull. Chem. Soc. Jpn.* **1990**, *63* (10), 3022-3023. DOI: 10.1246/bcsj.63.3022.

(6) Larson, M. L.; Moore, F. W. Synthesis and Properties of Molybdenum(III) Acetylacetonate. *Inorg. Chem.* **1962**, *1* (4), 856-859. DOI: 10.1021/ic50004a030.

(7) Johnson, A.; Everett, G. W. Comparison of proton and deuteron nuclear magnetic resonance of some paramagnetic transition metal complexes. I. *Journal of the American Chemical Society* **1972**, *94* (5), 1419-1425. DOI: 10.1021/ja00760a001.

(8) Tkachov, R.; Stepien, L.; Roch, A.; Komber, H.; Hennersdorf, F.; Weigand, J. J.; Bauer, I.; Kiriy, A.; Leyens, C. Facile synthesis of potassium tetrathiooxalate – The “true” monomer for the preparation of electron-conductive poly(nickel-ethylenetetrathiolate). *Tetrahedron* **2017**, *73* (16), 2250-2254. DOI: 10.1016/j.tet.2017.03.010.

(9) Liebing, P.; Schmeide, M.; Kühling, M.; Witzorke, J. The Alkali Metal Salts of Methyl Xanthic Acid. *Eur. J. Inorg. Chem.* **2020**, *2020* (25), 2428-2434. DOI: 10.1002/ejic.202000258.

(10) Andrez, J.; Pecaut, J.; Bayle, P. A.; Mazzanti, M. Tuning lanthanide reactivity towards small molecules with electron-rich siloxide ligands. *Angew. Chem. Int. Ed.* **2014**, *53* (39), 10448-10452. DOI: 10.1002/anie.201405031.

(11) Bartoli, G.; Bosco, M.; Guerrieri, A.; Dalpozzo, R.; De Nino, A.; Iantorno, E.; Palmieri, G. Reaction of dianions of acyclic β-enamino ketones with electrophiles. vii. synthesis of 5-(monoalkylamino)-3-oxo γ,δ-unsaturated acids and esters and of 3-(monoalkylamino)-5-oxo β,γ-unsaturated esters. *Gazz. Chim. Ital.* **1996**, *126* (1), 25-29.

(12) Finger, L. H.; Guschlbauer, J.; Harms, K.; Sundermeyer, J. N-Heterocyclic Olefin-Carbon Dioxide and -Sulfur Dioxide Adducts: Structures and Interesting Reactivity Patterns. *Chem. Eur. J.* **2016**, *22* (45), 16292-16303. DOI: 10.1002/chem.201602973.

(13) Dolomanov, O. V.; Bourhis, L. J.; Gildea, R. J.; Howard, J. A. K.; Puschmann, H. OLEX2: a complete structure solution, refinement and analysis program. *J. Appl. Crystal.* **2009**, *42* (2), 339-341. DOI: 10.1107/s0021889808042726.

(14) Sheldrick, G. M. SHELXT - integrated space-group and crystal-structure determination. *Acta Cryst.* **2015**, *71* (Pt 1), 3-8. DOI: 10.1107/S2053273314026370.

(15) Sheldrick, G. M. A short history of SHELX. *Acta Cryst.* **2008**, *64* (Pt 1), 112-122. DOI: 10.1107/S0108767307043930.

(16) Bacher, A. D.; Sens, I.; Müller, U. Ein neuer Zugang zu Tetrathiooxalaten. Die Kristallstruktur von $(NEt_4)_2[C_2S_4]$ / A Novel Access to Tetrathiooxalates. Crystal Structure of $(NEt_4)_2[C_2S_4]$. *Z. Naturforsch. B* **1992**, *47* (5), 702-705. DOI: 10.1515/znb-1992-0516.

(17) Jeroschewski, P.; Hansen, P. Tetrathiooxalate-Darstellung, Eigenschaften und Reaktionen. *Sulfur Rep.* **1986**, *7* (1), 1-37. DOI: 10.1080/01961778608082501.

(18) Breitzer, J. G.; Chou, J.-H.; Rauchfuss, T. B. A New Synthesis of Tetrathiooxalate and Its Conversion to $C_3S_5^{2-}$ and $C_4S_6^{2-}$. *Inorg. Chem.* **1998**, *37* (8), 2080-2082. DOI: 10.1021/ic971327c.

(19) Breitzer, J. G.; Holloway, G. A.; Rauchfuss, T. B.; Salata, M. R.; Kee, C. L.; Yan, Y. K. Electrochemical Synthesis of Tetraethylammonium Tetrathiooxalate. In *Inorganic Syntheses: Volume 36*, Inorganic Syntheses, 2014; pp 195-198.

(20) *Gaussian 09, Revision A.02*; Wallingford CT, 2016. (accessed 23.07.2024).

(21) *Chemcraft - graphical software for visualization of quantum chemistry computations. Version 1.8, build 682.* https://www.chemcraftprog.com (accessed 12.08.2024).

(22) Jeroschewski, P. Elektrochemische Darstellung von Tetraalkylammoniumsalzen der Tetrathiooxaisäure. *Z. Chem.* **1981**, *21* (11), 412-412. DOI: 10.1002/zfch.19810211115.